Dihydroartemisinin efficiently Induces Cytotoxicity in Normoxic and Hypoxic Cancer Cells and Improves Radiotherapy

Inaugural-Dissertation

zur

Erlangung des Doktorgrades

Dr. rer. nat.

der Fakultät für

Biologie

an der

Universität Duisburg-Essen

vorgelegt von

Sina Bader

aus Weingarten

Juli 2021

Die der vorliegenden Arbeit zugrundeliegenden Experimente wurden am Institut für Zellbiologie (Tumorforschung) in der Abteilung für Molekulare Zellbiologie am Universitätsklinikum Essen, der Universität Duisburg-Essen durchgeführt.

1. Gutachter: PD Dr. rer. nat. Justine Rudner

2. Gutachter: Prof. Dr. rer. nat. Christian Johannes

Vorsitzender des Prüfungsausschusses: Prof. Dr. phil. nat. George E. Iliakis

Tag der mündlichen Prüfung: 12.01.2022

DOI: 10.17185/duepublico/75334
URN: urn:nbn:de:hbz:464-20220215-121954-9

In the context of this doctoral thesis, the following articles were published:

Bader S, Wilmers J, Pelzer M, Jendrossek V, Rudner J. *Activation of anti-oxidant Keap1/Nrf2 pathway modulates efficacy of dihydroartemisinin-based monotherapy and combinatory therapy with ionizing radiation.* Free Radical Biology and Medicine, 2021(168): p. 44-54

Bader S, Wilmers J, Ontikatze T, Ritter V, Jendrossek V. Rudner J. *Loss of pro-apoptotic Bax and Bak increases resistance to dihydroartemisinin-mediated cytotoxicity in normoxia but not in hypoxia in HCT116 colorectal cancer cells.* Free Radical Biology and Medicine, 2021(174): p. 157-170

“Life is pleasant. Death is peaceful. It's the transition that's troublesome.”

Isaac Asimov (1920 - 1992)

Index

1 Introduction

1.1 Cancer incidence and mortality

In 2020, 19.3 million patients were diagnosed with cancer. Death from cancer is globally the second leading cause of deaths after ischemic heart diseases. According to the GLOBOCAN database, breast, lung and colorectum cancers were the most frequently diagnosed tumor entities in the general population. With regard to mortality, lung, colorectum and liver cancers accounted for more than one third of cancer related deaths worldwide (Fig. 1.1).

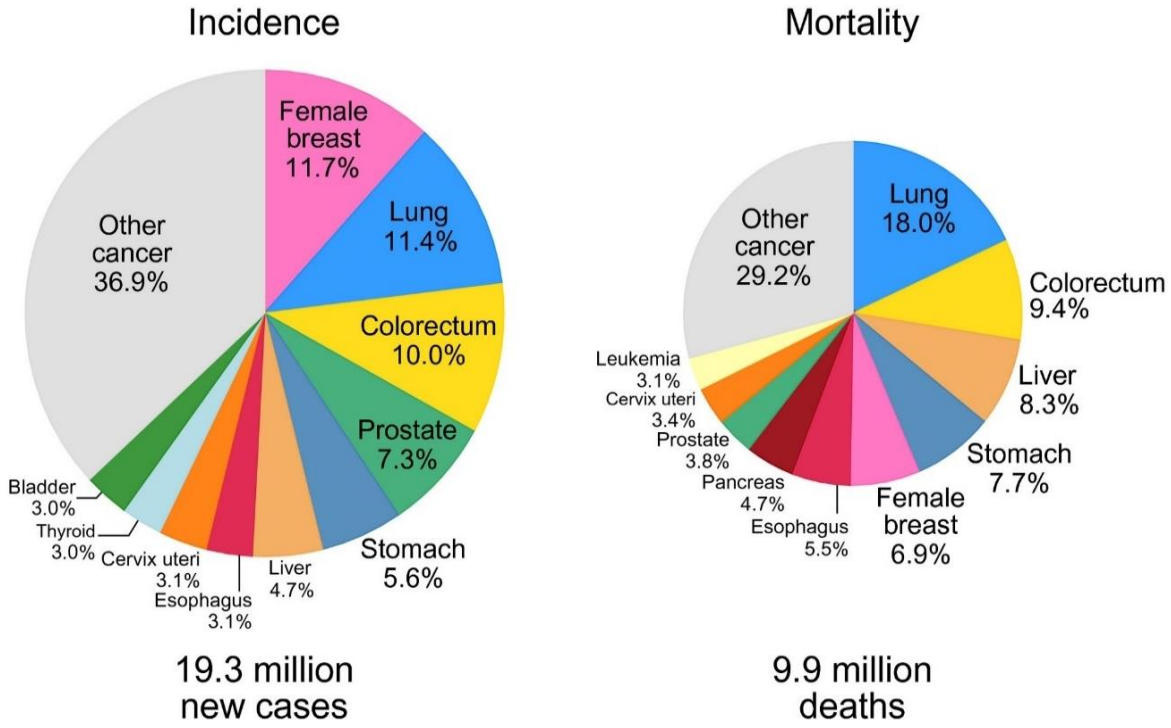

Figure 1.1 Worldwide cancer incidence and mortality for the 10 most common cancers in 2020 in men and women. *The most often diagnosed cancer entities were female breast, lung and colorectum cancer. Lung, colorectum and liver cancer account for one third of cancer mortality [1]*

Although treatment of cancer has greatly improved over the last decades, almost 10 million people died from cancer in 2020 [1]. The conventional therapies have been refined, but they often fail to cure cancer due to high resistance of tumor cells and severe effects on normal tissue. In addition, a partial remission in response to therapy frequently results in tumor recurrence afterwards with increased resistance of mutated cells to the therapy applied [2]. Hence, the search for new pharmacological agents with a more efficient and more specific anti-cancer activity is ongoing with the goal to advance the rate of complete and durable clinical response in patients.

1.2 Radiotherapy

1.2.1 Application of radiotherapy in cancer treatment

Along with chemotherapy and surgery, radiotherapy is one of the standard treatment options for cancer patients. Approximately 50% of all cancer patients receive radiotherapy during their course of illness. Usually, radiotherapy is applied adjuvant to kill cancer cells which remained in the body after surgical removal, or neoadjuvant to shrink the tumor volume before surgery [3]. Radiotherapy is either administered alone or in combination with chemotherapeutic drugs to increase the anti-neoplastic effect. The use of each modality mainly depends on the cancer cell histology, anatomic location, stage of the tumor and patient's fitness [4]. The most common application technique for treating cancer with radiation is fractionated radiation therapy, in which the intended dose of radiation is applied in multiple fractions over several weeks. A commonly used regimen consist of 5 fractions per week of 1 - 3 Gy daily doses to reach a total dose of 60 – 70 Gy depending on the tumor entity [210]. The advantage of this procedure is mainly based on three factors: firstly, *repair* of sublethal injury in healthy cells between fractions, resulting in lowered normal tissue toxicity. Secondly, the *redistribution* of the cell cycle of surviving tumor cells, since the highest sensitivity to radiation is given in M and late G2 phase, while cells in late S phase are highly resistant. Thirdly, the *reoxygenation* of hypoxic cancer cells, since radiation kills a greater proportion of aerated cells, while hypoxic cells are highly resistant. The accumulation of a hypoxic cell population after irradiation can be avoided by application of radiotherapy in multiple fractions, allowing reoxygenation of hypoxic cells before receiving the next radiation dose [5]. Consequently, the therapeutic window – the range, in which the irradiation dose could safely be applied due to different sensitivity of normal and tumor tissue – is increased. Therefore, the fractionated-dose radiotherapy has become the standard application procedure targeting the tumor tissue.

The most frequently applied form of radiation in cancer therapy is ionizing radiation (IR), which is defined as the energy required to eject electrons from the orbit of an atom, causing that atom to become charged or ionized. Ionizing radiation is applied as electromagnetic waves or particles. In radiotherapy, the most common energy sources are electromagnetic particles called photons such as X-rays or γ-rays, which are both indirectly ionizing. Their absorption results in the production of fast recoil electrons that in turn are able to ionize other atoms and produce damage in biologic material [6]. Thus, X-rays and γ-rays do not differ in the way they act, but in the way they are

generated. X-rays are produced by linear accelerators, such as X-ray tubes. These are electrical devices in which electrons are emitted from the cathode and accelerated in the direction of an anode. When the highly energetic electron hits the anode – which is usually made of tungsten, molybdenum or copper – they transfer their kinetic energy to atoms of the anode while deaccelerating, thereby creating photons, among which the braking radiation (X-rays) is used to irradiate tumors. In the present study, low linear-energy-transfer with X-rays was employed to irradiate tumor cells. In contrast, γ-rays are generated by the decay of radioactive isotopes (e.g., cobalt-60, caesium, radium) [3, 6]. Moreover, radiation beams can also originate from electrons, protons or heavy ions which are generated by specific cyclotrons [3, 7].

Radiotherapy is commonly applied using the described external beam radiation therapy (EBRT), but sometimes brachytherapy is used. Brachytherapy allows a radiation treatment from inside the body by deposing radioactive material very close or inside the tumor tissue. Most often, it is used to treat rare pediatric cancers and has the advantage of using a higher total dose while treating a smaller area than EBRT [8].

1.2.2 Mechanisms of IR-induced cytotoxicity

On the cellular level, IR affects biomolecules by direct and indirect actions. When radiation is absorbed by biological material, the produced recoil electron can directly ionize a critical target in the cell, such as DNA, proteins or lipids. Alternatively, the electron interacts with other cellular atoms or molecules to produce free radicals that in turn damage targeted structures (Fig. 1.2) [9, 11, 155]. This effect is termed indirect action and occurs mainly by radiolysis of water, the major constituent of cells (~ 80%). During radiolysis, water undergoes a breakdown into ionized water (H_2O^+) and hydrated electrons (e_{aq}^-). Subsequently, free radicals such as the highly reactive hydroxyl radicals (·OH) or superoxide anions ($O_2^{\cdot -}$) are generated, which damage cellular macromolecules by oxidation [10, 11]. Using X-rays during irradiation, about two thirds of the cellular damage is attributed to the indirect action [6]. The importance of reactive oxygen species (ROS), such as hydroxyl radicals or superoxide anions, in radiation-induced cytotoxicity becomes apparent in cancer cells, irradiated in an oxygen deprived environment, in which IR-induced ROS production is decreased and cancer cell survival therefore improved [12, 13].

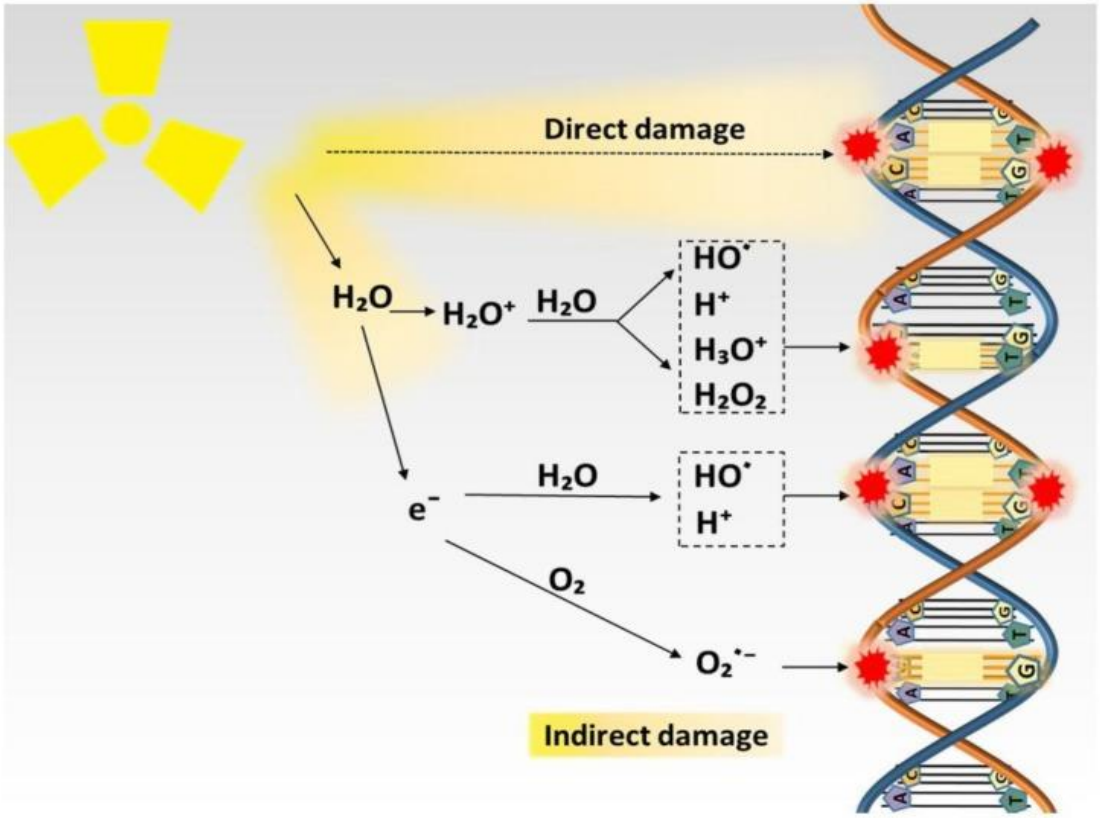

Figure 1.2 The direct and indirect action of ionizing radiation. *Direct action: The produced recoil electron directly ionizes a critical target in the cell, such as DNA. Indirect action: The secondary electron interacts with other intracellular molecules, most likely water, to produce free radicals such as the highly reactive hydroxyl radical (·OH) or super oxide anions ($O_2^{\cdot-}$) that in turn induce cellular damages [14].*

Although IR is capable of damaging all cellular biomolecules, DNA damage, particularly double strand breaks (DSB) are considered to be the major lesion responsible for the anti-neoplastic effect [15]. DSBs are highly deleterious for fast proliferating tumor cells, since they can cause mutations (point mutations, deletions, translocations) as well as lethal chromosome or chromatid aberrations [211]. An early cellular response to DNA damage is the induction of cell cycle arrest in G1/S or G2/M phase to allow processing of lesions and prevent entering S and M phase with damaged DNA [155]. In order to enable repair factors access to the site of damage, phosphorylation of the H2A histone family member X (γH2A.X) occurs in response to DSBs. Thus, detection of γH2A.X has become a well-established method to analyze chromatin modifications linked to DNA DSBs and repair [16]. The main mechanisms by which DSBs are eliminated include the error-free homologous recombination repair (HRR), the error-prone non-homologous end-joining (NHEJ) and as a backup alternative NHEJ. The fast-occurring error-prone NHEJ is active throughout the cell

cycle, while the error-free HRR and the error-prone alternative NHEJ are cell-cycle dependent. Alternative NHEJ operates with a higher efficiency in G2 phase, while HRR is only available in late S and G2 phase and depends on the availability of an undamaged sister chromatid [212, 213]. Due to oncogene-induced replication stress and acquired defects in DNA repair pathways, cancer cells have a higher DSB burden than healthy cells. This, most likely, contributes to specificity of radiation-induced cytotoxicity to cancer cells [17].

Radiotherapy aims to induce cellular damage that exceeds the repair capacity of tumor cells, resulting in replicative or reproductive death. The most frequent mechanism leading to cell death is mitotic catastrophe, a delayed-mitosis-linked cell death occurring from DNA damage or malfunctions in the mitotic machinery. In response to radiation it is caused by damaged chromosomes while cells attempt to divide [6]. Death occurs in the first or subsequent divisions following irradiation when sufficient genetic damage and chromosomal aberrations are accumulated [18].

1.3 Hypoxia limits radiation-induced cytotoxicity

1.3.1 Tumor hypoxia physiology

Tumor hypoxia is defined by reduced concentrations of oxygen relative to the physiological oxygenation level of the respective tissue. Hypoxia commonly occurs in approximately 50 – 60% of human solid tumors as a consequence of the fast expanding tumor tissue and an abnormal vascular network [19]. Hypoxia is highly dynamic with respect to its intensity and duration. Typically, hypoxia is classified in two main types: acute and chronic hypoxia [24, 214].

Chronic hypoxia occurs as a result of expanding tumor tissue around blood vessels and affects cancer cells that spread beyond the diffusion distance of oxygen in biological material [19]. Cells exposed to chronic hypoxia can remain viable for hours to days [20]. To escape from cell death and enable reoxygenation, cells exposed to persistently low oxygen levels induce angiogenesis, the formation of new capillaries from pre-existing vessels. Angiogenic signaling, such as the release of the vascular endothelial growth factor (VEGF), is initiated by stabilization of the hypoxia-inducible factors (HIF) [21, 215]. HIFs are a family of transcription factors, whereof HIF1 is the most studied one. HIF1 is composed of two subunits – HIF1α and HIF1β – of which HIF1α levels are regulated by hydroxylation of two prolyl residues, catalyzed by oxygen-sensing prolyl hydroxylase domain proteins (PHD). Under normoxic

conditions, HIF1α hydroxylation results in binding of the von Hippel-Lindau protein (VHL) and subsequent ubiquitination and proteasomal degradation [21]. Under conditions of low oxygen availability, hydroxylation is markedly reduced, resulting in HIF1α stabilization and dimerization with HIF1β. The heterodimer binds to DNA, driving transcription of HIF1-inducible genes [216]. In addition to angiogenic signaling, the transcription factor also promotes cell detachment, migration and invasion by downregulation of adhesion proteins such as cadherins and induction of matrix degrading enzymes [19, 215, 217]. Moreover, HIF1 regulates metabolic adaption to low oxygen availability, by induction of glucose transporters and glycolytic enzymes. Collectively, HIF1 transcriptionally regulates a wide array of genes promoting survival and adaption to unfavorable oxygen conditions [217, 218].

In contrast to chronic hypoxia, acute hypoxia emerges spontaneously for instance due to a limited perfusion caused by occluded blood vessels [22]. Cancer cells are frequently exposed to acute, perfusion-limited hypoxia, since tumors are characterized by a chaotic architecture of the vascular network, consisting of immature and malformed vessels that contribute to an inadequate blood flow [23]. Transient closing or blockage of malformed vessels results in dynamically changing perfusion of the surrounding tissue [22]. Changing oxygen concentrations result repetitively in transient hypoxic phases followed by reoxygenation, also termed as cycling hypoxia [219]. Research of the past decades revealed that acute and cycling hypoxia leads to a more aggressive phenotype than chronic hypoxia [24]. This is mainly based on the clonal selection of death resistant cancer cells that have adapted to unfavorable and changing oxygen conditions. Cells exposed to hypoxia can become resistant to apoptosis at multiple levels. A previous publication revealed that hypoxia hinders the translocation of the pro-apoptotic protein Bax to mitochondrial membrane, thereby preventing induction of the intrinsic apoptosis pathway. In addition, hypoxia-dependent inhibition of apoptosis could be related to an increased expression of the anti-apoptotic inhibitor of apoptosis protein 2 (IAP-2), which inhibits activated caspases [25].

Altogether, hypoxia drives malignant progression and is therefore a prognostic factor for poor survival. Since hypoxia contributes to resistance towards radiotherapy and several chemotherapeutic drugs, it is considered a major obstacle in treatment of locally advanced solid tumors [13, 26, 27].

1.3.2 Mechanism of hypoxia-dependent radioresistance

The efficacy of IR to induce permanent and irreparable oxidative damage is strongly influenced by the intracellular oxygen availability. In normoxic conditions, IR-induced DNA radicals react with molecular oxygen to form peroxy radicals, considered as permanent damage leading to strand breaks (Fig. 1.3). In hypoxia, the lack of oxygen hampers the formation of peroxy radicals and, thus, reduction of DNA radicals. As a consequence, less DNA strand breaks are produced, thereby lowering radiation-induced cytotoxicity in hypoxia [14, 28]. The reduced efficacy to induce DNA breaks in a hypoxic environment results in a 2 – 3-fold increased radiation dose required for equal cell killing as in normoxia [27, 28]. This dose ratio is known as the oxygen enhancement ratio (OER).

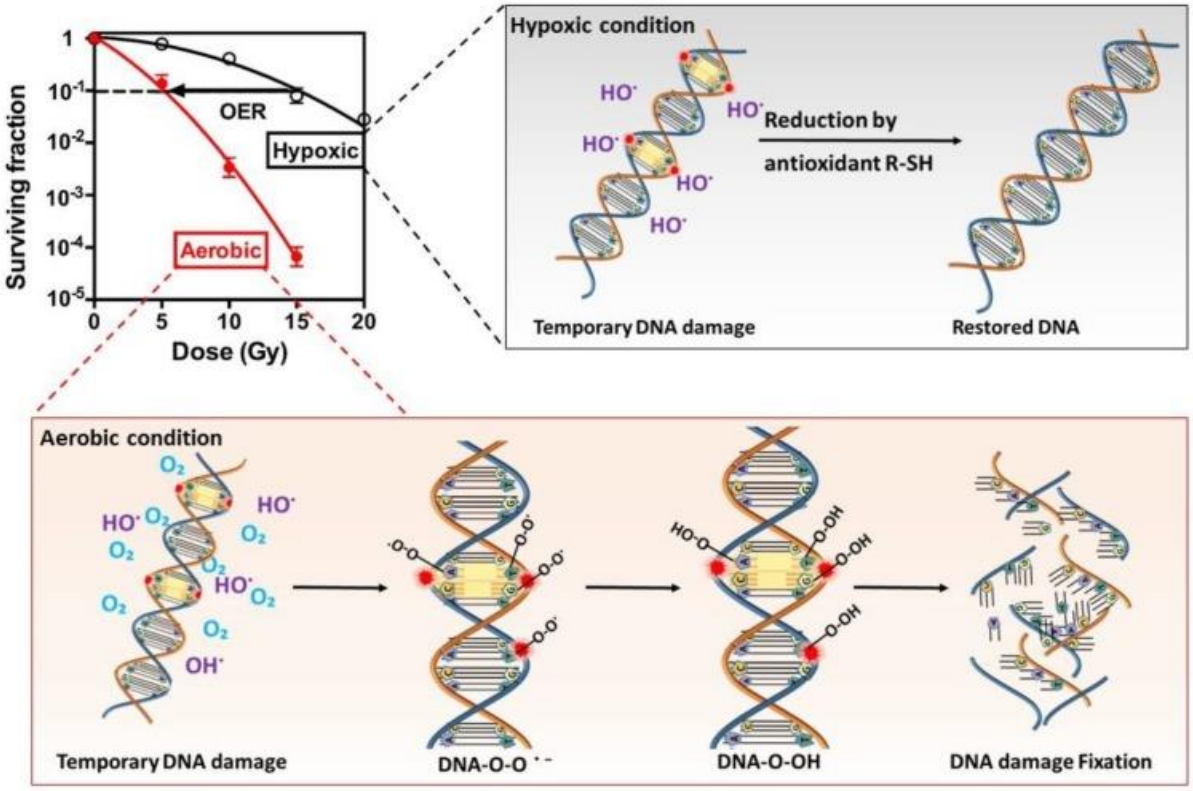

Figure 1.3 Oxygen-dependent fixation of radiation-induced DNA damage. *In normoxia, molecular oxygen reacts with IR-induced DNA radicals, creating permanent peroxy radicals and strand breaks. In hypoxia, the lack of oxygen enables repair of DNA radicals. As a consequence, generation of strand breaks and subsequent cell death decrease. The oxygen enhancement ratio (OER) or hypoxic radioresistance can be represented by the ratio of the dose required in hypoxic condition divided by the dose required in aerobic conditions for equivalent eradication of cancer cells [14].*

1.4 ROS and the antioxidative system

1.4.1 ROS and oxidative damages

ROS are inevitable by-products of aerobic metabolism. They include for instance superoxide anions ($O_2^{\cdot-}$), singlet oxygen ($^1O_2$), the highly reactive hydroxyl radical ($\cdot OH$) or the highly diffusible hydrogen peroxide (H_2O_2). At low levels, ROS can act as second messengers and activate signalling pathways that regulate cell survival, proliferation and metabolic processes. On the contrary, increased ROS stress can cause oxidative injuries and cell death [29, 30]. Hence, the maintenance of an appropriate ROS level is of central importance for cellular function.

Mitochondria are considered as the major source of intracellular ROS production. Specifically, the mitochondrial complexes I and III of the electron transport chain (ETC) contribute to approximately 45% of intracellular ROS production through one-electron reduction of molecular oxygen, resulting in generation of superoxide anions [31]. The generated superoxide anions are subsequently converted into the highly diffusible second messenger H_2O_2 through superoxide dismutase (SOD) followed by catalase- and glutathione peroxidase-dependent detoxification [32]. Alternatively, Fenton reactions catalyze the production of highly reactive hydroxyl and hydroperoxyl radicals [33]. Other endogenous ROS sources are for instance NADPH oxidases, β-oxidation of fatty acids in peroxisomes or the process of oxidative protein folding in the endoplasmatic reticulum (ER) [34].

Exposure of cells to high ROS levels can cause oxidative damage to biomolecules [35]. The highly reactive sulfhydryl groups of proteins, particularly of methionine and cysteine residues, are especially prone to modifications during oxidative insult [35, 36]. While site-specific thiol oxidation serves as a sensor for the regulation of protein function in some cases, the majority of proteins may lose their function by unspecific oxidation events [37]. ROS-induced thiol modifications include the reversible formation of sulfenic acids (R-SOH), which can either interact with a second cysteine resulting in intramolecular or intermolecular protein disulfides, or react with thiol reductants such as glutathione (GSH) to become S-glutathionylated (R-SSG) (Fig. 1.4). Reduction of these reversible modifications is catalyzed by glutaredoxins (Grx) or thioredoxin reductases (Trx). Alternatively, sulfenic acids may be further oxidized to sulfinic (R-SO2H) and sulfonic acids (R-SO3H), both of which represent irreversible modifications [35, 37]. Undesirable thiol (over)oxidation by severe oxidative stress can impair cellular processes and cell viability [38].

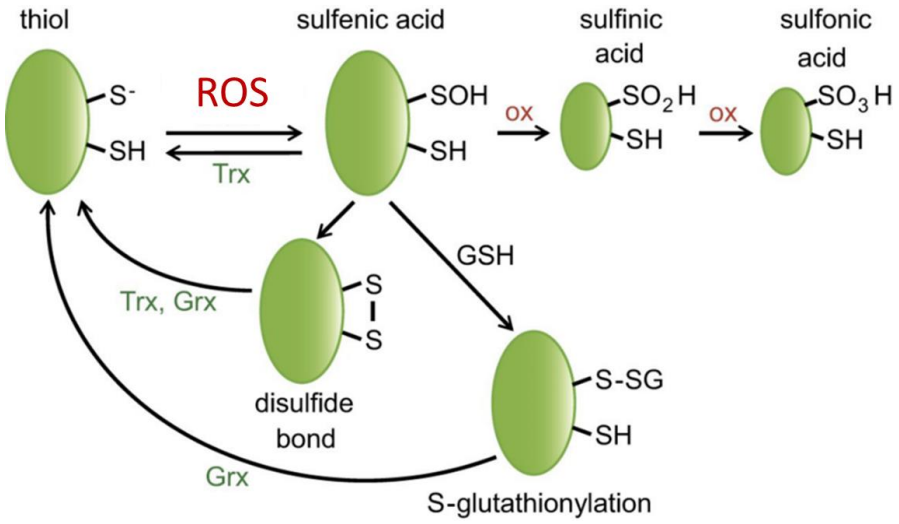

Figure 1.4 ROS-induced cysteine modifications. *The initial products of ROS-induced thiol oxidation are highly reactive sulfenic acids that can form intramolecular or intermolecular protein disulfides or react with glutathione (GSH) to become S-glutathionylated (R-SSG). These modifications are reversible. The reduction is catalyzed by glutaredoxins (Grx) or thioredoxin reductases (Trx). Under severe oxidative conditions, sulfenic acids may be further oxidized to sulfinic and sulfonic acids, both representing irreversible modifications [35].*

ROS can also oxidize lipids. A major contributor to the initiation of lipid peroxidation is the cytosolic liable iron pool. Via Fenton reaction, unbound iron ions generate highly reactive hydroxyl and peroxyl radicals that interact with lipids [33]. Most often, polyunsaturated fatty acids (PUFAs) are affected. This reaction leads to formation of carbon-centered lipid radicals (L·) that propagate lipid peroxidation via a *chain reaction* (Fig.1.5). During propagation, L· molecules instantly react with oxygen to lipid peroxide radicals (LOO·). These radicals react with hydrogen from other lipid molecules to form lipid hydroperoxides (LOOH) thereby generating new L· molecules [39]. This propagation process continues until its termination by reaction of LOO· with antioxidant molecules. The originated primary peroxidation product LOOH can be repaired by glutathione peroxidase 4 (GPx4). Provided with a cationic surface near the catalytic center to interact with polar heads of phospholipids, GPx4 is the unique enzyme capable of reducing the hydroperoxide group (R-OOH) of membrane-forming phospholipids [40]. Alternatively, LOOH can be converted into toxic and mutagenic secondary peroxidation products, such as 4-hydroxynonenal (4HNE) and malondialdehyde (MDA), both of which covalently react with nucleic acids, phospholipids or proteins, resulting in further irreversible modifications [41].

Conclusively, excessive oxidation of lipids can cause severe cellular damage and induce cell death, particularly iron-dependent ferroptosis [42].

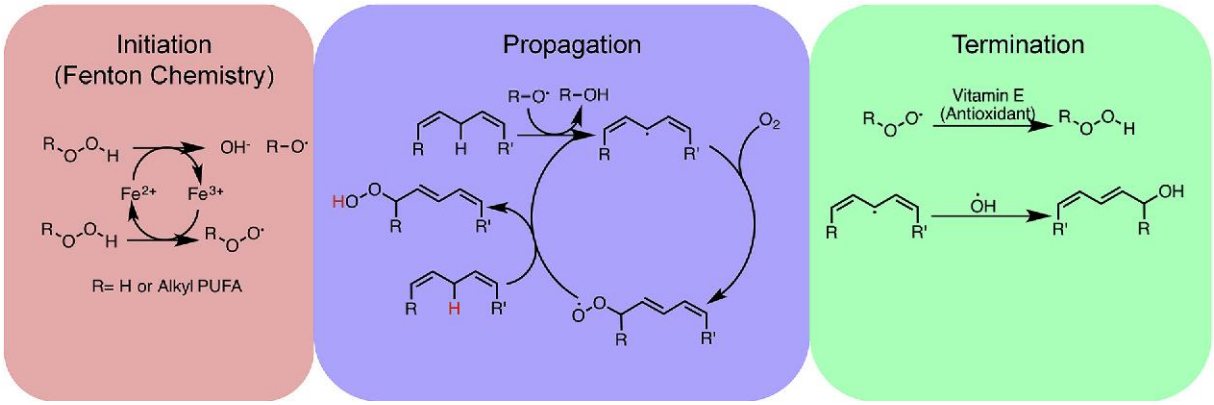

***Figure 1.5 Three steps of non-enzymatic lipid peroxidation**. In the first step lipid radicals are generated by redox active iron (initiation). In the second step, radicals abstract hydrogen from other lipids leading to formation of new radicals (propagation). Propagation continues until termination by antioxidants or reaction with another radical [42].*

Since all intracellular molecules are susceptible to oxidative stress, DNA can also be a target for ROS. The diversity of oxidative DNA lesions is large and includes a vast array of base modifications, abasic sites or deoxyribose damage and could even result in single or double strand breaks. Most of the created DNA lesions are repaired by base excision repair (BER) or nucleotide excision repair (NER) [43]. Due to this efficient, error-free repair machinery, oxidation of nuclear DNA results rarely in mutations. Less is known about repair mechanisms of mitochondrial DNA (mtDNA), but the proximity to the ROS producing ETC makes mtDNA specifically prone to oxidative modifications. Oxidative lesions are detected more often in mtDNA than in nuclear DNA [44]. Consequently, unrepaired lesion can result in mtDNA mutations which, in turn, may facilitate neoplastic transformation.

The degree of intrinsic oxidative stress depends on the dynamic balance between ROS generation and elimination. To keep ROS levels at non-toxic concentrations, cells harbor a battery of antioxidative defence mechanisms. These systems are commonly divided in two groups: non-enzymatic and enzymatic antioxidants. Small molecules, such as GSH, flavonoids, vitamins A, C and E count among non-enzymatic antioxidants, while enzymatic antioxidants include for instance superoxide-dismutase (SOD), catalase, peroxiredoxins (PRX) or glutathione peroxidases (GPx) [29, 30].

1.4.2 The antioxidative glutathione system

GSH, a tripeptide composed of glutamate, cysteine and glycine is considered the most abundant intracellular antioxidant. Its major function is the detoxification of xenobiotic compounds and electrophiles by spontaneous conjugation. Alternatively, the detoxification process can be enzymatically catalyzed by GPx proteins and glutathione-S-transferase (GST). Most of the intracellular glutathione is utilized by GPx to neutralize ROS, generated during cell metabolism [45-47]. The enzyme family of GPx proteins consists of eight sequentially numbered isoenzymes located in the cytosol and mitochondria with unique roles but similar mechanism [30]. During detoxification process, the reduced form of glutathione (GSH) becomes oxidized, thereby linking two molecules via disulfide bridge (GSSG). This reaction can be reversed by glutathione reductases in the presence of NADPH (Fig. 1.6) [46]. In cells, the ratio between the reduced and oxidized form (GSH/GSSG) is usually greater than 100 but decreases under conditions of oxidative stress [29]. The high abundancy of GSH, together with the ability to scavenge ROS and repair oxidative damage at lipids and proteins, emphasizes the high relevance of this system in the maintenance of intracellular redox homeostasis.

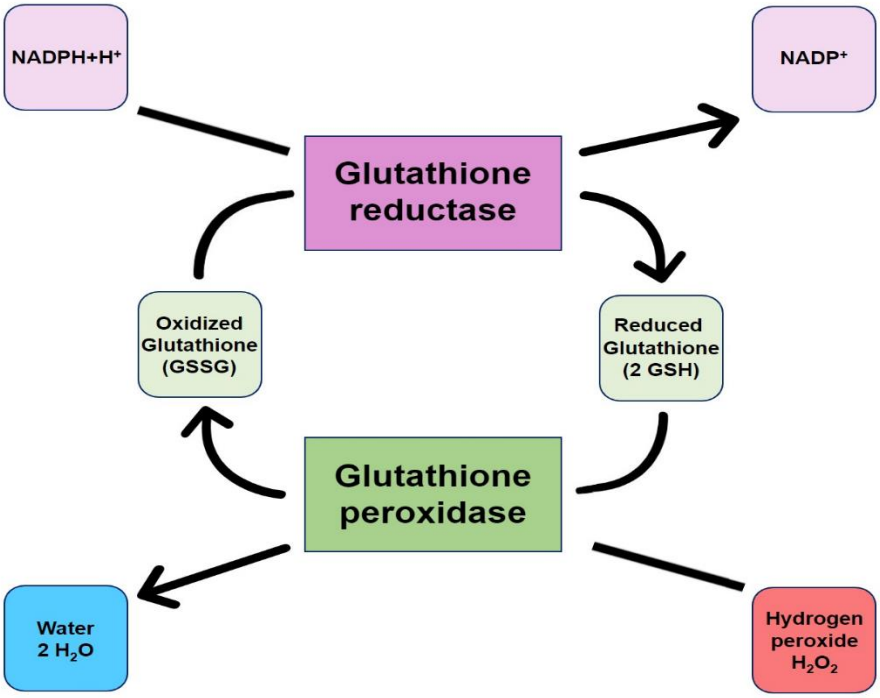

Figure 1.6 The glutathione redox cycle. *Peroxides produced endogenously by cellular metabolism or by exogenous oxidants are detoxified by members of the enzyme family of glutathione peroxidases (GPx). Thereby, two molecules glutathione form a disulfide bridge creating oxidized glutathione (GSSG). Subsequently, GSSG is reduced by glutathione reductases (GR), which use NADPH as a source of reducing equivalents.*

Glutathione biosynthesis involves a two-step and ATP-dependent enzymatic reaction that starts with the conjugation of cysteine and glutamate by γ-glutamate-cysteine ligase (GCL). This enzyme is composed of two subunits; one catalytic (GCLC) and one modifier subunit (GCLM). In the second step, glutathione synthetase catalyzes the reaction of y-glutamyl-cysteine with glycine. Together with the intracellular cysteine availability, this step is rate-limiting in glutathione biosynthesis [48]. Cysteine can be provided by one-carbon metabolism as homocysteine. However, the major source of intracellular cysteine is the uptake of extracellular cystine, the oxidized dimeric form of cysteine [49]. Cystine is imported by the sodium independent, chloride dependent cystine–glutamate antiporter in the plasma membrane, also known as system Xc or xCT (Fig. 1.7) [50].

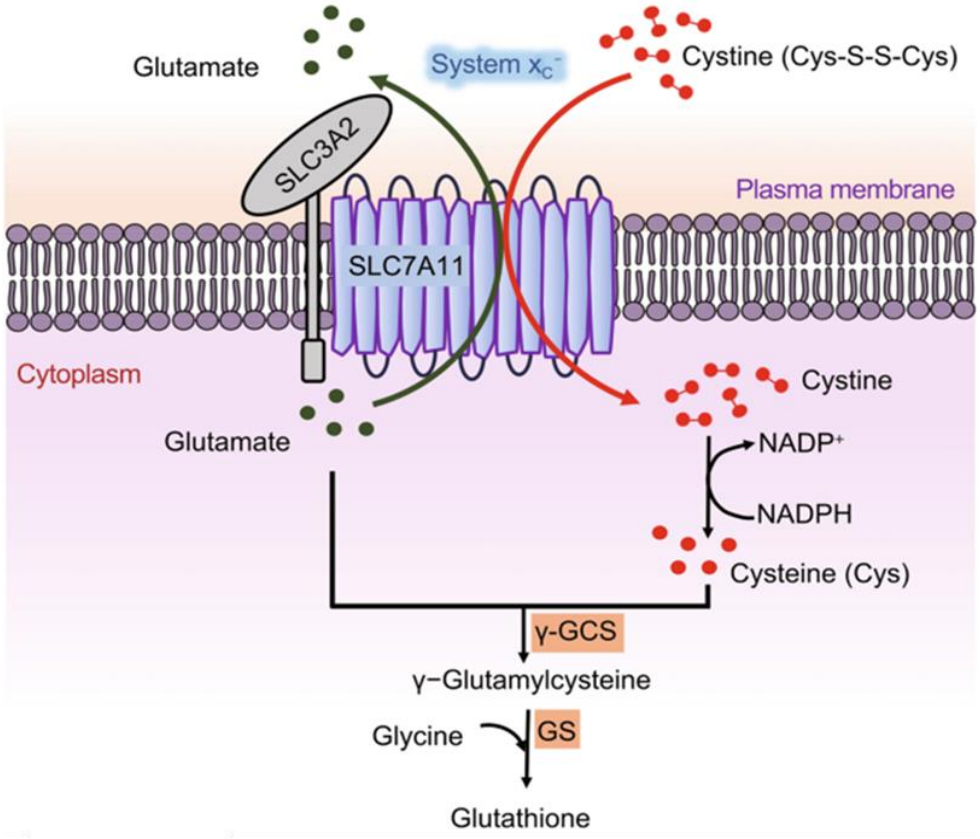

Figure 1.7 Structure and function of the cystine–glutamate antiporter xCT. *xCT is a heterodimer consisting of the light chain subunit SLC7A11 and the heavy chain subunit SLC3A2. In exchange of glutamate, cystine is imported into the cell and subsequently reduced to cysteine by NADPH. Cysteine can be used for biosynthesis of glutathione, a tripeptide composed glutamate, cysteine and glycine [51].*

xCT is located at the cell surface and consists of a light chain subunit SLC7A11 with 12 transmembrane domains and a heavy chain subunit SLC3A2, that are linked together by disulfide bridges. The light chain SLC7A11 primarily mediates the import

of extracellular cystine. In exchange for glutamate at an obligatory molar ratio of 1:1, cystine is imported into the cell, where it is converted into cysteine in a NADPH-dependent reaction [51-53]. xCT as well as several other proteins of the glutathione system are transcriptionally regulated by the antioxidative Kelch-like ECH-associated protein 1 (Keap1)/ Nuclear factor erythroid 2-related factor 2 (Nrf2) pathway [54].

1.4.3 The antioxidative Keap1/ Nrf2-pathway

In the past decades, researchers uncovered the Keap1/Nrf2 pathway as an important defense mechanism against oxidative and electrophilic stress and, thus, this pathway attracted increasing interest. Meanwhile, it is considered as leading regulator of the antioxidant response [55]. Nrf2 activates the transcription of a wide range of cytoprotective genes, including proteins of the glutathione synthesis pathway, antioxidant proteins involved in oxidative damage repair, as well as drug-metabolizing enzymes and xenobiotic transporters [55-57]. In the basal state, Keap1 interacts with Nrf2 and the Cul3-containing E3 ubiquitin ligase, resulting in ubiquitination and proteasome-dependent degradation of the complex (Fig. 1.8) [58]. Under conditions of oxidative and xenobiotic stress, Keap1 functions as a sensor protein. Thereby, critical cysteine residues in Keap1 are modified through electrophilic reaction, resulting in conformational change of this protein. Subsequently, Nrf2 dissociates from the complex and translocates into the nucleus, where it binds to antioxidant response elements to activate transcription of effector genes [59, 60]. Because of its safeguarding role against toxic and carcinogenic compounds, Nrf2 is commonly considered as a major regulator of cell survival, protecting cells from aging, (photo-)oxidative stress, diabetes, neurodegenerative and cardiovascular diseases as well as inflammation and cancer [57, 61].

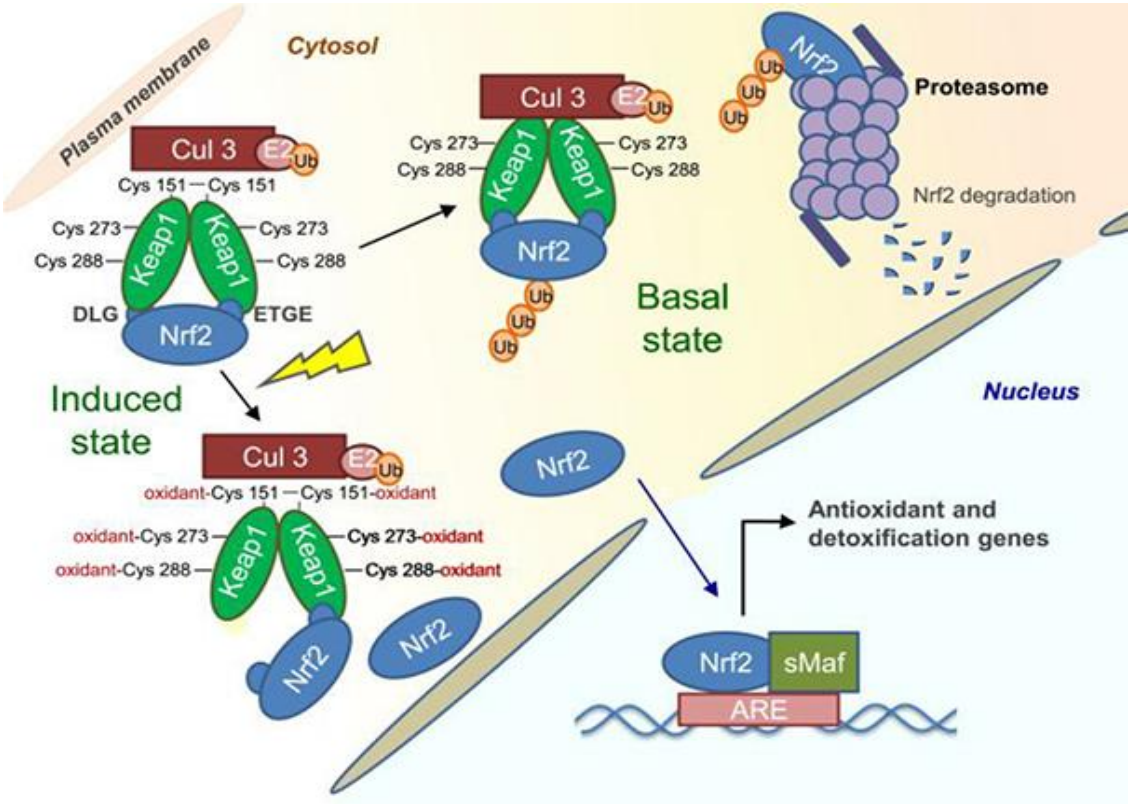

Figure 1.8 Regulation of the antioxidant Keap1/Nrf2 pathway*. In the cytosol, Keap1 usually interacts with Nrf2 and the Cul3-containing E3 ubiquitin ligase, resulting in Nrf2 ubiquitylation and proteasomal degradation. In response to oxidative stress, critically cysteine residues of Keap1 become oxidized, resulting in dissociation of Nrf2 from the complex and translocation into the nucleus. Nrf2 activates transcription of genes involved in antioxidant response and detoxification [62].*

1.4.4 ROS and the antioxidative defense promote a tumorigenic phenotype in cancer cells

Previous publications have demonstrated that malignant cells are in general under increased oxidative stress compared to their heathy counterparts. This feature can be ascribed to oncogenic transformation as well as metabolic- and microenvironment-associated adaption processes [63-66]. Several oncogenes such as *K-RAS* and *c-MYC* drive intracellular ROS production [67-69]. In addition, tumor cells have a higher mtDNA mutation frequency [70], which is accompanied by an increased metabolic activity to support anabolic processes involved in proliferation and growth [71]. Thus, mitochondria produce large amounts of ROS, which accelerates the accumulation of oxidative injuries and genetic instability [66]. Moreover, tumor hypoxia can additionally facilitate cellular ROS production. [72].

ROS play a dual role in tumor cells. On one hand, excessive ROS production further enhances genetic instability and activates molecular pathways that promote tumor growth and malignant progression. On other hand, increased oxidative stress can

induce cell death when the damage exceeds the antioxidative and repair capacity of the cell (Fig. 1.9) [73-75]. In order to keep ROS levels below the cytotoxic threshold and prevent cell death, tumor cells constantly activate antioxidative defense mechanisms [64, 66, 76]. Highlightening the *dark side of antioxidants,* several researchers recently suggested not to consider antioxidants as tumor suppressors any longer [76, 77]. Blocking protective pathways that allow tumor survival and boosting ROS production at the same time, might increase tumor cell death in response to therapy and proof beneficial to cancer patients.

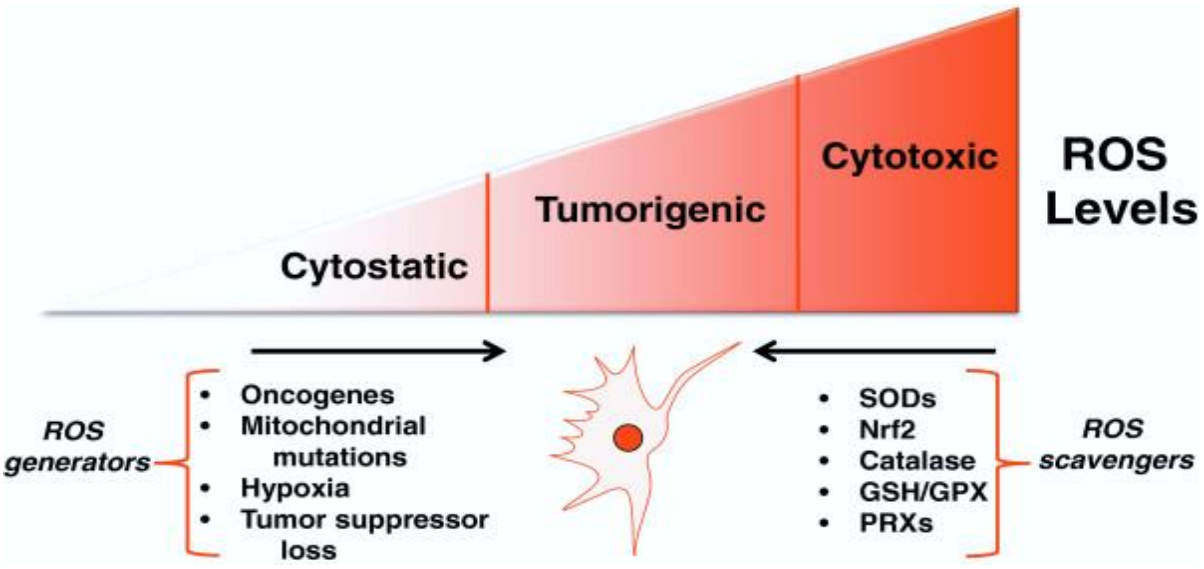

Figure 1.9 Balance between ROS generation and ROS elimination promotes tumorigenesis. *Oncogenes, mitochondrial mutations, hypoxia and the loss of tumor suppressors increase ROS production and contribute to malignancy. Higher expression of antioxidant proteins in tumor cells prevent increased ROS generation and cell death induction in response to oxidative damage [78].*

1.5. Anti-malaria drugs as novel tool in cancer treatment

1.5.1 Artemisinin and its derivatives in malaria therapy

The anti-malaria drug artemisinin is a sesquiterpene trioxane lactone that was first isolated from the sweet wormwood (*Artemisia annua L*). In traditional Chinese medicine, this herb has been used for thousands of years to treat chills and fever [79]. Artemisinin is reduced into the active metabolite dihydroartemisinin (DHA), representing the starting compound for the development of first-generation derivatives including artemether and artesunate (Fig. 1.10 a). Collectively, artemisinins represent a new class of antimalarial therapeutics which are effective even against chloroquine-resistant *Plasmodium falciparum*, the pathogen causing malaria. These drugs are toxic

to the parasites at nanomolar concentrations, while acting more efficiently and less toxic than chloroquine [80, 81]. Nowadays, artemisinin and its derivatives represent the first-line medication in malaria treatment. They are usually administered orally or parenterally to treat both, *Plasmodium falciparum*-induced uncomplicated and *Plasmodium vivax*-induced complicated malaria. In order to reduce the likelihood of developing drug resistance, artemisinin combination therapies (ACT) have been recommended by the World Health Organization (WHO). ACT combines artemisinin-based compounds with drugs from a different class, such as chloroquine [81]. During the course of clinical application, a low toxicity and a high tolerability was recorded in millions of patients. Administration of artemisinins at high doses caused neurotoxicity in animal models and *in vitro* studies using neuronal cells [82-84]. In humans however, ACT-linked conspicuous changes in the neurological system could not be detected so far [85].

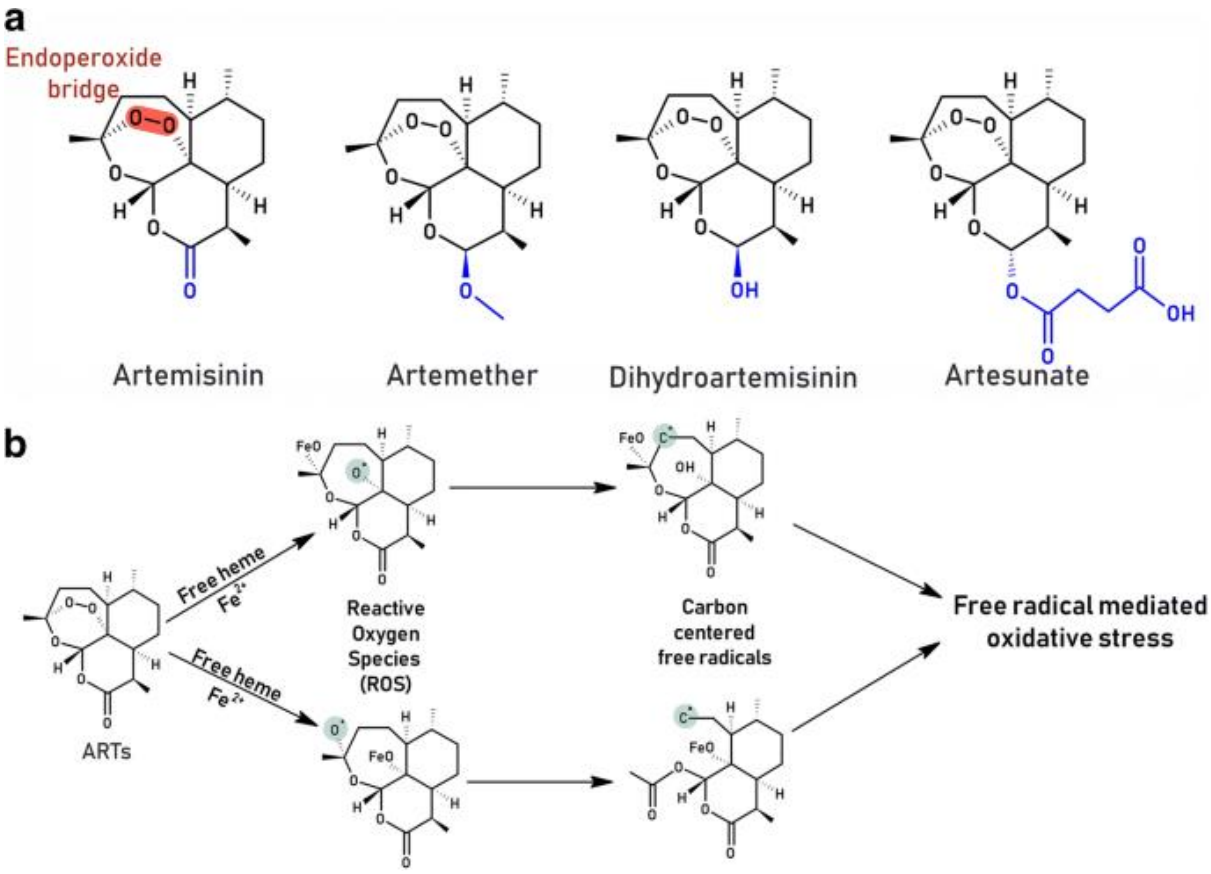

Figure 1.10 Chemical structure and proposed mechanism of activation of artemisinin and its derivatives. *(a) The endoperoxide bond is highlighted in red. Structural differences between derivatives are highlighted in blue. (b) In the proposed mode of action, artemisinins undergo reductive activation in the presence of free heme/Fe^{2+} ions at either O1 or O2 positions. Activation results in ROS production and rearrangement into carbon-centered free radicals [86].*

Although the effectivity of artemisinin and the related derivatives is well-established and well-examined in malaria patients, the precise mode of action of these drugs is still discussed. It is generally accepted that the highly reactive endoperoxide ring within these compounds is required for the anti-malaria response [81, 87, 88]. Likely, the peroxide bond (O-O) is cleaved in the acidic food vacuole of the parasite through interaction with heme [Fe(II)] during digestion of hemoglobin (Fig. 1.10 b) [89]. This iron-dependent reductive activation results in generation of reactive carbocations and ROS that may interact with biomolecules of the parasite. The produced radicals damage cellular membranes and oxidize proteins, resulting in alkylation and inhibition of nucleic acid synthesis [81, 90]. To-date, the precise chemical interaction between the essential endoperoxides of artemisinins and the parasite targets remain obscure. It is unclear, whether there is a single important target or multiple targets in *Plasmodium* [91]. Beyond that, research of the past decades investigating artemisinin and the related derivatives suggest a much broader field of possible applications, including the treatment of several parasitic and viral infectious diseases as well as inflammation and cancer [92].

1.5.2 Dihydroartemisinin (DHA) in cancer treatment

DHA, the active metabolite of artemisinin, contains a hydroxyl group that greatly improves its pharmacodynamic properties. Compared to artemisinin, this derivative displays an improved water solubility, an enhanced absorption and a wider distribution profile in patients, resulting in a 10-fold higher bioavailability. Moreover, DHA shows a 4 – 8 times stronger antimalaria activity with an improved tolerability in malaria patients [93, 94]. Due to its low toxicity and known safety, DHA has received increasing attention in cancer treatment. The anti-neoplastic activity of DHA was demonstrated in many different tumor entities including brain, lung, breast, prostate, colorectal and ovarian cancers [94]. The observed anti-neoplastic effects can be attributed to many different molecular mechanisms, including induction of cell cycle arrest, apoptosis and ferroptosis, inhibition of angiogenesis and metastasis, induction of autophagy and ER stress [95-98]. The observed anti-cancer activity of DHA and artemisinin requires ROS production and oxidative stress with subsequent oxidative damage to macromolecules and organelles. The severity and localization of DHA-induced oxidative damage is highly heterogenous, hindering the elucidation of the exact mechanism. Most likely, DHA-induced cytotoxicity is based on multiple mechanisms that are dose- and time-dependent and influenced by the genetic background of the targeted cell. In

previous *in vitro* studies, researchers detected synergistic effects when combining DHA with clinical cancer therapies, including chemotherapeutic drugs (e.g., paclitaxel, gemcitabine, doxorubicin) and drugs targeting specific proteins (gefitinib, ABT-263), but also radiotherapy [93]. However, clinical anti-cancer trials are scarce so far. One study could demonstrate that DHA administered in non-toxic concentrations improved the clinical symptoms in patients with advanced cervical cancer [99]. Using artesunate to treat patients with metastatic breast cancer, a phase I study detected a good safety profile [100]. In patients with colorectal cancer, a high tolerability and anti-proliferative properties of artesunate resulting in decreased tumor recurrence were observed [101]. However, the current pharmacokinetic properties restrict the application of higher doses and thus, a more efficient anti-cancer treatment. Artemisinins have a poor water solubility, short plasma half-life and low bioavailability upon oral administration that limit the clinical application in cancer therapies. In order to address this issue, new compound formulations with structural modifications or drug carrier and delivery systems are currently under investigation [94]. In addition, it remains to clarify whether combination therapies with DHA could reduce the toxic side effects of standard therapies in cancer patients. To accelerate the clinical application of DHA as a sensitizing drug in cancer therapy, the molecular mechanism of this drug must be completely elucidated, drug delivery systems improved and possible combination therapies tested.

1.6 Cell death mechanisms in response to artemisinin and its derivatives

1.6.1 Apoptosis

Apoptosis is a tightly regulated cell death program with characteristic morphological and molecular features. It is an important process in embryonic development and contributes to tissue homeostasis throughout life [102]. Morphologically apoptosis is characterized by cell shrinkage, nuclear DNA condensation and fragmentation as well as membrane blebbing [103, 104]. Biochemically, apoptosis can be distinguished from other cell death programs by activation of caspases, a family of cysteine proteases that cleave peptide bounds c-terminal of an aspartate residue. The caspase family consists of enzymes related to apoptosis as well as enzymes involved in cytokine maturation. The former are generally divided in two classes: initiator caspases, which include for instance caspase-8, -9 and -10, and effector caspases including caspase-3, -6 and -7.

Synthesized as catalytically inactive zymogens, initiator caspases become activated after recruitment to multimeric protein complexes formed in response to apoptotic signal due to proximity, while effector caspases are cleaved by initiator caspases. Activation of an effector caspase results in proteolytic cleavage of cellular biomolecules, ultimately resulting in apoptotic cell morphology [105, 106].

Apoptosis can be initiated either through the extrinsic death-receptor pathway or the intrinsic mitochondrial pathway, depending on the origin of the stimuli (Fig. 1.11). The extrinsic pathway is activated by binding of extracellular death ligands of the tumor necrosis factor (TNF) family to death receptors at the plasma membrane. The clustered ligand/receptor complex forms together with adaptor proteins such as Fas-associated protein with death domain (FADD) the death-inducing signaling complex (DISC) to recruit and activate the pathway-specific initiator caspase-8, which, in turn, activates effector caspases [18]. The mitochondrial apoptosis pathway is initiated in response to intrinsic stresses such as DNA damage, oncogenes, free radicals, hypoxia or survival factor deprivation. Such death stimuli induce pro-apoptotic signaling by mitochondrial outer membrane permeabilization (MOMP), allowing cytochrome c release from the mitochondrial intermembrane space into the cytosol. Together with the apoptotic protease activating factor 1 (APAF1) and the inactive initiator caspase-9, cytochrome c forms a complex known as the apoptosome. Complex formation results in recruitment and activation of the initiator caspase-9 followed by the activation of effector caspases [103].

The mitochondrial apoptosis pathway is tightly controlled by the B-cell lymphoma 2 (Bcl-2) family of proteins, which regulate mitochondrial permeability. Depending on its function and homology, the Bcl-2 family members can be divided into pro-apoptotic and anti-apoptotic proteins. The latter consists of Bcl-2, Bcl-xL, Bcl-w and Mcl-1 among others, containing at least three of the four homologues domains (BH1-4), while the former can be further subdivided into pore-forming proteins (Bax, Bak, Bok) consisting of BH1-3 and the BH3-only proteins (BID, Bad, Bim, Noxa and Puma), which possess only one homologues domain [103]. BH3-only proteins interact directly with Bax or Bak, thus activating these pro-apoptotic proteins. Alternatively, BH3-only proteins interact with anti-apoptotic Bcl-2 family members, thereby neutralizing their function and releasing pro-apoptotic Bax and Bak from the inhibitory complex with the anti-apoptotic proteins. Upon activation, pro-apoptotic proteins Bax and Bak form pores in the

mitochondrial outer membrane through which cytochrome c is released into the cytosol, where it facilitates caspase activation [107].

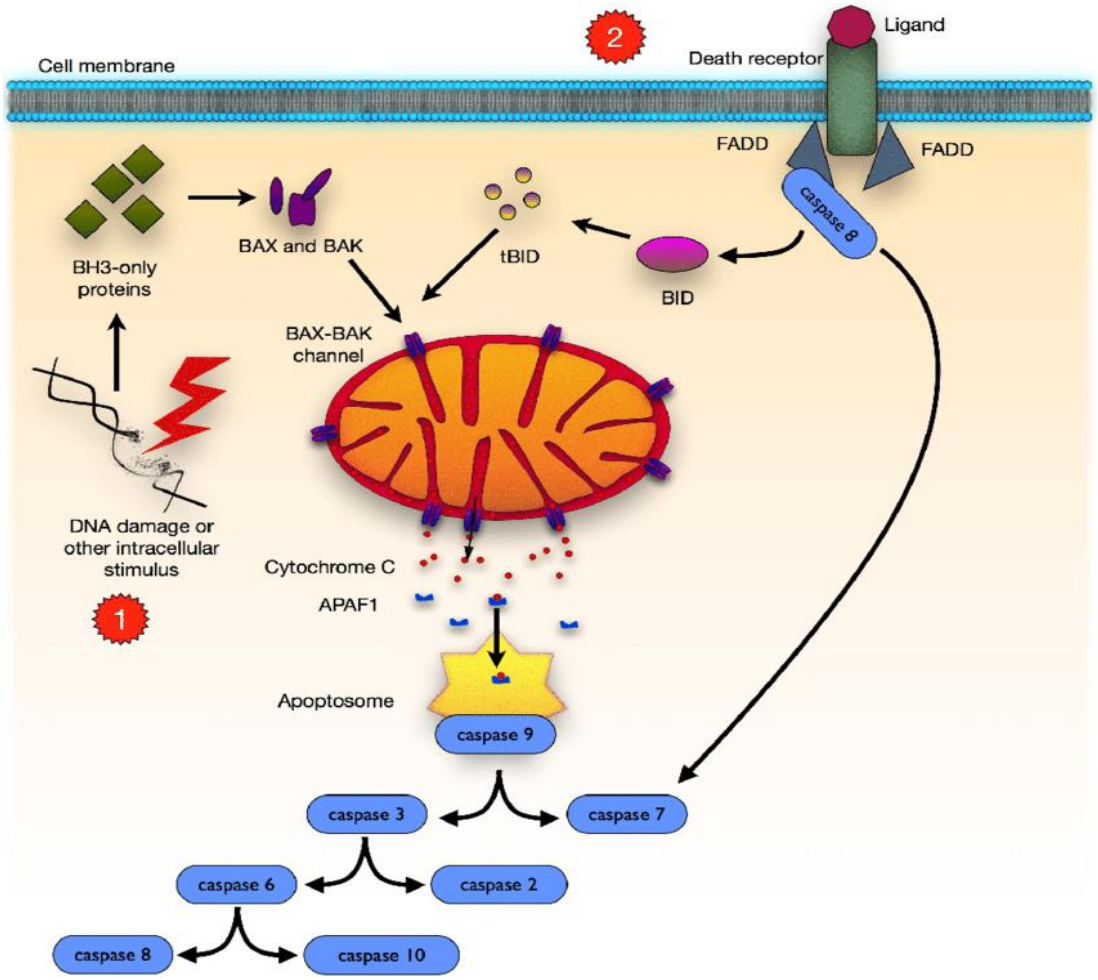

Figure 1.11 The extrinsic and intrinsic apoptosis pathway. *1) Intracellular death stimuli activate BH3-only proteins that facilitate pore formation of Bax and Bak in the mitochondrial outer membrane enabeling mitochondrial outer membrane permeabilization (MOMP) and cytochrome C release. into the cytosol, where, together with APAF1 and dATP, it forms the heptameric complex called apoptosome. Initiator caspase-9 is recruited and activated at the apoptosome and subsequently activates effector caspases in a cascade. 2) Binding of extracellular death ligands of the tumor necrosis factor family to death receptors activates the extrinsic pathway. The adaptor protein FADD translocates to the membrane, where it forms the death-inducing signaling complex (DISC) together with the activated and oligomerized death receptors. Upon recruitment to DICS, initiator caspase-8 is activated, resulting in sequential activation of effector caspases. In addition, caspase-8 is able to cleave pro-apoptotic BH3-only protein BID. The generated truncated BID (tBID) is able to bind to and activate pro-apoptotic Bax and Bak, thus linking extrinsic and intrinsic apoptosis pathway [108].*

Impaired apoptosis induction is considered as one of the major hallmarks of human cancers [109] and strongly contributes to therapy resistance [104, 110]. Cancer cells have evolved several strategies to escape from apoptosis. Overexpression of

anti-apoptotic proteins or decreased expression or dysfunction of pro-apoptotic proteins is often observed in human tumors [110]. Moreover, increased expression of inhibitors of apoptosis, for example X-linked inhibitor of apoptosis (XIAP), interferes with caspase activation by direct binding to activated caspases [111]. Presently, different compounds targeting extrinsic and intrinsic apoptosis pathway are under investigation with promising potential, but only few drugs were tested in clinical trials and approved for the treatment of cancer so far [112].

1.6.2 Autophagy

Autophagy is a highly conserved cellular mechanism to remove damaged or dispensable biomolecules or organelles by “self”-digestion. Autophagic processes distinguish between macroautophagy, microautophagy and chaperone-mediated autophagy. Of these three forms, macroautophagy is the best examined process [113]. Basically, autophagy is a protective process in response to microenvironmental stress such as starvation, hypoxia, heat stress or oxidative stress, allowing the cell to recycle cytoplasmic material and survive while adapting to environmental changes [18]. Autophagy is dysregulated in several human diseases including cancer [114].

Approximately 30 autophagy-related proteins have been characterized in yeast, and many mammalian homologs have been identified [113]. Generally, autophagy is induced by mammalian target of rapamycin complex 1 (mTORC1)-dependent or -independent pathways and starts with the formation of lipid-based membranes, so called phagophores (Fig. 1.12). In this process, autophagy reporter proteins such as the microtubule-associated protein 1A/1B-light chain 3 (LC3) are recruited to the forming phagophore. To this end, the cytosolic LC3I is lipidated to generate a LC3-phosphatidylethanolamine conjugate (LC3II). LC3II facilitates formation of autophagosomal membranes by engulfment of substrates targeted for degradation [115]. Once the mature autophagosome fuses with the lysosome, the substrates are degraded by hydrolases. After decomposition of substrates, the generated products can be recycled into cell metabolism [116, 117]. LC3II formation has been widely accepted as marker of autophagy induction [115].

Despite its protective qualities, emerging evidence indicates that autophagy is a crucial cell death process, in which the cell digests its contents until death (autophagy-associated cell death). However, it is still unclear which mechanisms promote autophagy’s protective and which promote its damaging role [118].

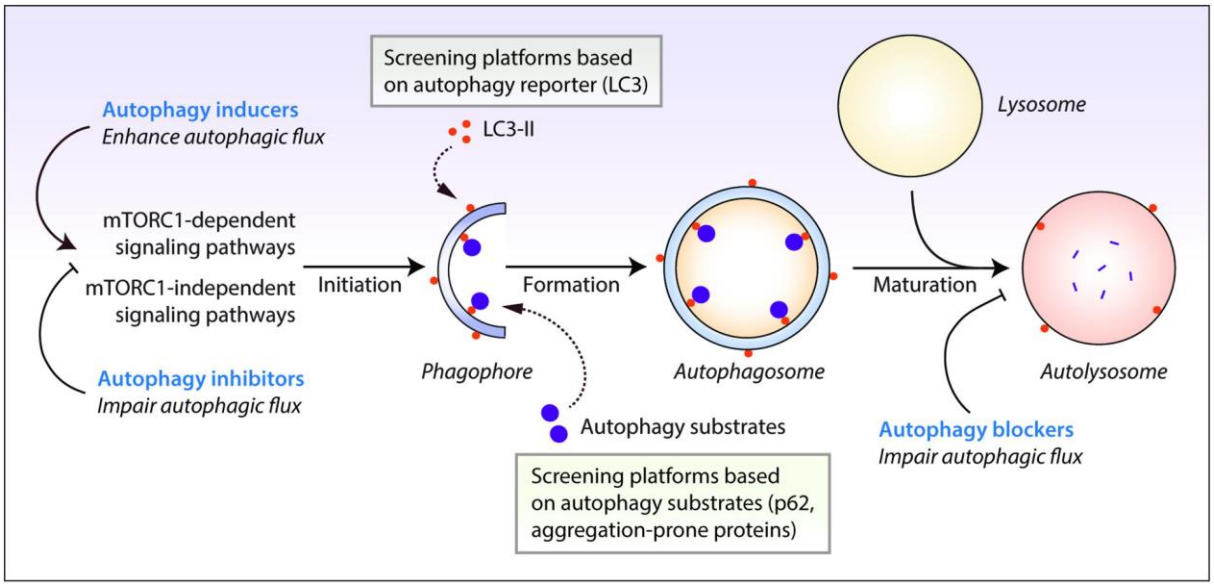

Figure 1.12 Autolysosome formation in autophagy. *mTORC1-dependent and -independent pathways initiate phagophore formation. LC3II is recruited to the phagophore and facilitates the engulfment of autophagy substrates during autophagosome biogenesis. The autophagosome fuses with a lysosome. The acidic environment in autolysosome allows the decomposition of autophagy substrates [119].*

1.6.3 Ferroptosis

Ferroptosis, a recently identified form of regulated cell death (RCD), is morphologically and mechanistically distinct from other RCDs such as apoptosis or autophagy-associated cell death. In particular, ferroptosis is characterized by an iron-dependent lipid peroxidation in response to accumulation of intracellular ROS. Under moderate ROS-stress, GPx4 counteracts oxidation of lipids using glutathione as a substrate in this detoxifying process [120-124]. Hence, decreased GPx4 activity or lowered glutathione levels in cells may result in ferroptosis [125]. The first compound discovered as an inducer of ferroptosis was the small molecule erastin. This compound triggers cell death by inhibition of the cystine-glutamate antiporter, leading to intracellular cysteine depletion and subsequently, decrease of glutathione levels. Lowered intracellular glutathione concentrations mitigate the antioxidant defence and thus, facilitate lipid peroxidation [120]. Meanwhile, numerous ferroptosis-inducing compounds have been identified, acting by diverse mechanisms (Fig. 1.13). Among these compounds are the GPx4 inhibitor RSL3, buthionine sulfoximine (BSO) which blocks GCL or agents which increase the intracellular iron abundance [122]. Inhibitors of ferroptosis include iron chelators such as deferoxamine (DFO) and lipophilic, radical trapping antioxidants such as vitamin E or ferrostatin [126].

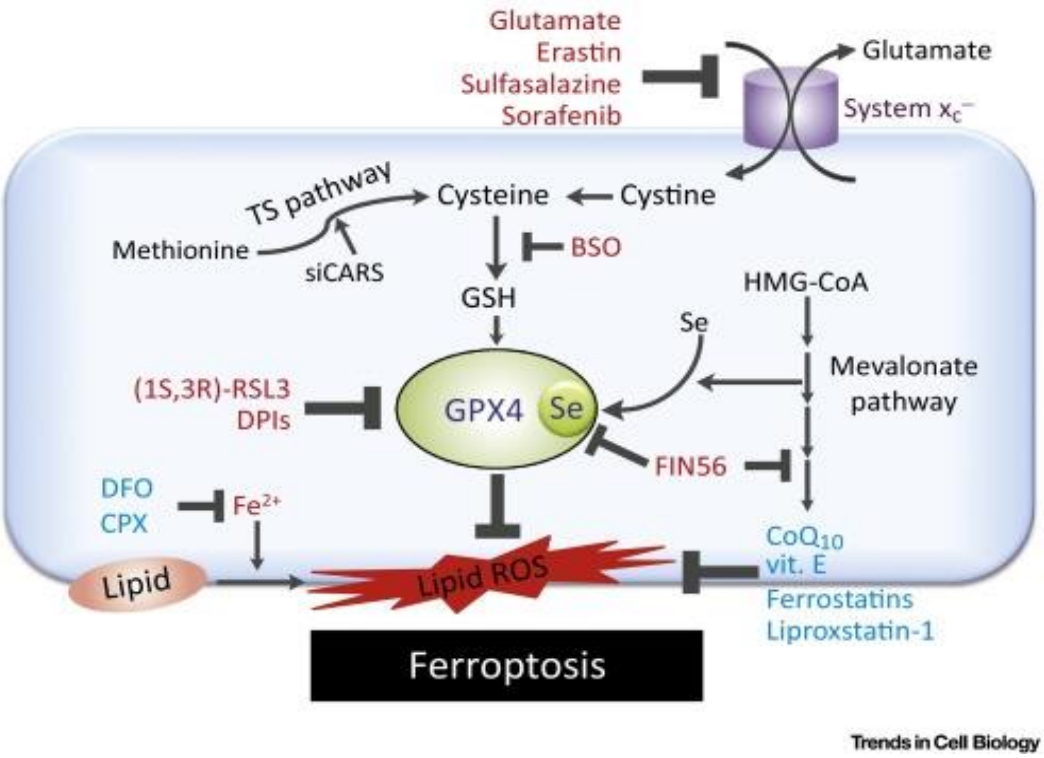

Figure 1.13 Inducers and inhibitors of ferroptosis. *Lipid peroxidation triggers ferroptosis and can be induced by interfering in the glutathione biosynthesis pathway, inhibition of GPx4, or an increase in intracellular, redox-active iron. Inhibitors of ferroptosis include iron-chelating agents or lipophilic, radical trapping antioxidants that prevent lipid peroxidation [126].*

Morphologically, ferroptosis is characterized by a loss of plasma membrane integrity accompanied by oncosis. The nuclei remain unaffected without chromatin condensation. Shrinking mitochondria with condensed membrane densities, reduced cristae and outer membrane rupture are other morphological changes during ferroptosis [121, 127, 128]. Despite the distinct alterations in mitochondrial morphology, their role of this organelle in ferroptosis is still under debate. The initial publication demonstrated that mitochondria are dispensable for ferroptosis induction [120]. In contrast, recent studies suggest that mitochondrial metabolism, including the mitochondrial tricarboxylic acid (TCA) cycle, the ETC, lipid metabolism and amino acid metabolism can regulate ferroptotic cell death [121, 125, 129]. Moreover, changes in iron homeostasis with altered generation of ROS production and lipid peroxidation have previously been linked to ferroptosis. As a key organelle regulating iron sulphur cluster assembly and insertion of heme groups into proteins, the involvement of mitochondria in the regulation of ferroptosis is evident [129].

1.7 Aims

A crucial factor contributing to radioresistance is hypoxia, a characteristic feature of most solid tumors [13, 26, 27]. A hypoxic environment limits ROS formation in cells after exposure to ionizing radiation [14, 28]. An improved antioxidative defense of tumor cells is another factor limiting efficacy of radiotherapy by interfering with ROS production and improving the removal of oxidative damage [12, 130, 131]. On the contrary, cellular antioxidative capacities are limited in tumor cells, constituting a specific vulnerability of transformed cells compared to normal cells [64, 66]. In the present study, we intended to boost ROS production using the prooxidative anti-malaria drug DHA.

The first aim of this study was the analysis of DHA-induced cellular damage and DHA-induced cell death in normoxia. Since oxidative stress may also result in the activation of protective mechanism, we intended to examine the activation of the pro-survival pathway by the transcription factor Nrf2. The lung adenocarcinoma cell line NCI-H460 and the colorectal cancer cell line HCT116 were chosen as experimental models because of their different response to DHA.

The second objective addressed the question whether additional treatment with the ROS-promoting drug DHA could improve the efficacy of radiotherapy by boosting ROS production. Since the prooxidative compound could activate protective pathways, it was possible that an additional treatment with DHA would even limit IR-induced cytotoxicity. While analyzing the feasibility of a combined therapy with DHA and IR, we also examined different treatment schedules to determine the most effective treatment strategy. In addition, the most effective application strategy was applied in a hypoxic environment to test whether DHA could overcome hypoxia-induced radioresistance.

The third aim of the present study intended to shed more light on the mechanism of DHA-induced cytotoxicity. Previous work in our laboratory suggested that apoptosis played a prominent role in DHA-induced cytotoxicity in colorectal cancer cells treated in hypoxia [132]. Thus, HCT116 colorectal cancer cells, that were either proficient or deficient in apoptosis induction through the intrinsic pathway, were chosen as experimental model. The dependency of the intrinsic apoptosis pathway in response to DHA-induced cytotoxicity was investigated in short- and long-term assays in normoxic as well as hypoxic conditions.

2 Material and Methods

2.1 Materials

2.1.1 General chemicals

Table 2.1 Utilized chemicals

Chemical	Manufacturer
Acetic acid	Sigma-Aldrich, St. Louis, MO, USA
Acrylamide (30%)	Roth, Karlsruhe, Germany
Ammonium persulfate (APS, 10%)	Roth, Karlsruhe, Germany
Aprotinin	Roth, Karlsruhe, Germany
α-tocopherol	Sigma-Aldrich, St. Louis, MO, USA
BODIPY 581/591 C11	Thermo Fisher Scientific, Waltham, MA, USA
Bovine Serum albumin (BSA)	New England Biolabs, Frankfurt am Main, Germany
Bromphenol blue	Roth, Karlsruhe, Germany
β-Mercaptoethanol	Roth, Karlsruhe, Germany
CHAPS	Sigma-Aldrich, St. Louis, MO, USA
Citric acid	Merck KGaA, Darmstadt, Germany
Coomassie Brilliant Blue	Sigma-Aldrich, St. Louis, MO, USA
Crystal violet	Roth, Karlsruhe, Germany
Deferoxamine	Sigma-Aldrich, St. Louis, MO, USA
D-glucose	Sigma-Aldrich, St. Louis, MO, USA
Dihydroethidium (DHE)	Sigma-Aldrich, St. Louis, MO, USA
Dimethyl sulfoxide (DMSO)	Sigma-Aldrich, St. Louis, MO, USA
ECL Western Blotting Detection Reagents Prime (Amersham)	Sigma-Aldrich, St. Louis, MO, USA
ECL Western Blotting Detection Reagents Select (Amersham)	Sigma-Aldrich, St. Louis, MO, USA
EDTA (Ethylendiaminetetraacetic acid)	Sigma-Aldrich, St. Louis, MO, USA

Ethanol (100%)	UME Apotheke, Essen, Germany
FACS Clean	Dickinson, Franklin Lakes, NJ, USA
FACS Flow	Dickinson, Franklin Lakes, NJ, USA
FACS Rinse	Dickinson, Franklin Lakes, NJ, USA
Fetal calve serum (FCS)	Biochrom AG, Berlin, Germany
Formaldehyde	Roth, Karlsruhe, Germany
Glutaraldehyde	Roth, Karlsruhe, Germany
Glycerol	Roth, Karlsruhe, Germany
Glycine	Merck KGaA, Darmstadt, Germany
HEPES	Thermo Fisher Scientific, Waltham, MA, USA
Hoechst 33342	Thermo Fisher Scientific, Waltham, MA, USA
Isopropanol	Sigma-Aldrich, St. Louis, MO, USA
Leupeptin	Roth Karlsruhe, Germany
L-glutamine	Sigma-Aldrich, St. Louis, MO, USA
Methanol	Roth, Karlsruhe, Germany
MitoSox™ Red	Thermo Fisher Scientific, Waltham, MA, USA
ML385	Selleckchem, München, Germany
Page Ruler, pre-stained protein ladder	Thermo Fisher Scientific, Waltham, MA, USA
Paraformaldehyde (PFA)	Biochrom AG, Berlin, Germany
Pepstatin	Roth, Karlsruhe, Germany
Phenylmethanesulfonyl fluoride	Sigma-Aldrich, St. Louis, MO, USA
Phosphate buffered saline (PBS)	Gibco Life Technologies, Thermo Fisher Scientific, Waltham, MA, USA
Propidium iodide (PI)	Sigma-Aldrich, St. Louis, MO, USA
Sodium citrate	Merck KGaA, Darmstadt, Germany

Sodium chloride (NaCl)	Roth, Karlsruhe, Germany
Sodium dodecyle sulfate (SDS)	Roth, Karlsruhe, Germany
Sodium fluoride (NaF)	Sigma-Aldrich, St. Louis, MO, USA
Sodium orthovanadate (Na_3VO_4)	Sigma-Aldrich, St. Louis, MO, USA
Sodium pyruvate	Sigma-Aldrich, St. Louis, MO, USA
Tetramethylethylenediamin (TEMED)	Roth, Karlsruhe, Germany
Tris (Tris-hydroxymethylaminomethane)	Roth, Karlsruhe, Germany
Triton X100	Sigma-Aldrich, St. Louis, MO, USA
Trypan blue	Sigma-Aldrich, St. Louis, MO, USA
Trypsin-EDTA (0.05%)	Biochrom AG, Berlin, Germany
Tween20	Sigma-Aldrich, St. Louis, MO, USA

2.1.2 Kits

Table 2.2 Utilized commercial kits

Chemical	**Manufacturer**
DC Protein Assay	BIO-RAD, Hercules, CA, USA
EdU Assay	Life technologies, Carlsbad, Ca, USA
Glutathione assay kit	Sigma-Aldrich, St. Louis, MO, USA
qPCR MasterMix for SYBR Green	Thermo Fisher Scientific Waltham, MA, USA
QuantiTect Reverse Transcription Kit	Eurogentec, Seraing, Belgium
RNeasy Mini Kit	Qiagen, Venlo, Netherlands
Seahorse XF Mito Stress Test Kit	Agilent Technologies, Santa Clara, CA, USA

2.1.3 Antibodies

Table 2.3 Antibodies applied for immunofluorescence staining (IF), Western blot (WB) analysis and flow cytometry (FC)

Antibody	Origin	Dilution	Manufacturer
Anti-mouse (HRP-conjugated)	goat	1:2000 (WB)	Cell Signaling Technologies Danvers, MA, USA
Anti-rabbit (HRP-conjugated)	goat	1:2000 (WB)	Cell Signaling Technologies Danvers, MA, USA
Anti-sulfenic acid	rabbit	1:500 (IF) 1.1000 (WB)	Merck KGaA, Darmstadt, Germany
Bak	rabbit	1:1000 (WB)	Cell Signaling Technologies Danvers, MA, USA
Bax (D2E11)	rabbit	1:1000 (WB)	Cell Signaling Technologies Danvers, MA, USA
β-actin	mouse	1:20000 (WB)	Sigma-Aldrich St. Louis, MO, USA
Cleaved caspase-3 (Asp175)	rabbit	1:1000 (WB)	Cell Signaling Technologies Danvers, MA, USA
Keap1	rabbit	1:1000 (WB)	Cell Signaling Technologies Danvers, MA, USA
LC3B	rabbit	1:200 (FC)	MBL International Corporation, Woburn, MA, USA
Nrf2	rabbit	1:1000 (WB)	Cell Signaling Technologies, Danvers, MA, USA
Nrf2	rabbit	1:500 (IF)	Abcam, Cambridge, United Kingdom
PARP (46D11)	rabbit	1:2000 (WB)	Cell Signaling Technologies Danvers, MA, USA
pH2A.X	rabbit	1:1000 (WB)	Cell Signaling Technologies Danvers, MA, USA
SLC7A11	rabbit	1:1000 (WB)	Cell Signaling Technologies Danvers, MA, USA

2.1.4 Media and commercial buffers

Table 2.4 Utilized media and commercial buffers

Medium/Buffer	Manufacturer
PBS	Life technologies, Carlsbad, Ca, USA
RPMI 1640	Life technologies, Carlsbad, Ca, USA
Seahorse XF Base Medium	Agilent Technologies, Santa Clara, CA, USA
Seahorse XF Calibrant	Agilent Technologies, Santa Clara, CA, USA

2.1.5 qRT-PCR primers

All primers were produced by Eurofins.

Table 2.5 qRT-PCR primer sequences

Primer		Sequence (5'-3')
GAPDH	forward	ATG CAG TGG CAG TGA CCT TT
	reverse	GGC AAC AAA GAT CGG AAC TG
SLC7A11	forward	TGC ACC ACC AAC TGC TTA GC
	reverse	GGC ATG GAC TGT GGT CAT GAG

2.1.6 Buffers and solutions

Table 2.6 Composition of staining solutions for flow cytometric analyses

Staining solution	Components	Concentration
Lipid peroxidation	BODIPY 581/591 C11 *in RPMI*	1 µM
DHE	DHE *in PBS*	5 µM
EdU	EdU *in RPMI*	10 µM
Nicoletti	Sodium citrate Triton X-100 Propidium iodide *in PBS*	0.1% (w/v) 0.1% (v/v) 50 µg/mL
PI exclusion	Propidium iodide *in PBS*	10 µg/mL
TMRE	tetramethylrhodamine ethyl ester *in PBS*	25 nM

Table 2.7 Composition of staining solutions for cell survival assays

Solution	Components	Concentration
Coomassie brilliant blue	Coomassie brilliant blue	0.05% (w/v)
	Methanol	20% (v/v)
	Acetic acid *in A. bidest*	7.5% (v/v)
Crystal violet	Crystal violet *in PBS*	0.1% (w/v)

Table 2.8 Composition of media for Seahorse XF cellular bioenergetic assay

Assay	Components	Concentration
Mito stress test	Seahorse XF Base Medium	
	Pyruvate	1 mM
	L-glutamine	2 mM
	D-glucose	10 mM

Table 2.9 Composition of buffers and solutions for protein analysis

Buffer/Solution	Components	Amount/Concentration
Lysis buffer	HEPES (pH 7.5)	50 mM
	sodium chloride	150 mM
	Triton X-100	1% (v/v)
	EDTA	1 mM
	sodium pyrophosphate	10 mM
	sodium fluoride	10 mM
	sodium orthovanadate	2 mM
	phenylmethanesulfonyl fluoride	100 mM
	Aprotinin	5 µg/mL
	Leupeptin	5 µg/mL
	Pepstatin A	3 µg/mL
	in H_20	

4x SDS sample buffer	Glycerol Tris-HCl (pH 6.8) SDS Bromphenol blue β-mercaptoethanol *in H_2O*	40% (v/v) 240 mM 8% (w/v) 0.04% (w/v) 10% (v/v)
15% SDS PAGE resolving gel (for 1 gel)	H_2O Acrylamid (30%) Tris-HCl (1.5 M, pH 8.8) SDS (10%) APS (10%) TEMED	3.4 mL 7.5 mL 3.8 mL 0.150 mL 0.150 mL 0.006 mL
12% SDS PAGE resolving gel (for 1 gel)	H_2O Acrylamid (30%) Tris-HCl (1.5 M, pH 8.8) SDS (10%) APS (10%) TEMED	4.9 mL 6 mL 3.8 mL 0.150 mL 0.150 mL 0.006 mL
5% SDS PAGE stacking gel (for 1 gel)	H_2O Acrylamid (30%) Tris-HCl (1.5 M, pH 8.8) SDS (10%) APS (10%) TEMED	5.9 mL 5 mL 3.8 mL 0.150 mL 0.150 mL 0.006 mL
10x SDS running buffer	H_2O Acrylamid (30%) Tris-HCl (1 M, pH 6.8) SDS (10%) APS (10%) TEMED	3.4 mL 0.83 mL 0.63 mL 0.05 mL 0.05 mL 0.005 mL
10x Transfer buffer	Tris- HCl Glycine SDS *in H_2O; adjusted to pH 8.3*	250 mM 192 mM 1% (w/v)
10x TBS-T	Tris NaCl Tween-20 *Adjusted to pH 7.4*	0.5 M 1.5 M 1% (v/v)
Blocking solution	Non-fat dry milk *in 1x TBS-T*	5% (w/v)

2.1.7 Consumables

Table 2.10 Consumable material

Chemical	Manufacturer
Cell culture 6-well plates	Eppendorf AG, Hamburg, Germany
384-well qPCR plates	4titude, Wotton, United Kingdom
Cell culture 12-/96-well plates	TPP AG, Transadingen, Switzerland
Cell culture dishes (10 cm)	Sarstedt AG&Co, Nümbrecht, Germany
Cell culture flasks (T75/ T175 cm2)	Sarstedt AG&Co, Nümbrecht, Germany
Combitips advanced®	Eppendorf AG, Hamburg, Germany
Cover slides	Engelbrecht GmbH, Edermünde, Germany
Cryo tubes	Roth, Karlsruhe, Germany
Flow cytometry tubes	BD Falcon, Franklin Lakes, NJ, USA
Filter CellTrics 30 µm	Sysmex Partec GmbH, Görlitz, Germany
GasPak™ Anaerobe Pouch System	BD Diagnostics, Franklin Lakes, NJ, USA
Microscope slides Superfrost Plus	Thermo Scientific, Waltham, MA, USA
Objective slides	Engelbrecht GmbH, Edermünde, Germany
Pasteur pipettes	Brand, Wertheim, Germany
Pipette tips	Starlab, Hamburg, Germany
PVDF membrane	Roth, Karlsruhe, Germany
qPCR seal	4titude, Wotton, United Kingdom
Reaction tubes	Sarstedt AG&Co, Nümbrecht, Germany
Seahorse XF96 cell culture microplates	Agilent Technologies, Santa Clara, CA, USA
Seahorse XF96 sensor cartridges	Agilent Technologies, Santa Clara, CA, USA
Serological pipettes	Sarstedt AG&Co, Nümbrecht, Germany
Whatman paper	Roth, Karlsruhe, Germany

2.1.8 Technical equipment

Table 2.11 Applied technical equipment

Device	Manufacturer
AriaMx Real-Time PCR System	Agilent Technologies, Santa Clara, CA, USA
Blotting chamber Trans-Blot®	Bio Rad GmbH, Munich, Germany
Calibur Flow Cytometer	BD Biosciences, Franklin Lakes, USA
Cell culture incubator C200	Labotect, Rosdorf, Germany
Cell scraper	Sarstedt AG&Co, Nümbrecht
Centrifuge 5417 R	Eppendorf
Centrifuge Biofuge® pico	Heraeus Instruments
Centrifuge Megafuge™ 1.OR	Heraeus Instruments
Chemiluminescence imaging system Fusion Solo	PeQLab GmbH, Erlangen, Germany
FUSION Solo	VILBER LOURMAT Deutschland GmbH, Eberhardzell, Germany
GelCount™ colony counter	Oxford Optronix, Oxford, UK
Incubator (37° C / 60° C)	Astel Jouan, Thermo Fisher Scientific Inc., Waltham, MA, USA
Inverses light microscope DM IL	Leica Microsystems GmbH, Wetzlar, Germany
Inverses microscope DM IRB	Leica Microsystems GmbH, Wetzlar, Germany
Invivo2 400 hypoxia chamber	Ruskinn Technology , Bridgend, United Kingdom
Laminar-flow bench	BDK Luft und Reinraumtechnik GmbH, Sonnenbühl-Genkingen, Germany
Magnetic stirrer RH basic 2	IKA-Werke GmbH, Staufen, Germany
Microplate reader, Synergy H1	BioTek, Winooski, VT, USA
Mr. Frosty Freezing Container	Thermo Fisher Scientific Inc., Waltham, MA, USA
Nanodrop ND-1000 Spectrophotometer	PeQLab GmbH, Erlangen, Germany
pH electrode edge	Hanna Instruments, Woonsocket, RI, USA

Pipetboy acu 2	Integra, Zizers, Swiss
Pipette Eppendorf Research Plus	Eppendorf AG, Hamburg, Germany
Power supply PowerPac HC	Bio-Rad GmbH, München, Germany
Protein electrophoresis system	Biometra, Göttingen, Germany
Seahorse XFe 96 Analyzer	Agilent Technologies, Santa Clara, CA, USA
ThermoMixer® comfort	Eppendorf AG, Hamburg, Germany
Vortexer Reax 2000	Heidolph, Schwabach, Germany
Water bath	GFL, Burgwedel, Germany
X-Rad 320 irradiator	Precision X-Ray Inc., Brandford, CT, USA

2.1.9 Software

Table 2.12 Applied software and tools

Software	**Manufacturer**
AriaMx	Agilent Technologies, Santa Clara, CA, USA
BLAST 2.2	National Center for Biotechnology Information (NCBI)
FlowJo	FlowJo, LLC, Ashland, OR, USA
Fusion	Vilber Lourmat, Eberhardzell, Germany
GelCount™ 1.4	Oxford Optronix, Milton, United Kingdom
GraphPad Prism 7	GraphPad Software Inc., La Jolla, CA, USA
Image J	Wayne Rasband, NIH,Bethesda, MD, USA
KC4™	BioTek Instruments
Microsoft office	Microsoft Corporation, Redmont, WA, USA
Primer-BLAST	National Center for Biotechnology Information (NCBI)
Wave Desktop 2.6	Agilent Technologies, Santa Clara, CA, USA
Zen	Carl Zeiss AG, Oberkochen, Germany

2.2 Cell lines and cultivation

NCI-H460 lung adenocarcinoma cells were obtained from ATCC (Bethesda, USA). NCI-H460 MitoTimer cells expressing the oxidation sensitive fluorescent protein targeted to mitochondrial matrix were generated by stable transfection using a vector as described before [133]. HCT116 wild type (wt) cells and HCT116 $Bax^{-/-}Bak^{sh}$ cells were kindly provided from P.T. Daniel (Berlin, Germany). Protein expression of Bax and Bak was verified by Western blot analysis. The phenotype of all cell lines was checked regularly before data acquisition using light microscopy and cell identity was verified by short tandem repeat analysis. Cells were routinely tested for mycoplasma contamination.

Cells were maintained and grown in a humified incubator at 37 °C and 5% CO_2 in RPMI1640 medium supplemented with 10% (v/v) fetal calf serum (FCS). Hypoxic cells were incubated at 37 °C, 0.2% O_2 and 5% CO_2 in a humidified hypoxia work station. Cells were split at a confluence of 70 – 80% and cultured for a maximum of 20 passages. During passaging, cells were washed with PBS to remove FCS-containing medium before detachment with Trypsin-EDTA at 37 °C. Cells were seeded in fresh medium at appropriate dilutions in 75 cm^2 cell culture flasks. For seeding of specific cell numbers, cell suspension was diluted with trypan blue (5:1), a membrane impermeable dye, that stains only cells with damaged membranes, in order to distinguish alive and dead cells. Cells were counted using a Neubauer counting chamber.

For conservation, cells were centrifuged for 5 minutes at 1400 rpm and resuspended in freezing medium containing 20% FCS and 10% DMSO at 10^6 cells/ml. The cell suspension was transferred to cryo tubes and subsequently frozen at -80 °C. The next day, cryo tubes were transferred to liquid nitrogen for long time storage. For recultivation, cells were briefly thawed in a water bath at 37 °C and immediately transferred to cell culture flasks with complete medium. After 6 – 8 h, medium was replaced by the appropriate culture medium.

2.3 Irradiation and drug treatment

Irradiation and drug treatment occurred one day after plating. Prior to any treatment, medium was removed and replaced by fresh culture medium. Cells were treated with DHA at concentrations between 6.25 and 50 µM. Controls were incubated with the solvent DMSO at respective concentration. For combined treatments with DFO (50 µM), α-tocopherol (10 µM), ML385 (12.5–50 µM), erastin (10 µM), chloroquine (20 µM) or N-acetylcysteine (2 mM), cells were incubated with the respective inhibitor 1 h prior to treatment with DHA. Cells were irradiated with a X-ray machine operated at 320 kV, and 12.5 mA in presence of a 1.65-mm aluminum filter. Irradiation was carried out at a distance of 50 cm and a dose rate of ~3.7 Gy/min. Cells were irradiated with a total dose of 2 Gy at room temperature and returned to the incubator immediately after exposure to IR. For treatment in hypoxia, cells, medium and other solutions were transferred to the hypoxia chamber 2 h before treatment starts to enable equilibration. To irradiate cells in a hypoxic environment, cell culture plates were pouched in air-tight plastic bags.

2.4 Flow cytometry

In this study, flow cytometry was used to analyze lipid peroxidation, ROS production in mitochondria and in whole cell, cell death induction, apoptosis induction, cell cycle distribution, mitochondrial membrane potential (MMP) dissipation and autophagy induction. In all assays, cell culture medium and supernatants from washing steps were collected to include also detached cells in analysis. Cells were harvested by Trypsin-EDTA incubation and spun down by centrifugation for 5 minutes at 1400 rpm. Cell pellets were resuspended in 200 µl of the corresponding dye solution or PBS. Flow cytometric measurements were performed with FACS Calibur cytometer and analyzed with Flowjo software. The first step of analysis aimed to identify and gate the population while excluding the debris.

2.4.1 Lipid peroxidation

Lipid peroxidation was detected using the lipid peroxidation sensor BODIPY 581/591 C11. The lipophilic dye indicates lipid peroxidation by shifting the fluorescence from red to green upon oxidation. The dye was applied at a concentration of 1 µM one hour prior to drug treatment. At indicated time points, cells were analyzed by flow cytometry using channel FL-1 and FL-3 to determine green and red fluorescence intensity (FI), respectively. The ratio of mean fluorescence intensity was calculated (mean green

FI/mean red FI). An increased green fluorescence and decreased red fluorescence indicates lipid peroxidation.

2.4.2 Total ROS production

Total cellular ROS production was analyzed using the membrane permeable, oxidation-sensitive dye dihydroethidium (DHE). Oxidation by superoxide results in formation of 2-hydroxyethidium. Non-specific oxidation occurring from other sources of ROS results in formation of ethidium. Total fluorescence of both oxidation products was analyzed in channel FL-2. For this purpose, cells were stained with 5 µM DHE for 15 min at 37°C and washed with PBS. The percentage of DHE-positive and DHE-negative cells was determined. To block ROS formation, cells were pre-treated with 2 mM N-acetyl cysteine (NAC).

2.4.3 Mitochondrial ROS production using MitoSox

Mitochondrial ROS production was analyzed using MitoSox^{TM} Red. The fluorogenic dye is a derivative of DHE provided with a cationic triphenylphosphonium substituent to specifically target mitochondria. Oxidation of MitoSox^{TM} Red by superoxide results in its hydroxylation, generating 2-hydroxyethidium. Emission of the oxidized dye product was detected in channel FL-2. For this purpose, cells were stained with 5 µM MitoSox^{TM} Red/PBS for 30 min at 37°C. For further analysis, mean fluorescence intensities were calculated.

2.4.4 Mitochondrial ROS production using MitoTimer

Mitochondrial ROS production was analyzed using NCI-H460 cells expressing the oxidation sensitive MitoTimer. The fluorescent protein indicates ROS production at the mitochondria by shifting the fluorescence from green to red upon oxidation. At indicated time points, cells were harvested as described above and subsequently resuspended in PBS for analysis. The mean fluorescence intensity was detected using channel FL-1 (green) and FL-3 (red). An increased red fluorescence and decreased green fluorescence indicates enhanced mitochondrial ROS production (mean red FI/mean green FI).

2.4.5 Propidium iodide (PI) exclusion assay

Cell death was quantified by PI exclusion assay. This method is based on the DNA-intercalating, membrane-impermeable dye propidium iodide which accumulates only in dead cells. Cell death was detected 48 h following treatment with DHA. To this end,

cells were collected and stained with 10 µg/ml PI/PBS for 30 min in the dark. PI-positive (dead) cells were determined by flow cytometry using channel FL-2 (Fig. 2.1).

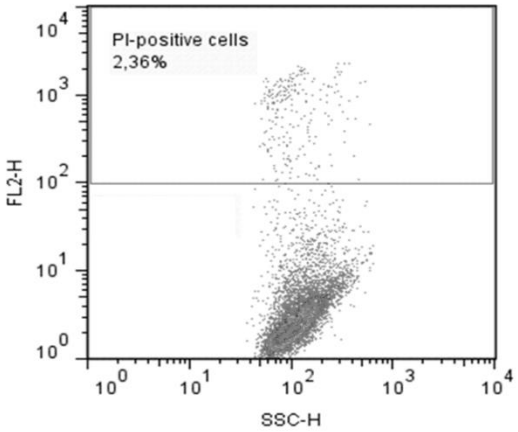

Figure 2.1 Representative dot plot gating dead cells. *Viable cells with intact membranes are depicted by low fluorescence intensity and dead cells by high fluorescence intensity.*

2.4.6 Determination of apoptosis induction

Nicoletti et al. published a method to analyze cell cycle distribution and apoptotic cells within a population using flow cytometry [134]. Similar to the PI exclusion assay, this method is based on the DNA-intercalating dye propidium iodide. By addition of the detergent Triton X-100 and citrate to PBS, cell membranes become permeable for PI enabling the dye to enter all cells and intercalate with DNA. PI intercalation is proportional to DNA content. After flow cytometric analysis in channel FL-2, results are portrayed in a histogram according to the fluorescence intensity (Fig. 2.2). The histogram is characterized by two sharp peaks for cells in G0/G1 phase and for diploid cells in G2/M phase. The fluorescent signal between the two peaks indicates cells in S-phase. Apoptotic cells are visualized by sub-G1 peak as a result of DNA fragmentation, which is a late occurring event during apoptosis. For analysis of DNA fragmentation, cells were incubated for 30 minutes in the dark in PBS containing 0.1% sodium citrate, 0.05% Triton X- 100 and 50 µg/ml propidium iodide.

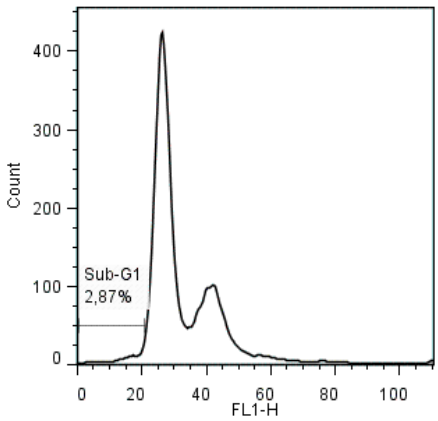

Figure 2.2 Representative histogram analyzing cells with fragmented DNA (sub G1 population).

2.4.7 Analysis of mitochondrial membrane potential with TMRE staining

In cells with an intact proton gradient and mitochondrial membrane potential (ΔΨm), the cationic and lipophilic fluorescent dye tetramethylrhodaminethylester (TMRE) accumulates at the inner mitochondrial membrane [135]. Therefore, TMRE accumulation can be used to assess the number of viable cells with an intact mitochondrial membrane potential (high ΔΨm). In contrast, dead cells are characterized by dissipation of the mitochondrial membrane potential (low ΔΨm) resulting in a decreased fluorescence signal (Fig. 2.3). To determine cells with dissipated membrane potential, cells were incubated for 30 minutes at 37° C with 25 nM TMRE in PBS. TMRE fluorescence was analyzed in channel FL-2. Cells with low TMRE intensity were considered dead.

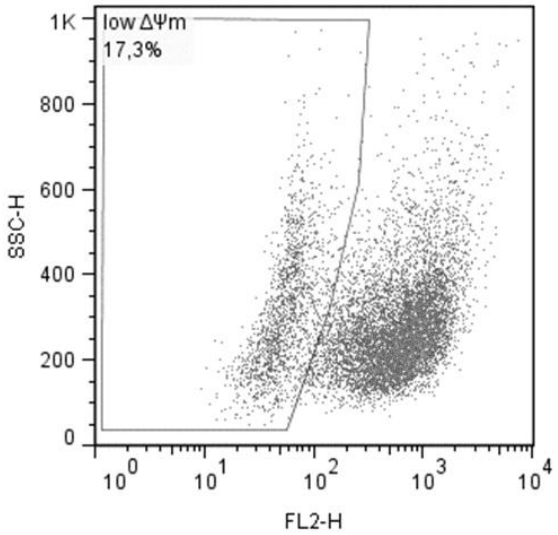

Figure 2.3 Representative dot plot gating dead cells. *Cells with intact mitochondria have a high ΔΨm, depicted by a high fluorescence intensity following TMRE-staining. In dying cells with damaged mitochondria ΔΨm is dissipated, depicted by a weaker fluorescence intensity.*

2.4.8 Analysis of proliferation and cell cycle distribution with EdU/PI staining

Proliferation was analyzed using a Click-iT EdU FACS Kit, which is based on the detection of the incorporated thymidine analog EdU into newly synthesized DNA. The assay uses click chemistry to detect incorporated 5-ethynyl-2'-deoxyuridine (EdU) by coupling a fluorophore to the thymidine analog. The reaction is based on a copper catalyzed interaction between an alkyne located at the ethyl moiety of EdU and picolyl azide, which is coupled to Alexa Fluor 488 dye. The assay was performed according to the manufacturers protocol. Cells were incubated for 30 min with 10 µM EdU in cell culture medium. Subsequently, cells were harvested, fixed and permeabilized with the

provided fixative and saponin-based permeabilization solution according to manufacturer's protocol. After click labeling wit Alexa Fluor 488, cells were additionally stained with 10 µg/ml PI/PBS for 30 min in the dark for cell cycle analysis. Cells were analyzed by flow cytometry using channel FL-1 for Alexa Fluor 488 and FL-2 for PI (Fig.2.4).

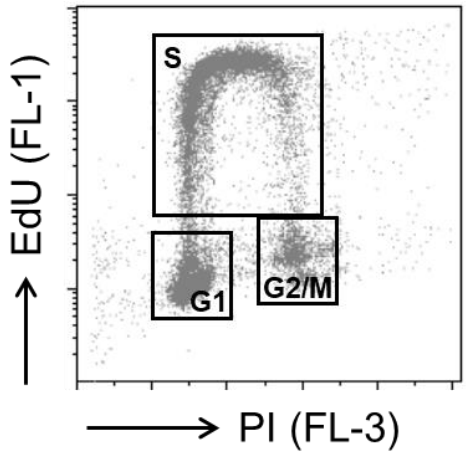

Figure 2.4 Representative dot plot for analysis of EdU incorporation and cell cycle analysis after double staining with EdU-Alexa Fluor 488 and PI.

2.4.9 Analysis of autophagy induction

Autophagy induction was quantified by flow cytometric analysis of autophagosome-associated LC3BII. Before detection of LC3BII, cytoplasmic LC3BI was extracted from the cell using saponin extraction buffer [136]. In contrast, the lipidated LC3BII is inserted into membranes of autophagosomes and, therefore, cannot be washed out with saponin extraction buffer. Consequently, saponin extraction of LC3BI allows the quantification of intracellular LC3BII levels, using antibody against endogenous LC3B. Saponin extraction was conducted by incubation of harvested cells with 0.05% saponin/PBS for 5 min. Afterwards, cells were incubated with 1 µg/ml mouse-anti LC3B antibody for 30 min. After washing with PBS, cells were incubated for further 30 min with Alexa 488^{TM}-coupled anti-mouse antibody. Fluorescence was detected in channel FL-1. For further analysis, mean fluorescence intensities were used.

2.5 Microscopic analysis

2.5.1 Immunofluorescence staining

Cells were placed on coverslips in multi-well plates and treated the next day. At indicated time points after treatment, cells were washed with PBS and fixed for 10 minutes with 4% PFA/PBS at room temperature. In order to detect intracellular proteins, cells were permeabilized for 10 minutes with 0,2% Triton X-100/PBS. After further washing steps, coverslips were incubated for 1 h at room temperature or overnight at 4 °C with 2% goat serum in PBS to block unspecific binding sites. The blocking buffer was removed and cells were incubated for 1 h at room temperature with the respective primary antibody diluted in blocking buffer. After three further washing steps, cells were incubated in the dark for 1 h at room temperature with the corresponding secondary antibody, diluted 1:400 in PBS and supplemented with 3 µM Hoechst 33342 (2'-[4-Ethoxyphenyl]-5-[4-Methyl-1-Piperazinyl]-2,5'-bi-1H-Benzimidazol-Trihydrochlorid-Trihydrat). For detection of sulfenic acids, cells were treated with 10 mM dimedone 2 h prior to cell fixation. Fixation and permeabilization of dimedone-labeled cells were carried out by incubation with ice-cold methanol for 3 min on ice to circumvent interaction of dimedone with aldehyde. Incubation with the respective antibodies and Hoechst staining were conducted as described above. After the final washing steps, cells on coverslips were mounted inversely onto microscope glass slides using DAKO mounting medium. Finally, slides were dried at least one night at 4 °C before microscopic analysis. Analysis of the samples was conducted using a Zeiss Axiovert 200 fluorescence microscope with ApoTome and ZEN imaging software.

2.5.2 Staining of apoptotic cells with Hoechst 33342 and propidium iodide

To distinguish between apoptotic and non-apoptotic, necrotic cell death, cells were stained with the two DNA-binding dyes Hoechst 33342 and propidium iodide. The membrane-permeable blue fluorescence dye Hoechst 33342 enters every cell, while the red fluorescence dye PI accumulates in dead cells only. Apoptotic cells are characterized by condensed nuclear DNA. During the initial phase of apoptosis, the plasma membrane remains intact and condensed DNA in nuclei appears blue, while cells loose membrane barrier function in the last phase, allowing PI accumulation in the nuclei (red nuclei with condensed DNA). Necrotic cells possess a normal nuclei

morphology but accumulate PI (red nuclei without DNA condensation), while viable cells do not accumulate PI (blue nuclei without DNA condensation).

Cells were seeded on 12-well plates and treated the next day in normoxia or hypoxia. After 48 h, cells were stained with 3 µM Hoechst 33342 and 50 µg/ml PI for 15 min in the dark before taking images using a fluorescence microscope with Hg 50 W lamp and a broadband emission filter.

2.5.3 Lipid peroxidation

Lipid peroxidation was visualized using the fluorescent probe BODIPY 581/591 C11. Cells were plated on coverslips and incubated with 1 µM BODIPY 1 h prior to drug treatment. At indicated time points, cells were washed with PBS, fixed with 4% PFA for 10 min and stained with 3 µM Hoechst 33342 for 15 min. After further washing steps, coverslips were inversely mounted onto glass slides with DAKO mounting medium. Slides were examined with a Zeiss Axiovert 200 fluorescence microscope using respective filters, ApoTome and ZEN imaging software.

2.6 Protein analysis

2.6.1 Protein purification

Cells were seeded in 10 cm cell culture dishes and treated the next day. 24 h after treatment, the medium was removed and washes with PBS. The following steps were carried out on ice to prevent degradation of proteins. For whole cell protein extraction, cells were shortly incubated with 100 – 200 µl lysis buffer and subsequently scratched from the dishes using a cell scraper. The lysates were incubated on ice for 30 minutes. Following incubation, lysates were centrifuged at 13.000 rpm for 15 minutes at 4 °C and the supernatants containing the solubilized proteins were collected. Determination of protein concentration was carried out using DC Protein Assay kit following the manufacturer’s protocol. Protein concentrations were calculated according to a bovine serum albumin (BSA) standard curve. Lysates within a sample set were adjusted to the same concentration with lysis buffer and complemented with an appropriate volume of 4x SDS sample buffer containing 10% 2-mercaptoethanol. For protein denaturization, samples were incubated at 95 °C for 10 minutes and subsequently stored at -20 °C.

To detect oxidized proteins by Western blot, sulfenic acids need to be labeled with dimedone before protein purification. Therefore, cells were incubated with 10 mM dimedone 2 h prior to cell lysis, which was then performed as described above.

2.6.2 SDS PAGE and Western blot analysis

Proteins were separated by sodiumdodecyl-sulfate polyacrylamide gel electrophoresis (SDS PAGE) under reducing condition using polyacrylamide gels at 12% or 15%. Samples and a pre-stained protein sample standard (PageRuler™) were loaded onto gels and proteins were separated overnight until sufficiently separated at 40 V using 1x SDS running buffer. In order to transfer proteins onto methanol-activated PVDF membranes, a tank transfer system was used at 1.5 A for 1.5 h in 1x transfer buffer. Afterwards, membranes were incubated for 1 h in blocking solution containing 5% non-fat milk at room temperature to block unoccupied binding sites. Primary antibodies were diluted in 1x TBS-T buffer containing 5% BSA. Anti-sulfenic acid antibody for detection of oxidized proteins was diluted in 1x TBS-T containing 5% non-fat milk. Membranes were incubated with the respective antibodies at 4 °C overnight. After three washing steps with 1x TBS-T buffer, membranes were incubated for 1 h at room temperature with the appropriate secondary antibody, diluted 1:2000 in 1x TBS-T buffer containing 5% non-fat milk. Following three further washing steps with 1x TBS-T buffer, detection of the protein bands was conducted following incubation with ECL Prime or Select detection reagent using chemiluminescence imager Fusion Solo and Fusion software. Densitometric quantification of protein levels was performed using ImageJ software. Normalization of densitometric results was carried out to β-actin before second normalization to respective non-treated controls. All Western blot experiments were repeated at least twice in independent experiments until otherwise stated.

2.7 Analysis of cellular bioenergetics

2.7.1 Seahorse XF Extracellular Flux Analyzer

The Seahorse XF technology was developed to conduct an automatic analysis of cellular energy metabolism in real-time. The device allows label-free analysis of metabolic changes after drug treatment and comparison of bioenergetic phenotypes. The technology is based on the measurement of the oxygen consumption rate (OCR) and extracellular acidification rate (ECAR) of viable cells in a multi-well plate, indicating mitochondrial respiration and glycolysis, respectively. The key parameters of these two main energy-generating pathways, the OCR and ECAR, are detected simultaneous by changes of dissolved oxygen and free proton concentrations by solid state sensors residing 200 µm above the cell monolayer. During performance of metabolic assays,

specific inhibitors, stimulators or substrates that interfere with oxidative phosphorylation and glycolysis are sequentially injected through built-in ports at intervals of approximately 5 – 8 minutes to analyze changes in cellular metabolism in real-time. Analysis of the capability of cells to respond to inhibition of metabolic pathways, enables estimation of cellular fitness and energetic flexibility.

2.7.2 Seahorse XF mito stress test

In this study, the Seahorse XFe 96 analyzer was used to evaluate DHA-induced effects on mitochondrial function. Cells were seeded at 7.500 cells/well in 100 µl complete medium on XF96 micro-plates to reach an optimal cell density of 60 – 80% at the time point of measurement. The next day, cells were treated with DHA in normoxia or hypoxia. 6 – 8 replicates for each cell line and condition were analyzed at the same time. 24 h after treatment, medium was exchanged by 180 µl XF base medium per well containing 1 mM pyruvate, 2 mM glutamine and 10 mM glucose. Plates were incubated for 1 h at 37 °C under CO_2-free conditions. Mitochondrial function was examined using Seahorse XF mito stress test kit with respective inhibitors of oxidative respiration and performed according to the manufacturers protocol.

The method is based on analysis of oxygen and proton concentrations following sequential injection of inhibitors, targeting distinct components of the ETC (Fig. 2.5). Initially, the device measures the basal OCR before injecting the first inhibitor. Afterwards, Oligomycin inhibiting ATP synthase (complex V) is injected at a final concentration of 1 µM. The occurring decrease of the OCR indicates the amount of oxygen consumed for mitochondrial ATP generation and is calculated as follows:

$$ATP\ production = basal\ OCR_{\ before\ oligomycin} - minimum\ OCR_{\ after\ oligomycin}$$

Subsequently, Fluoro-carbonyl cyanide phenylhydrazon (FCCP) is injected into the wells. For NCI-H460 cells a final concentration of 2 µM was used, while HCT116 cells were treated with 1.5 µM FCCP. FCCP depolarizes the mitochondrial membrane resulting in an uninhibited electron flow through the ETC and forces maximal oxygen consumption by complex IV. This indicates the maximal respiratory capacity of the cells and reveals the distinct utilization of mitochondrial respiration under basal conditions. Thus, the spare respiratory capacity is calculated as follows:

$$Spare\ respiratory\ capacity = maximal\ respiration - basal\ respiration$$

To evaluate the mitochondrial proton leak and subtract oxygen consumption of non-mitochondrial respiration, rotenone, an inhibitor of complex I and antimycin, an inhibitor

of complex III are injected together. Both inhibitors were used at final concentrations of 0.5 µM to completely shut down the ETC and mitochondrial oxygen consumption. The detected remaining oxygen consumption after injection can be allocated to non-mitochondrial respiration. The proton leak at mitochondria can be calculated as follows:

Proton leak = minimum OCR $_{after\ oligomycin}$ *– non-mitochondrial respiration*

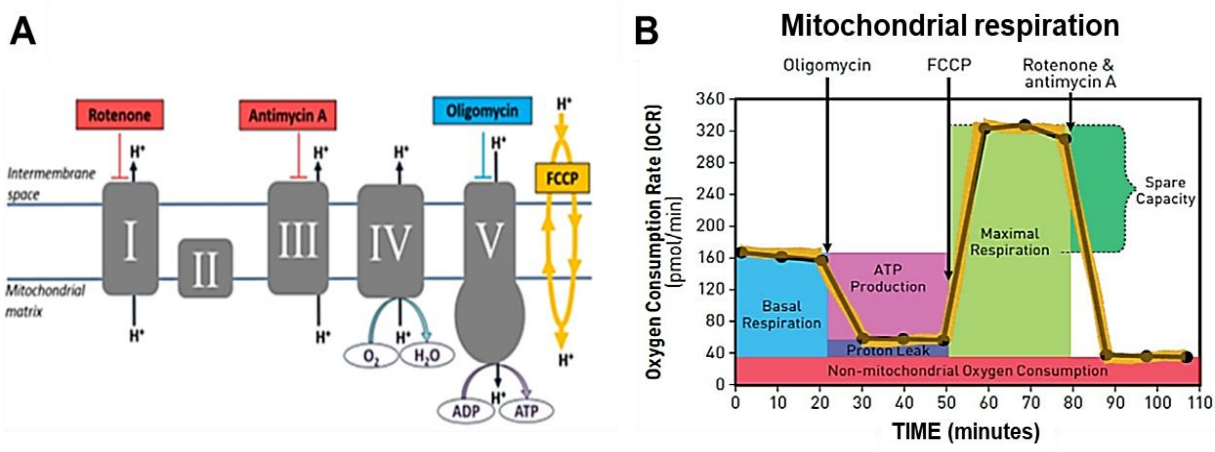

Figure 2.5 Seahorse XF mito stress test modulators and their impact on key parameters of mitochondrial respiration. *(A) Rotenone and antimycin A inhibit complexes I and III, oligomycin inhibits ATP synthase (complex V) and FCCP uncouples oxygen consumption from ATP production. (B) Key parameters of mitochondrial function. Basal respiration is measured prior to inhibitor injection. ATP production, maximal respiration, and non-mitochondrial respiration, are assessed by detecting changes of the OCR in response to compound injection. Moreover, these parameters reveal proton leak and spare respiratory capacity [137].*

Since OCR sensitively depends on the number of cells per well, normalization with Hoechst 33342 was performed to determine the DNA content and estimate the actual cell number in each well. At the end of the measurement, Hoechst was injected into each well at a final concentration of 10 µg/ml. After incubation of 10 minutes, fluorescence was measured at an excitation wavelength of 360 nm and an emission wavelength of 465 nm using an ELISA reader. OCR data were normalized to DNA content before further analysis using Wave 2.4 software.

2.8 Determination of intracellular glutathione levels

GSH is an important antioxidant and its intracellular concentration is an indicator for the antioxidative capacity. Glutathione exists in two different forms: the reduced sulfhydryl (GSH) and the oxidized from, glutathione disulfide (GSSG). In this study, a glutathione assay kit was used to determine the total amount of intracellular glutathione. The method is based on the continuous catalytic reduction of glutathione with 5,5′-dithiobis-(2-nitrobenzoic) acid (DTNB) to produce the chromophore TNB. In order to detect total glutathione levels, oxidized glutathione is reduced by glutathione reductase and NADPH. The product, TNB, is measured photometrically at 412 nm.

The assay was performed according to the manufacturers protocol. Cells were seeded in 75 cm^2 flasks and treated the following day as indicated in normoxia or hypoxia. 24 h later, cells were harvested and 5 x 10^6 cells of each sample collected and washed with PBS. Cell pellets were suspended in 90 µl 5% 5-sulfosalicylic acid solution to deproteinize samples during cell lysis. Cell membranes were disrupted by two short freezing/thawing cycles in liquid nitrogen and a 37 °C water bath to release glutathione from the cell. Subsequently, samples were placed on ice for 10 minutes to allow complete deproteinization. After centrifugation, supernatants were collected and if necessary, stored at -80 °C until further processing. For glutathione analysis, 10 µl of the samples were added in a 96-well microplate and incubated for 5 min at room temperature with 150 µl potassium phosphate buffer (95 mM) containing DTNB (0.03 mg/ ml) and glutathione reductase (0.115 units/ ml) in order to recycle the oxidized GSSG to GSH. For the standard curve, 10 µl GSH solution at appropriate concentration was added in respective well. Directly after adding 50 µl NADPH solution to a final concentration of 50 µM, the optical density (OD) was determined photometrically at 412 nm every minute for 5 minutes. Total glutathione concentrations were calculated according to the calculated standard curve.

2.9 Colony formation assay

The colony formation assay (CFA) analyzes reproductive cell death by detecting cells, that have retained the ability to undergo unlimited cell division before and after treatment. To analyze clonogenic survival after drug treatment or ionizing radiation in normoxia and severe hypoxia, cells were seeded in triplicates at various concentrations (HCT116: 200 – 12800, NCI-H460: 200 – 6400 cells per well) on 6-well

plates. The next day, cells were preincubated with the Nrf2 inhibitor ML385 1 h before treatment with DHA. For combined treatment with IR, cells were irradiated with 2 Gy and treated with DHA or the respective solvent volume immediately after irradiation. Alternatively, cells were irradiated with 2 Gy 24 h before treatment with DHA or vice versa. For treatment under hypoxic conditions, cells were exposed to hypoxia 2 h before treatment. 24 h after incubation in hypoxia, cells were replaced to normoxia to allow growth of single cell colonies. After 8 – 10 days, medium was removed and cells were fixed for 10 minutes with 3.7% paraformaldehyde and permeabilized with 70% ethanol for another 10 minutes. Subsequently, cells were stained with 0.05% Coomassie Brilliant Blue for at least 1 h and rinsed with water before drying. Colonies (>50 cells/colony) were counted using the GelCount™ colony counter and respective software. Finally, the plating efficiency (PE) was calculated according to the colony number and seeded cells in non-treated controls:

PE (%) = (counted colonies control / seeded cell number control) x 100

To determine the survival fraction (SF), the ratio of counted colonies to seeded cells in each treatment condition was calculated and normalized to respective non-treated controls:

SF (%) = (counted colonies $_{treatment}$ / seeded cell number $_{treatment}$) x PE

Survival curves were performed using Excel software by plotting DHA concentration (linear) versus surviving fractions (logarithmic).

2.10 Crystal violet assay

The crystal violet assay is commonly used to determine cell survival upon drug treatment by staining of viable, attached cells. Dying cells detach and are removed during initial washing steps.

HCT116 wt and HCT116 Bax$^{-/-}$Bak^{sh} cells were seeded in 96-well plates and treated with DHA the next day in normoxia or hypoxia. After 48 h, cells were washed with PBS, fixed with 1% glutaraldehyde for 15 min and stained with 0.1% crystal violet for 25 min. To remove the unbound dye, cells were washed with PBS. After that, cells were treated with 0.2% Triton X-10/PBS to solubilize the bound crystal violet dye. Subsequently, Absorption was measured photometrically at a wavelength of 540 nm using an ELISA reader. The optical density at 540 nm is proportional to the number of attached cells. The effect of DHA treatment was calculated by normalization to values of solvent-treated controls (0 µM DHA).

2.11 Quantitative real time PCR

2.11.1 Principle and utilization of qRT-PCR

Conventional polymerase chain reaction (PCR) allows the amplification of specific DNA sequences using primers that are complementary to the sequence of interest. Primers are extended by DNA polymerase to generate copies, so-called amplicons, which double with every cycle. The quantitative real time polymerase chain reaction (qRT-PCR) was performed employing SYBR® Green dye which is fluorescent when intercalating with double stranded DNA. At the end of each cycle, the fluorescence intensity is detected. With every cycle, the fluorescence signal increases as a function of the target gene's initial amount.

In this work, the SLC7A11 gene expression was analyzed. Simultaneously, a reference gene (here: GAPDH) was amplified. To this end, the isolated mRNA was transcribed into cDNA before amplification by qRT-PCR.

For relative quantification, the cycle Ct was identified, at which the fluorescent signal raised above the threshold in the linear range. ΔCt values were calculated for each probe (ΔCt = Ct(SLC7A11)- Ct(GAPDH)). The changes in SLC7A11 gene expression after treatment were calculated by the 2ΔCt method (2ΔCt = ΔCt(treated probe) - ΔCt(solvent-treated probe)).

2.11.2 RNA isolation and cDNA synthesis

Cells were seeded on 6-well plates and treated with DHA with or without ML385 for 12 hours the next day. After incubation, cells were harvested and washed with PBS. RNA isolation was performed using RNeasy® Mini Kit according to the manufacturer's protocol. All steps were carried out on ice to avoid RNA degradation. RNA concentration in samples was determined using Nanodrop™. If necessary, eluates were stored at -80 °C until further processing. Synthesis of cDNA was conducted with the QuantiTect® Reverse Transcription Kit using 1 µg purified RNA according to the manufacturer's protocol. cDNA was stored at -20 °C.

2.11.3 Primer design

Primers were designed using NCBI's online tool Primer-BLAST (https://www.ncbi.nlm.nih.gov/tools/primer-blast). Cross-reactivity was excluded by Blast 2.2 database comparison. Primers were designed in an intron with a size of 22 base pairs. PCR products were 150 – 250 base pairs in size with a GC content of

50 – 60% and annealing temperature of 59 – 61 °C. Primers were manufactured by Eurofins.

2.11.4 qRT PCR

The reaction mixtures for qRT PCR were prepared with qPCR MasterMix for SYBR® Green I according to the manufacturer's protocol (Table 2.13).

Table 2.13 Composition of qRT-PCR mater mix

Component	Volume
2x reaction buffer	5 µl
Primer forward (10 µM)	0.2 µl
Primer reverse (10 µM)	0.2 µl
SYBR® Green I	0.3 µl
ddH_2O	2.3 µl

8 µL reaction mixture and 2 µL (= 2 ng) cDNA were added per well in a 96-well qPCR plate. qRT-PCR was performed using the Agilent AriaMx Real-Time PCR system according to cycling conditions shown in Table 2.14.

Table 2.14 qRT-PCR cycling conditions

Step	Temperature	Time	Cycles
Uracil-N-Glycosilase (UNG) activation	50 °C	2 min	1
DNA Polymerase activation UNG inactivation	95 °C	10 min	1
Denaturation	95 °C	15 s	50
Annealing and extension	60 °C	1 min	
Melting curve analysis	60 – 95 °C	+ 0.5 °C every 3 s	

Samples containing cDNA and controls containing water were run in triplicates. Normalized target gene expression was calculated with the 2ΔCt method [138].

2.12 Analysis of patient data

The prevalence of Keap1 mutations in different tumors was analyzed by performing a pancancer study. To this end, accessible data at the cbioportal platform (http:// www.cbioportal.org/) was used by filtering studies for indicated tumor entities performed by “The Cancer Genome Atlas” (TCGA) project.

Survival analysis of patients undergoing radiotherapy was performed using data accessible at the KM Plotter platform (http://kmplot.com/analysis/). Patients with lung cancer were divided in two groups according to the median expression of the respective gene. Overall survival of the low expressing cohort was compared to the high expressing cohort.

2.13 Statistics

At least three independent experiments were performed, unless otherwise stated. Data represent mean values ± standard deviation (SD). The results were subjected to statistical analysis using GraphPad Prism 7 software. Statistical significance was calculated by t-test or for multiple comparison using ANOVA followed by Bonferroni post-hoc test. A p-value ≤ 0.05 was considered significant. Significance levels are indicated with asterisk as follows: * $p \leq 0.05$; ** $p \leq 0.01$; *** $p \leq 0.001$; **** $p \leq 0.0001$.

3 Results

3.1 DHA induces iron-dependent oxidative damages at lipids and proteins and affects mitochondrial function

In the first set of experiments, DHA-induced damage at lipids, proteins and mitochondria were analyzed. Oxidation of lipids was measured by flow cytometry and imaged by fluorescence microscopy using the lipophilic oxidation sensor BODIPY 581/591 C11. The fluorescent probe indicates oxidation of lipids by a shift from red to green fluorescence (Fig.3.1 A). Treatment of NCI–H460 lung adenocarcinoma and HCT116 colorectal cancer cells with DHA for 24 h potently induced lipid peroxidation in both cell lines. DHA-induced lipid peroxidation was slightly but insignificantly higher in HCT116 (3.8-fold) compared to NCI-H460 cells (2.6-fold) (Fig. 3.1 A). Pretreatment with 50 µM Deferoxamine (DFO), an iron-chelating compound, abrogated DHA-induced lipid peroxidation, confirming the drugs dependency on redox-active iron for its activation. These observations were further affirmed by fluorescence microscopy (Fig. 3.1 B). Upon treatment with DHA, green fluorescence of the lipophilic oxidation sensor BODIPY 581/591 C11 increased. This is visualized in a shift from yellow to green in merged images. Treatment with DFO resulted in formation of droplet-like structures, in which BODIPY 581/591 C11 accumulates, and prevented DHA-induced increase in green fluorescence.

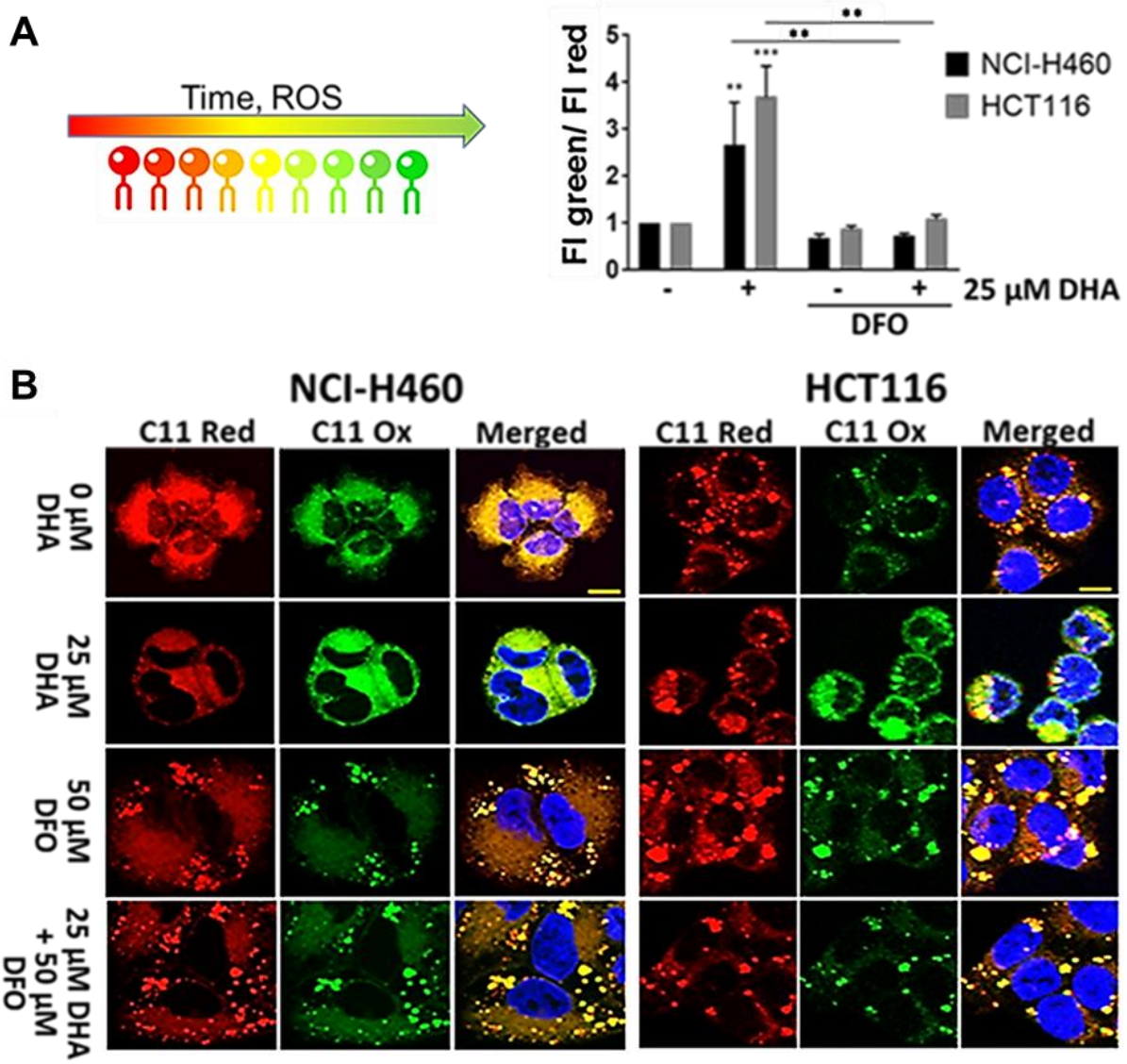

Figure 3.1 DHA increases iron-dependent lipid peroxidation in NCI–H460 and HCT116 cells. *Cells were treated for 24 h with DHA (0 µM, 25 µM) alone or in combination with 50 µM of the iron-chelating agent DFO, which was added 1 h prior to DHA treatment. Lipid peroxidation was detected using the lipophilic oxidation sensor BODIPY 581/591 C11. (A) The ratio of oxidized (green)/reduced (red) dye was detected by flow cytometry measuring mean fluorescence intensity (FI). (B) Representative fluorescence images of BODIPY-C11 oxidation were depicted. Scale bar, 10 µm. Co-treatment with DFO prevents DHA-induced lipid peroxidation in NCI-H460 and HCT116 cells. (A): Means ± SD (n=3). **, p < .01; ***, p < .001 (ANOVA with Bonferroni post-hoc test). Significance was calculated to vehicle-treated (0 µM DHA) respective controls until otherwise indicated by bars.*

Oxidation of proteins particularly occurs at reactive thiol groups of cysteines, which are especially prone to modifications during oxidative stress [139]. Changes in the intracellular thiol redox status were analyzed by Western blot using a specific antibody that detects sulfenic acids, the initial oxidation product (Fig.3.2 A). Non-treated HCT116 cells displayed higher basal protein oxidation in whole cell lysates compared to non-treated NCI–H460 cells. Treatment with DHA for 24 h increased sulfenic acid

formation in both cell lines but was more pronounced in HCT116 than in NCI-H460 cells. In both cell lines, protein oxidation was decreased by co-treatment with DFO, further confirming the relevance of iron for activation of DHA and the following oxidative damage.

Next, the intracellular localization of sulfenic acid formation was analyzed by fluorescence microscopy using NCI-H460 MitoTimer cells, which express the ROS-sensitive fluorescent protein targeted to mitochondrial matrix (Fig. 3.2 B). Fluorescence intensity of sulfenic acids (red) was increased following DHA treatment. The co-localization with the MitoTimer (green), indicated by yellow staining in merged images, revealed that DHA induces protein oxidation at mitochondrial proteins.

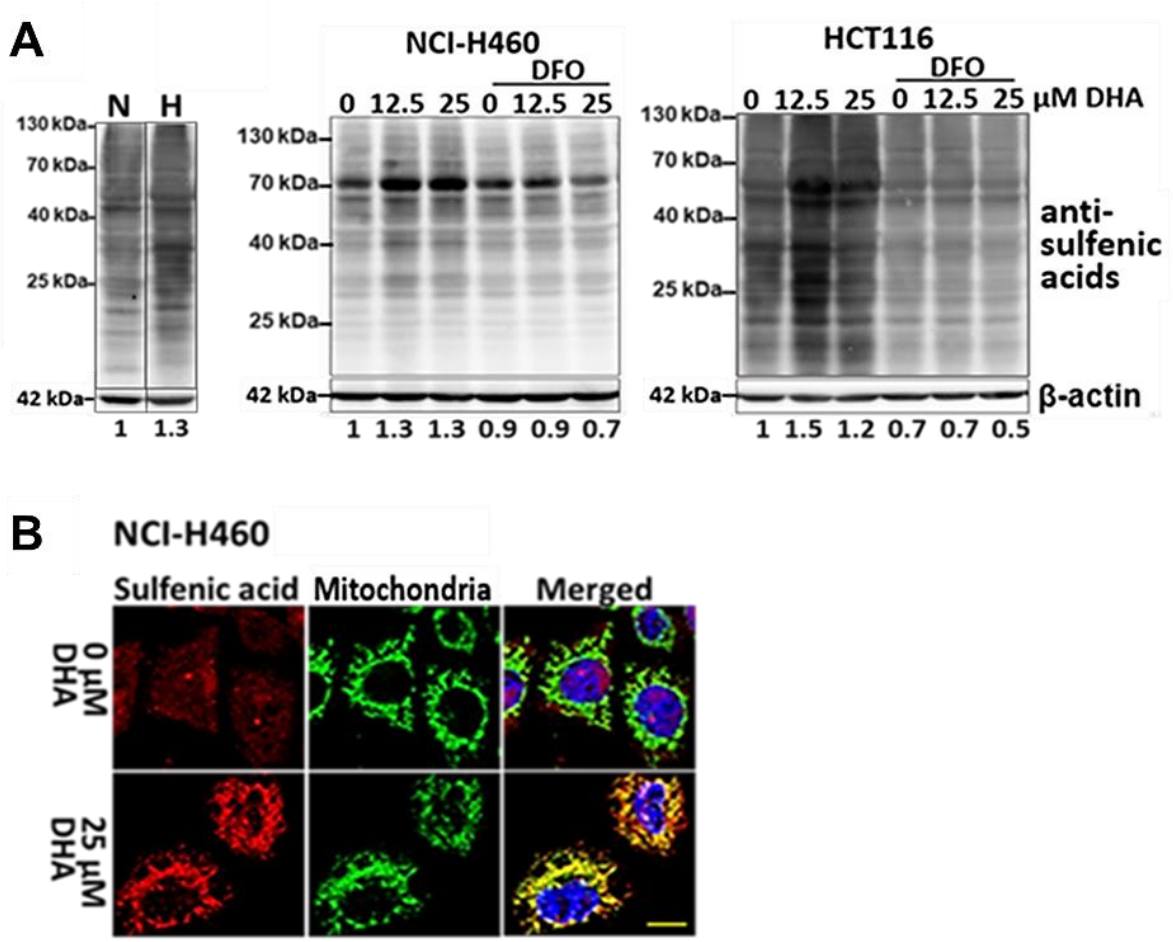

Figure 3.2 DHA increases iron-dependent protein thiol oxidation in NCI–H460 and HCT116 cells. *(A) Cells were treated for 24 h with DHA (0 µM, 12.5 µM, 25 µM) alone or in combination with 50 µM of the iron-chelating agent DFO. Dimedone-labeled sulfenic acids were detected by Western blot. Left panel shows steady-state protein oxidation in non-treated tumor cells. Densitometric analysis was performed by comparing probes blotted on the same membrane. Results are stated below the respective probes. Data shows representative blots of two independent experiments. (B) NCI-H460 cells expressing MitoTimer were treated for 24 h with DHA (0 µM, 25 µM) and subsequently fixed for analysis by fluorescence microscopy. Images show co-localization of oxidized thiol groups with MitoTimer. Scale bar, 10 µm.*

These results indicate an oxidative damage inflicted at mitochondria. In turn, damaged mitochondria are associated with an increased ROS production [140]. For this reason, we analyzed mitochondrial ROS production in NCI-H460 cells expressing the oxidation-sensitive MitoTimer by flow cytometry and fluorescence microscopy. Treatment with 12.5 – 50 µM DHA for 48 h induced a fluorescence shift from green (reduced) to red (oxidized), indicating increased mitochondrial ROS production (Fig. 3.3 A). In addition, treatment with DHA caused mitochondrial fragmentation observed by fluorescence microscopy. An altered morphology implies changes in mitochondrial function [141].

To examine mitochondrial function, we performed a mitochondrial stress test using the Seahorse XF analyzer. The basal respiration and mitochondrial ATP production in non-treated NCI-H460 cells was three and two times higher, respectively, than in non-treated HCT116 cells (Fig. 3.3 B). In both cell lines, treatment with low doses of DHA (6.25 – 12.5 µM) for 24 h was already sufficient to dramatically decrease mitochondrial respiration and ATP production. In HCT116 cells this effect was even more pronounced than in NCI-H460 cells (Fig. 3.3 C).

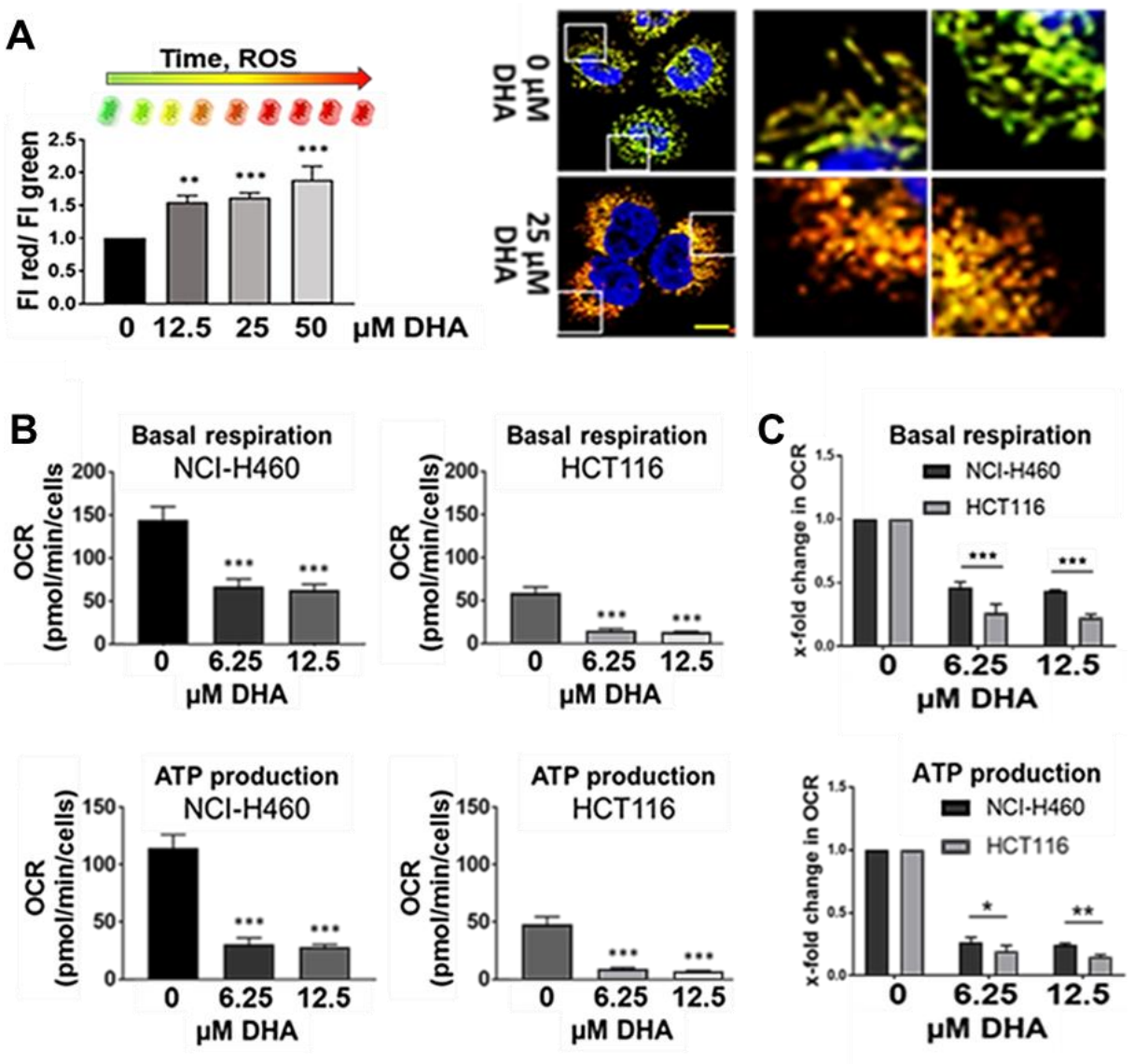

Figure 3.3 DHA increases mitochondrial ROS production and abrogates mitochondrial function in NCI-H460 and HCT116 cells. *(A) NCI–H460 MitoTimer cells were treated with DHA (0 µM, 12.5 µM, 25 µM, 50 µM) for 48 h. The ratio of oxidized (red)/reduced (green) MitoTimer was detected by flow cytometry measuring mean fluorescence intensity (FI). Data shows representative fluorescence images of NCI–H460 cells expressing MitoTimer 48 h after treatment with DHA (0 µM, 25 µM). Scale bar, 10 µm. (B, C) Mitochondrial function in NCI–H460 and HCT116 cells was examined 24 h after treatment with DHA (0 µM, 6.25 µM, 12.5 µM) using the seahorse analyzer. Upper graphs show DHA-induced decline of the basal respiration and lower graphs DHA-induced inhibition of ATP production, both depicted by decreased oxygen consumption rate (OCR). (C) Values were normalized to non-treated cells. DHA-induced abrogation of mitochondrial function was more pronounced in HCT116 than NCI-H460 cells. (A, B, C): Means ± SD (n=3). **, p < .01; ***, p < .001 (1-way ANOVA with Bonferroni post-hoc test). Significance was calculated to vehicle-treated (0 µM DHA) respective controls until otherwise indicated by bars.*

3.2 Prooxidative drug DHA activates the Keap1/Nrf2 pathway

DHA-induced lipid peroxidation (Fig. 3.1), the generation of sulfenic acids (Fig. 3.2 A) and abrogation of mitochondrial function (3.3 C) were more pronounced in HCT116 cells. These results suggest a higher susceptibility to oxidative stress-induced cytotoxicity in the colorectal cancer cell line HCT116 compared to the lung cancer cell line NCI-H460. To prove this assumption, cell death following treatment with DHA was analyzed by flow cytometry using propidium iodide exclusion assay (Fig. 3.4 A). HCT116 and NCI-H460 cells were treated with 12.5, 25 and 50 µM DHA for 48 h. HCT116 cells reacted more sensitive towards DHA-induced cell death. Treatment with the lowest DHA dose of 12.5 µM was sufficient to eradicate 20% of HCT116 cells, while it had no effect on NCI-H460 cells. Higher concentrations of DHA (25 and 50 µM) induced cell death in almost half as much NCI-H460 cells as HCT116 cells. More than 50% of HCT116 cells were eradicated using the highest concentration of 50 µM DHA. Based on the low sensitivity of NCI-H460 cells to DHA-induced cell death, we hypothesized that these cells have a better antioxidative defense than HCT116 cells, thus alleviating oxidative stress in response to DHA more efficiently than the colorectal cancer cells.

A commonly activated mechanism in response to oxidative stress is the Keap1/Nrf2 pathway. Upon dissociation of Keap1 from Nrf2, Nrf2 translocates to the nucleus and activates the transcription of antioxidant and detoxification genes [59, 60]. To analyze this pathway, we examined Nrf2 localization by fluorescence microscopy (Fig. 3.4 B). In HCT116 cells, Nrf2 localization is mainly cytosolic. Treatment with 25 µM DHA for 4 h induced Nrf2 translocation into the nucleus. This effect was prevented by co-treatment with the lipophilic antioxidant α-tocopherol. In contrast to HCT116 cells, Nrf2 was detected predominantly in the nucleus of non-treated NCI-H460 cells. As a result, only minimal additional accumulation in the nucleus could be observed upon DHA treatment. Western blot analysis revealed high basal Nrf2 levels in NCI-H460 cells, which scarcely increased 24 h after treatment with DHA (Fig 3.4 C). In contrast, the basal Nrf2 levels were low in HCT116 cells, but increased after treatment with DHA. Coincidentally, protein levels of Keap1, the cytosolic protein promoting Nrf2 ubiquitylation and degradation, decreased in these cells upon treatment with DHA. In NCI-H460 cells, Keap1 levels were constantly low and hardly affected by DHA. Iron depletion by DFO decreased the basal Nrf2 protein level in NCI-H460 cells, suggesting

an iron-dependent regulation of Nrf2 level. In HCT116 cells, iron depletion prevented DHA-induced upregulation of Nrf2 and decline of Keap1, revealing that Nrf2 upregulation is a consequence of iron-dependent DHA activation. Compared to HCT116 cells, non-treated NCI-H460 cells were characterized by higher basal Nrf2 and lower Keap1 levels. These results, together with the marked nuclear localization of Nrf2, suggest a constant activation of the Keap1/Nrf2 pathway in NCI-H460 cells, while Nrf2 becomes activated upon treatment with DHA in HCT116 cells.

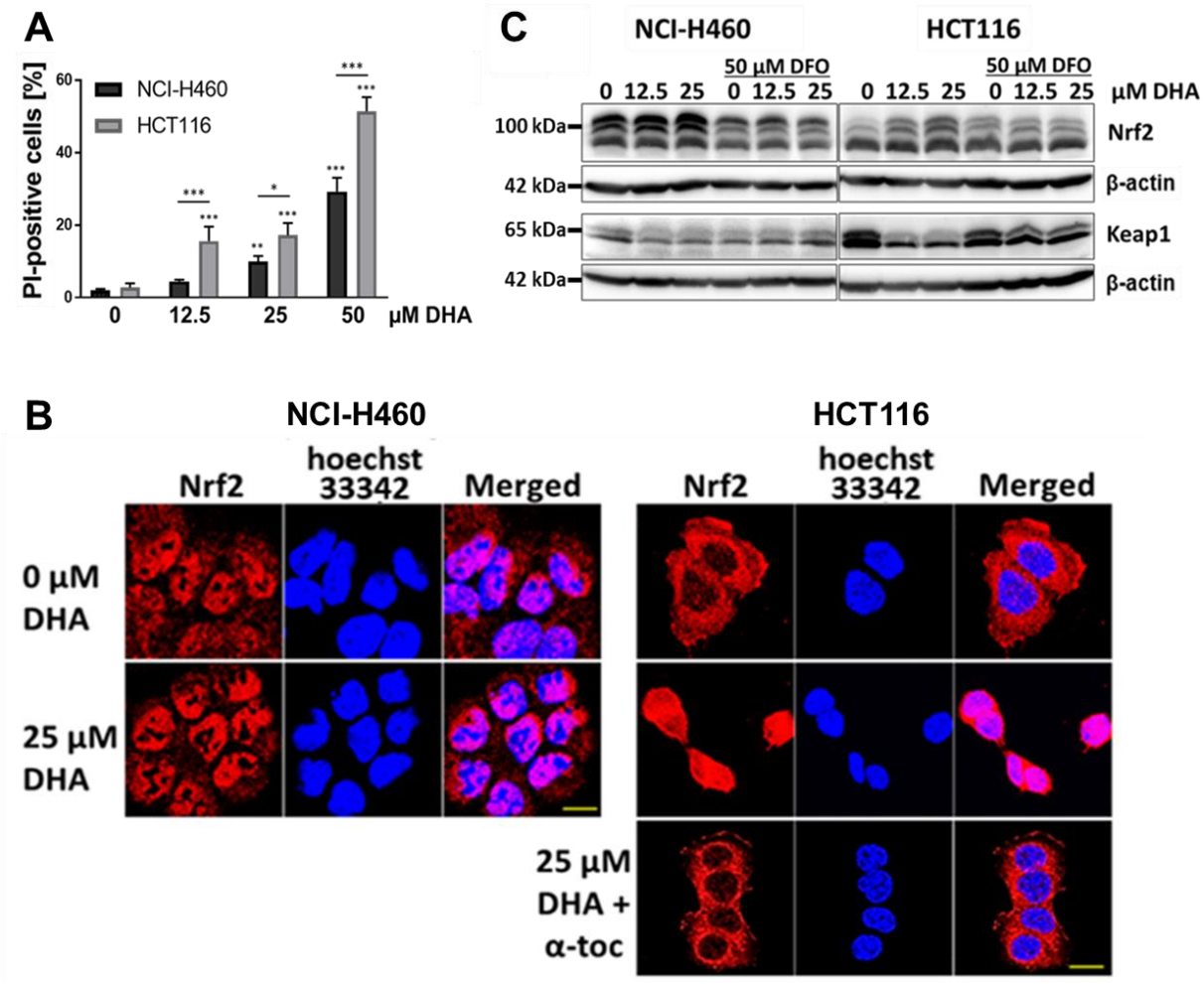

Figure 3.4 DHA-induced cell death and activation of the antioxidative Keap1/Nrf2 pathway is induced efficiently in Keap1 wildtype HCT116 compared to Keap1 mutant NCI-H460 cells. *(A) Cell death was analyzed 48 h after treatment with DHA (0 µM, 12.5 µM, 25 µM, 50 µM) by flow cytometry using PI exclusion assay. DHA-induced cell death was more efficient in HCT116 than in NCI-H460 cells. Means ± SD (n=3). *, p < .0.5; **, p < .01; ***, p < .001 (ANOVA with Bonferroni post-test). Significance was calculated to vehicle-treated (0 µM) respective controls until otherwise indicated by bars. (B) Localization of Nrf2 was detected by immunofluorescence 4 h after DHA treatment (0 µM, 25 µM). HCT116 cells were co-treated with the antioxidant α-tocopherol (10 µM) to abrogate ROS-induced nuclear translocation of Nrf2. (C) Protein expression of Nrf2 and Keap1 were detected 24 h after treatment with DHA (0 µM, 12.5 µM, 25 µM) by Western blot. Co-incubation with DFO (50 µM) prevented DHA-induced Nrf2-expression. Data shows representative blots from at least two independent experiments. Probes from both cell lines were detected on the same membrane.*

In accordance with these findings, other researchers described a Keap1 mutation located to the Nrf2 binding domain in NCI-H460 cells [142]. This raised the question whether Keap1 is more often mutated in lung cancers compared to other tumor entities. To examine Keap1 mutations in various tumors, accessible data from “The Cancer Genome Atlas” (TCGA) project was screened to perform a pancancer study (Fig. 3.5). Lung adenocarcinoma and lung squamous carcinoma (18% and 11%, respectively) contain the highest Keap1 mutation frequency, while Keap1 mutations occurred less frequent in colorectal cancer (1–2%) and other tumor types. This study emphasizes the medical relevance of Keap1 mutations in human lung cancers.

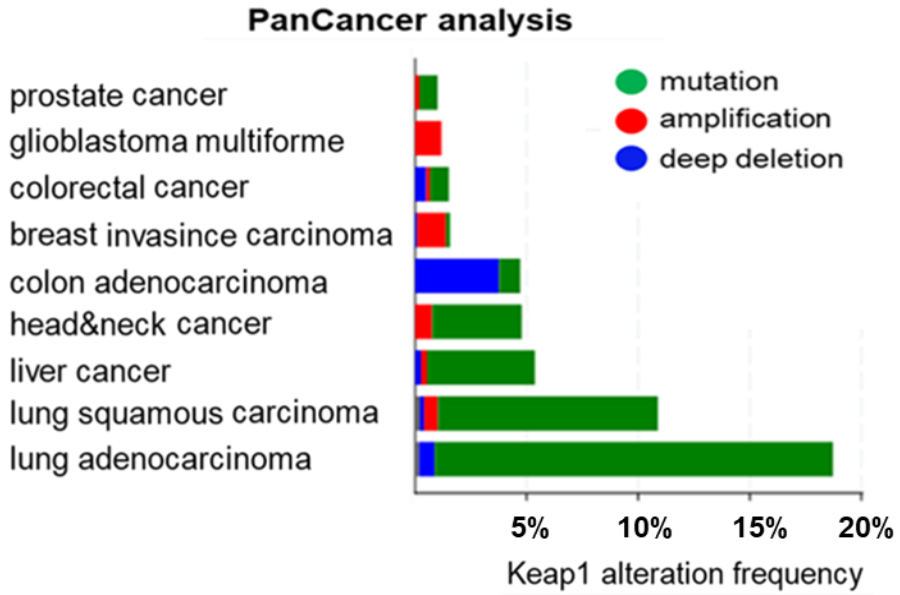

Figure 3.5 Keap1 mutations occur most frequently in lung cancers. *Pancancer analysis using data from “The Cancer Genome Atlas” (TCGA) project at cbioportal (http://www.cbio portal.org/) reveals the highest Keap1 mutation frequency in lung cancers but a low mutation frequency in colorectal cancer.*

3.3 Prooxidative drug DHA increases SCL7A11 expression and glutathione levels

To further examine activation of the Keap1/Nrf2 pathway and the downstream mechanisms, expression of the Nrf2 target gene SLC7A11 was analyzed. SLC7A11 is a subunit of the cystine/glutamate antiporter (xCT) promoting intracellular cystine import. Upon its conversion to cysteine, it fosters glutathione biosynthesis, thereby increasing the antioxidative capacity [51, 53]. Analysis by qRT-PCR revealed an approximately six times higher basal SLC7A11 mRNA expression in NCI–H460 than in HCT116 cells (Fig. 3.6 A left). Treatment with DHA (12.5 and 25 µM) induced a mild though significant (1.5- to 2-fold) upregulation of SLC7A11 gene expression in

NCI–H460 cells but clearly increased mRNA levels (6-fold) in HCT116 cells. Nrf2 inhibition with 50 µM ML385 completely prevented DHA-induced upregulation of SLC7A11 mRNA expression in NCI–H460 cells and partially in HCT116 cells (Fig. 3.6 A). ML385 is a small molecule that binds to Nrf2 and blocks its interaction with the DNA binding sequence, thereby preventing target gene expression [143]. In accordance with the SLC7A11 mRNA levels, Western blot analysis depicted a four times higher SLC7A11 protein expression in NCI–H460 compared to HCT116 cells (Fig. 3.6 B left). In addition, DHA-induced protein expression was prevented in NCI-H460 cells and decreased in HCT116 cells by co-treatment with ML385 (Fig 3.6 B).

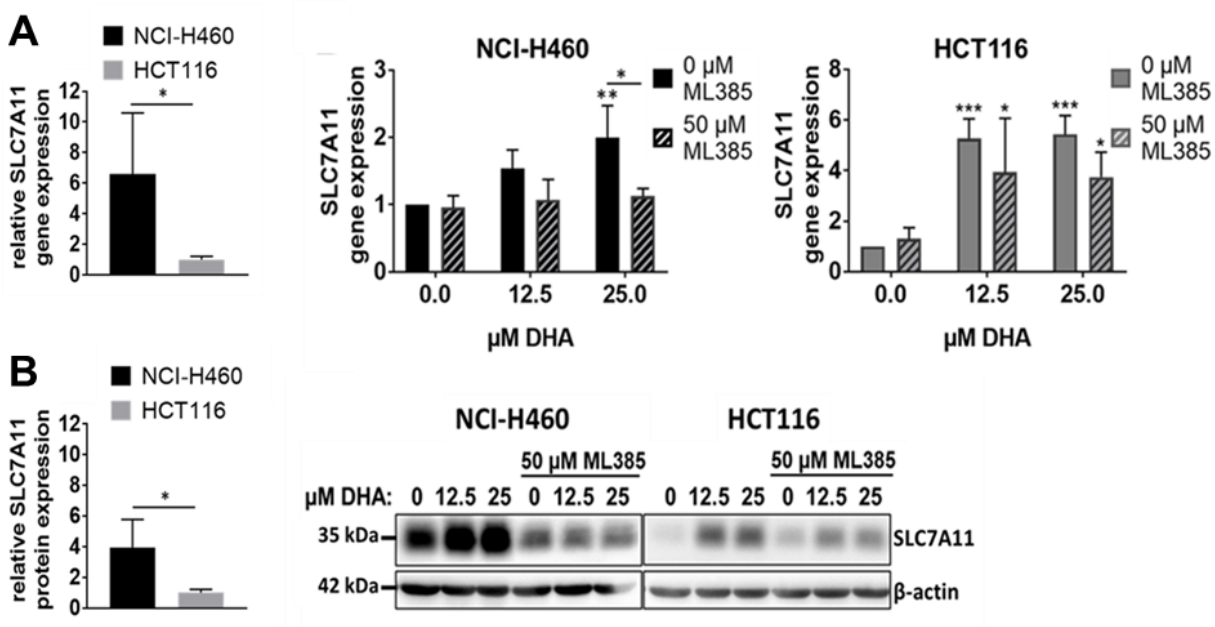

Figure 3.6 DHA-induced Nrf2 activation increases SLC7A11 expression in NCI-H460 and HCT116 cells. *(A) SLC7A11 mRNA expression was quantified by RT-qPCR and normalized to GAPDH. Basal levels of SLC7A11 mRNA expression are higher in NCI–H460 compared to HCT116 cells (left graph). Means ± SD (n=3). *, p < .0.5 (paired t-test). Gene expression of SLC7A11 was detected 12 h after treatment with DHA (0 µM,12.5 µM, 25 µM). DHA-induced SLC7A11 expression was decreased by co-incubation with 50 µM ML385. Means ± SD (n=3). *, p < .0.5; **, p < .01; ***, p < .001 (ANOVA with Bonferroni post-test). Significance was calculated to vehicle-treated (0 µM DHA) respective controls until otherwise indicated by bars. (B) Left panel: SLC7A11 protein expression was detected by Western blot and normalized to β-actin. Basal levels of SLC7A11 protein expression are approximately 4x higher in NCI–H460 compared to HCT116 cells. Right panel: Cells were treated with DHA (0 µM, 12.5 µM, 25 µM) for 24 h. DHA-induced SLC7A11 protein expression was partially decreased by ML385 (50 µM) in HCT116 cells, but completely abrogated in NCI–H460 cells. Data shows one representative blot of three independent experiments. Probes from both cell lines were detected on the same membrane.*

Following these observations, a biochemical analysis of glutathione concentration was performed to examine, whether DHA-induced upregulation of SLC7A11 affects intracellular glutathione levels (Fig. 3.7). Corresponding to the elevated SLC7A11 expression in NCI-H460 cells, basal glutathione levels were four times higher (20.39 ± 3.13 nmol/10^6 cells) than in HCT116 cells (5.69 ± 0.97 nmol/1 10^6 cells). Treatment with 25 µM DHA did not affect glutathione levels in NCI–H460 cells, but significantly increased glutathione levels (2.5-fold) in HCT116 cells. Co-treatment with the Nrf2 inhibitor ML385 completely abrogated DHA-induced increase of glutathione concentration in HCT116 cells. This data indicates Nrf2-dependent elevation of intracellular glutathione levels in colorectal cancer cells caused by DHA.

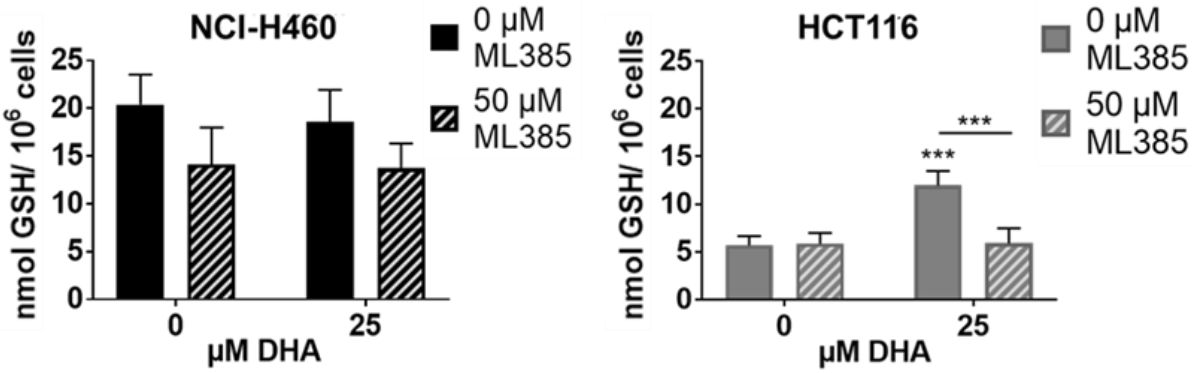

Figure 3.7 DHA-induced Nrf2 activation elevates glutathione levels in HCT116 cells. *Glutathione levels were analyzed in cell lysates of NCI–H460 and HCT116 cells using a glutathione assay kit. Cells were treated for 24 h with DHA (0 µM, 25 µM) alone or in combination with Nrf2 inhibitor ML385 (50 µM). Blocking Nrf2 activity prevented DHA-induced increase of intracellular glutathione concentration in HCT116 cells. Means ± SD (n=3). ***, p < .001 (ANOVA with Bonferroni post-test). Significance was calculated to vehicle-treated (0 µM) respective controls until otherwise indicated by bars.*

3.4 Activation of the Nrf2/Keap1 pathway limits DHA-induced cytotoxicity

Glutathione is the most abundant antioxidant in living organisms and holds a major role in ROS homeostasis and detoxification of ROS-inducing xenobiotics [45]. Thus, high glutathione levels might improve cell survival in response to DHA-induced oxidative damages and cell death. Vice versa, blocking the Nrf2-dependent increase of intracellular glutathione levels might enhance DHA-induced cytotoxicity. To prove this hypothesis, cell death was analyzed by flow cytometry 48 h after treatment with DHA in presence or absence of the Nrf2 inhibitor ML385 (50 µM) or erastin (10 µM), an

inhibitor of the xCT transporter. In HCT116 cells, that were more susceptible towards DHA-induced cytotoxicity than NCI-H460 cells, co-treatment with ML385 further enhanced cell death induction. In NCI-H460 cells, additional inhibition of Nrf2 was ineffective (Fig. 3.8 A). Interestingly, co-treatment with erastin significantly increased DHA-induced cell death in both, NCI–H460 and HCT116 cells (Fig. 3.8 B). These results demonstrate, that, within the first 48 h, the direct inhibition of cysteine import by erastin affects glutathione levels and cell death in NCI-H460 cells more efficiently than inhibition of SLC7A11 transcription. In HCT116 cells, both inhibitors improved cell death induction with comparable efficiency.

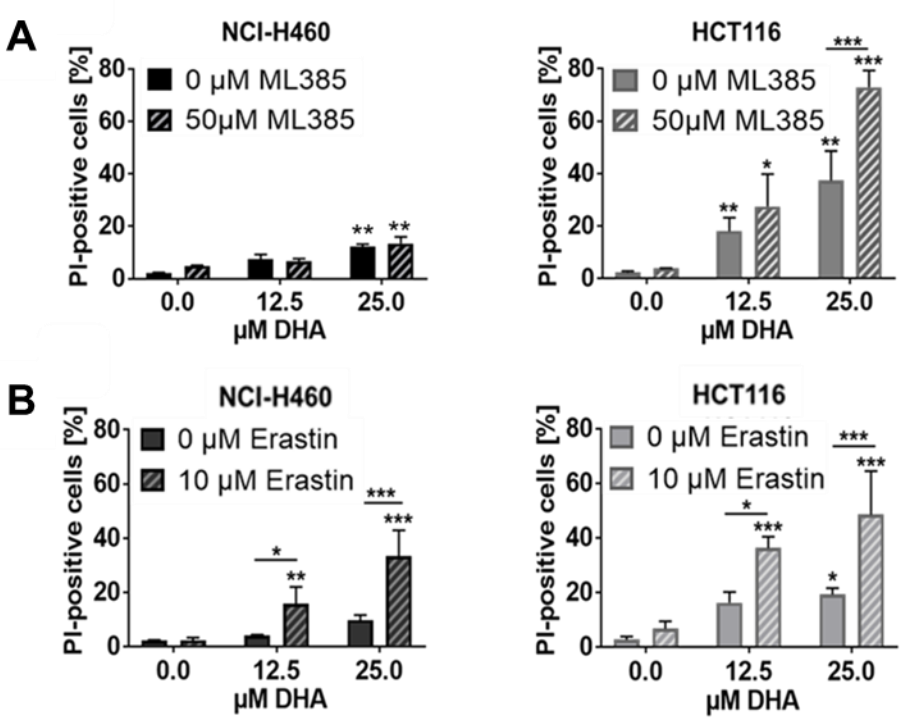

Figure 3.8 Targeting cysteine uptake sensitizes cancer cells to DHA-induced shot-term cell death. *NCI–H460 and HCT116 cells were treated with DHA (0 µM, 12.5 µM, 25 µM) for 48 h. Cell death was analyzed by flow cytometry using PI exclusion assay. (A) Cells were incubated with 50 µM ML385 1 h prior to DHA treatment. Inhibition of Nrf2 further increased DHA-induced cell death in HCT116 but not in NCI–H460 cells. (B) Cells were incubated with 10 µM erastin 1 h prior to DHA treatment. Co-treatment with erastin increased DHA-induced cell death in both cell lines. (A, B): Means ± SD (n=3). *, p < .05; **, p < .01; ***, p < .001 (ANOVA with Bonferroni post-hoc test). Significance was calculated to vehicle-treated (0 µM DHA) respective controls until otherwise indicated by bars.*

Due to the cytotoxic impact of ML385 and DHA in long-term experiments, both compounds were used at lower concentrations than in short-term experiments. To analyze long-term survival of tumor cells, a colony formation assay was performed. Single treatment with 12.5 µM of the Nrf2 inhibitor ML385 significantly lowered long-term survival in both, NCI-H460 and HCT116 cells (Fig. 3.9 A). Single treatment with

DHA, using 6.25 and 12.5 µM, decreased the clonogenic survival in both cell lines, but more efficiently in HCT116 than in NCI-H460 cells (Fig. 3.9 B). Additional treatment with the Nrf2 inhibitor ML385 further reduced the surviving fraction. Taken together, these results reveal that blocking Nrf2/Keap1 pathway clearly improves the anti-cancer activity of DHA, irrespective of Keap1 mutation.

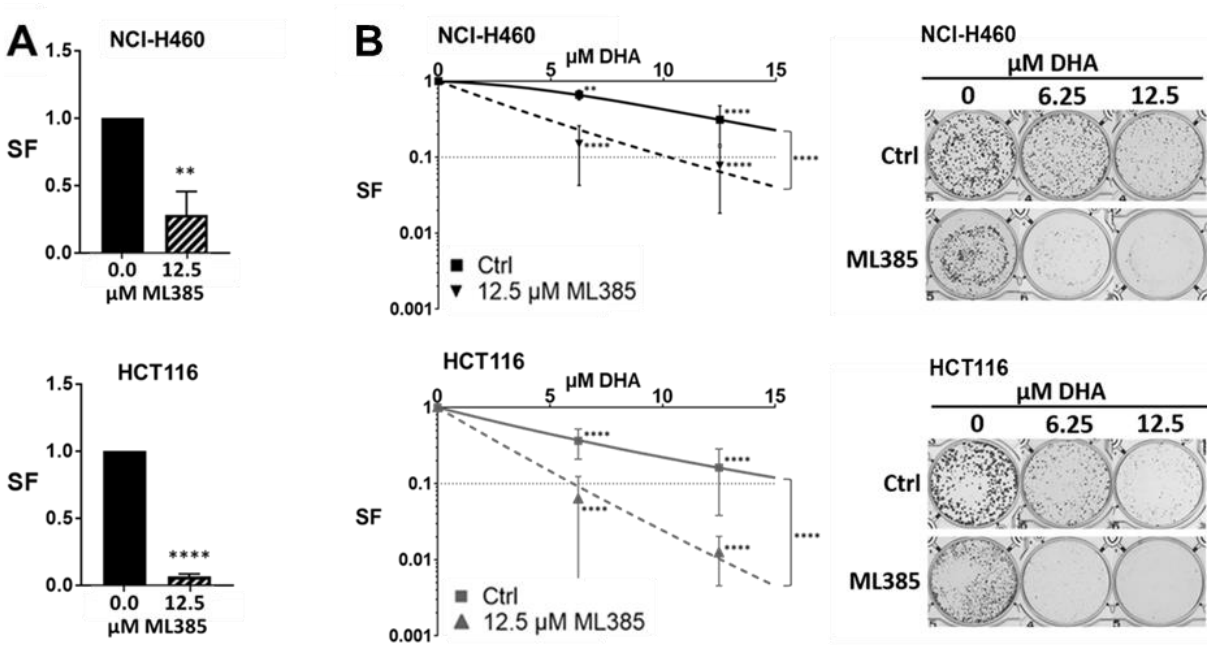

Figure 3.9 Targeting the Keap1/Nrf2 pathway sensitizes cancer cells to DHA-induced long-term cytotoxicity. *Clonogenic capacity of tumor cells was evaluated by colony formation assay. (A) Treatment with 12.5 µM ML385 over 9 days decreased the survival fraction (SF) of NCI–H460 and HCT116 cells. Values of ML385 treated cells were normalized to the plating efficiency of cells treated with solvent control (DMSO). (B) Cells were treated with DHA (0 µM, 6.25 µM, 12.5 µM) for 9 days. Co-treatment with 12.5 µM ML385 further improved DHA-induced eradication of clonogenic NCI–H460 and HCT116 cells. Values of DHA-treated cells were normalized to respective solvent-treated controls. Images show representative wells of a colony formation assay. (A, B): Means ± SD (n=3). **p < .01; ***, p < .001; ****, p < .0001 (ANOVA with Bonferroni post-hoc test).*

3.5 Combinatory therapy with ionizing radiation and DHA

So far, the results disclosed that DHA-induced cytotoxicity is limited by the antioxidative Keap1/Nrf2 pathway, independently of Keap1 mutations. The cytotoxicity of ionizing radiation also depends on ROS production and on the ability of tumor cells to prevent and repair ROS-induced oxidative damage [144, 145]. Using multi-variant analysis and the Kaplan-Meier Plotter, the outcome of radiotherapy in lung cancer patients was correlated with expression levels of genes regulated by the Keap1/Nrf2 pathway [146]. Expression levels of Keap1, Nrf2 and the two enzymes of the

glutathione biosynthesis pathway, CTH and GCLC, did not influence the median survival of patients receiving radiotherapy (Fig. 3.10 A, B, D, E). However, in patients with low expression of the Nrf2-target gene SLC7A11, radiotherapy significantly improved the clinical outcome with a median survival of 52 months compared to 26 months in the high expression cohort (Fig. 3.10 C).

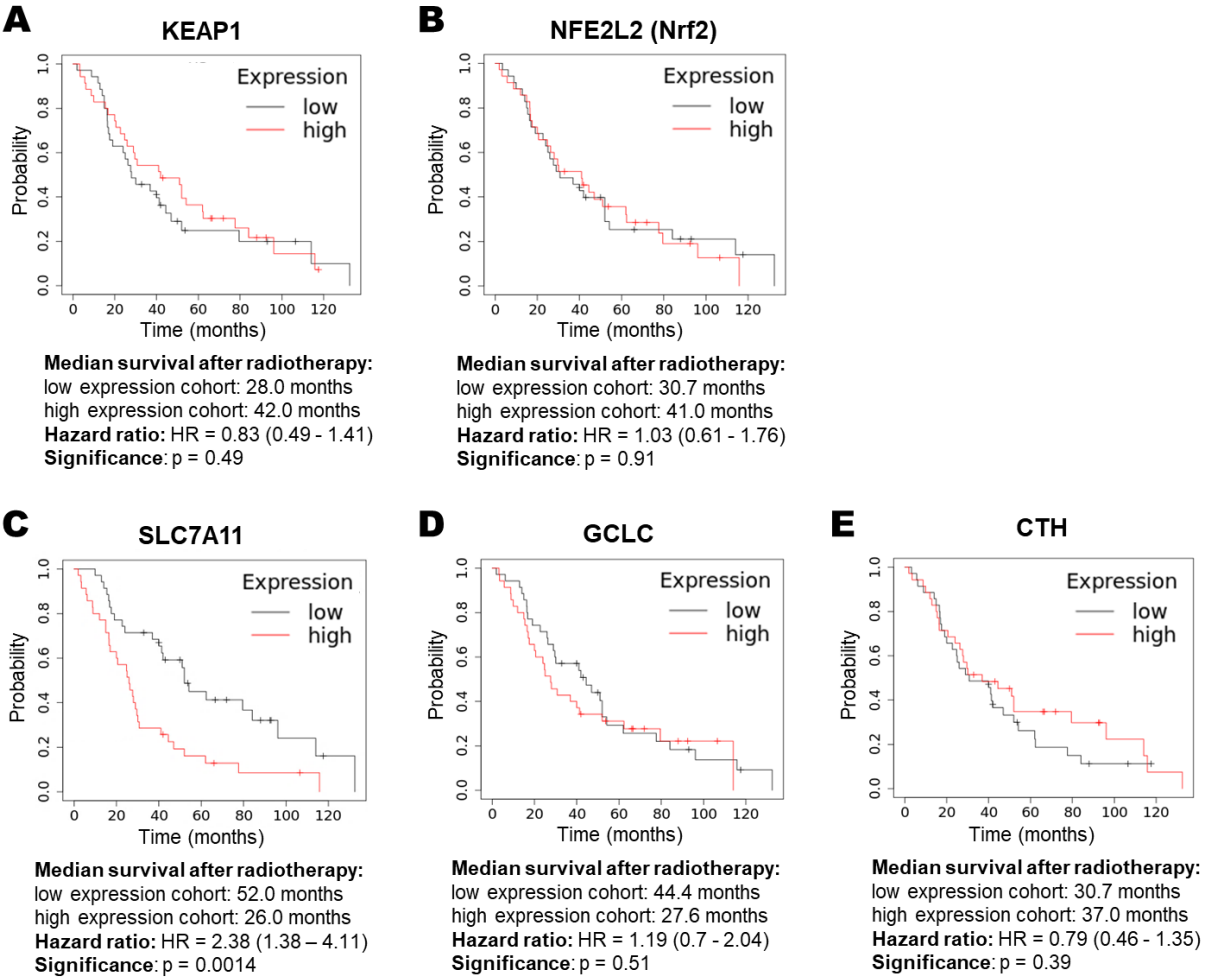

Figure 3.10 Survival of lung cancer patients receiving radiotherapy correlates with Nrf2 target gene SLC7A11*. Survival analysis was performed using data accessible at the KM-Plotter platform (http://kmplot.com/analysis/). Gene expression of Keap1 (A), Nrf2 (B) as well as the Nrf2 target genes GCLC (D) and CTH (E) did not influence survival after radiotherapy. However, lung cancer patients undergoing radiotherapy survive longer when expressing low levels of SLC7A11 (C).*

Next, we addressed the question whether treatment with DHA can improve radiotherapy. Thus, we analyzed long-term survival in response to IR and DHA alone or in combination. In the combined therapy, DHA was applied immediately after irradiation (Fig. 3.11). In both cell lines, irradiation with 2 Gy revealed a similar efficiency with a decrease of clonogenic survival by about 50%. To obtain a comparable toxicity with DHA, treatment at a concentration of 6.25 µM was enough in

HCT116 cells, while 12.5 µM DHA was required in NCI-H460 cells. The combinatory therapy reduced clonogenic survival in both cell lines more efficiently than any single treatment.

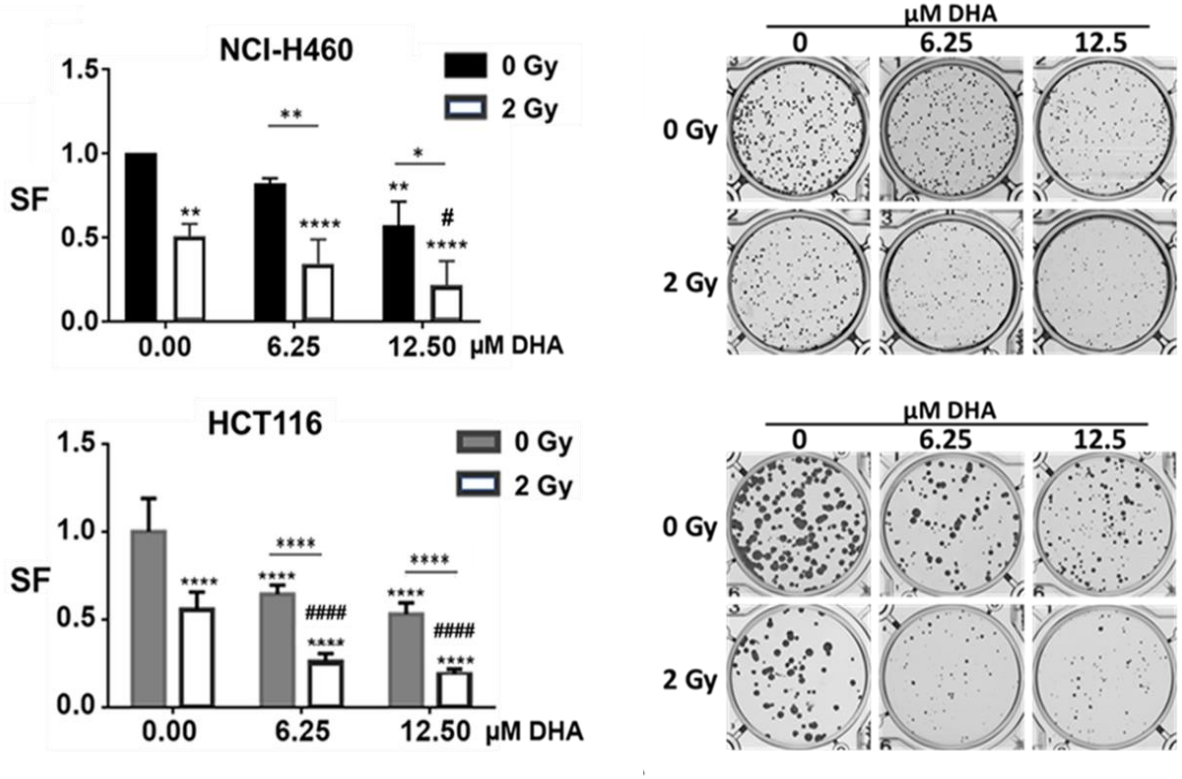

Figure 3.11 DHA improves the efficacy of radiation in NCI–H460 and HCT116 cells*. Clonogenic survival of NCI–H460 and HCT116 cells treated with DHA (0 µM, 6.25 µM, 12.5 µM) or in combination with IR (2 Gy) was evaluated by colony formation assay. Cells were irradiated and subsequently treated with DHA. The combined treatment decreased surviving fractions (SF) of both tumor cell lines more efficient than either single treatment. Images show representative wells of a colony formation assay. Means ± SD (n=3). *, p < .05; **, p < .01; ***, p < .001; ****/####, p < .0001; Significance was calculated to DMSO-treated (0 µM DHA) respective controls until otherwise indicated by bars. #### indicates significance to single treatment with IR.*

The previous results disclosed an activation of the antioxidative stress response after treatment with DHA, accompanied by an upregulation of SLC7A11 expression and a marked increase of intracellular glutathione levels in HCT116 cells. Based on these observations, we suspected that activation of the protective pathway by DHA could alleviate radiation-induced cytotoxicity. Therefore, we repeated long-term survival experiments with two distinct treatment schedules. In the first group, both cancer cell lines were irradiated with 2 Gy 24 h before adding DHA. In the second group, tumor cells received DHA treatment 24 h before irradiation with 2 Gy (Fig 3.12 A). In NCI-H460 cells both treatment approaches were similar effective and more toxic than

irradiation alone (Fig. 3.12 B, left graph). Accordingly, the treatment schedule did not influence the outcome of the combined therapy. In contrast, in HCT116 cells, the treatment schedule determined the efficacy of the combinatory therapy (Fig. 3.12 B, right graph). When HCT116 cells were irradiated before DHA application, the combined treatment was more toxic than single dose irradiation with 2 Gy. Conversely, when DHA treatment occurred 24 h before irradiation, the combined treatment was equally effective than irradiation alone. Hence, the additional cytotoxicity of the combined therapy was abolished. These results demonstrate an anti-neoplastic effect of DHA and a beneficial impact of the combined therapy with ionizing radiation, irrespective of Keap1 mutations. However, the treatment schedule needs to be considered carefully, particularly in cells that activate the protective Keap1/Nrf2 pathway.

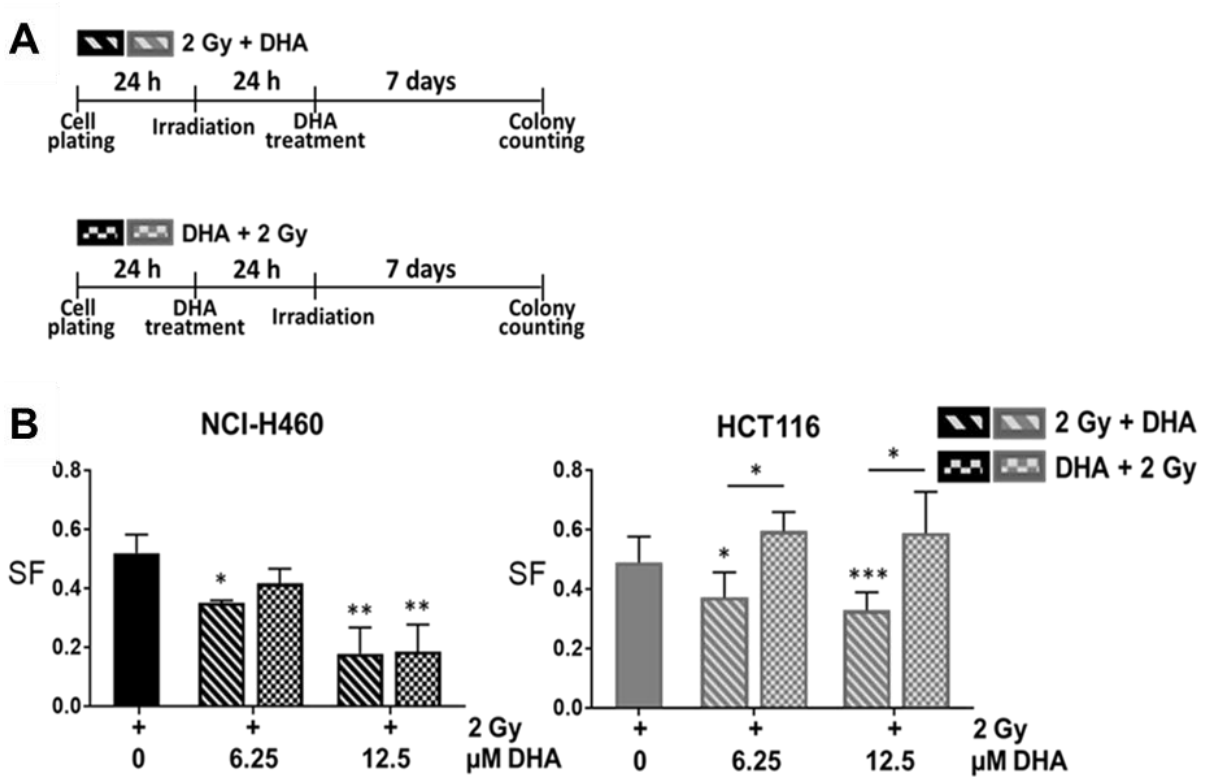

Figure 3.12 Treatment schedule of combinatory therapy determines efficacy in HCT116 cells. *Colony formation assay of NCI–H460 and HCT116 cells treated with IR (2 Gy) alone or in combination with DHA (0 µM, 6.25 µM, 12.5 µM) (A) Treatment schedule of the combinatory therapy was modified: In the first variation, cells were irradiated with 2 Gy 24 h before treatment with DHA (upper panel). In the second variation, cells were treated with DHA 24 h prior to irradiation with 2 Gy (lower panel). (B) Clonogenic survival of NCI–H460 and HCT116 cells treated according to the treatment schedule shown in A. Alterations in treatment schedule did not influence surviving fraction (SF) of NCI-H460 cells but determined efficacy in HCT116 cells. Means ± SD (n=3). *, p < .05; **, p < .01; ***, p < .001; Significance was calculated to DMSO-treated (0 µM DHA) respective controls until otherwise indicated by bars.*

3.6 Combined treatment of DHA and IR overcomes hypoxia-induced radioresistance

The previous results have demonstrated that a combined treatment of DHA and radiation can improve the efficacy of radiotherapy in normoxic conditions. However, most solid tumors are characterized by hypoxic regions that limit the cytotoxicity of radiotherapy and other ROS-dependent therapies. This phenomenon is based on the failure to produce permanent and irreparable oxidative damages in absence of molecular oxygen, that would provoke deleterious cellular damage, particularly DNA DSBs in presence of oxygen [14, 27]. Interestingly, certain publications disclosed an even more pronounced anti-neoplastic impact of artemisinin and the related derivatives in hypoxic than in normoxic conditions, especially when used at lower concentrations [132, 147-150]. In the following experiments, we therefore analyzed the cytotoxicity of a combined therapy of IR and DHA in hypoxia to prove whether additional application of DHA could improve the outcome of radiotherapy in conditions of low oxygen availability. Thus, we analyzed the clonogenic survival of tumor cells irradiated with 2 Gy and subsequently treated with DHA in severe hypoxia (0.2% O_2). 24 h after treatment, cells were replaced to normoxia to allow growth of single cell colonies. The results disclose that irradiation in hypoxic conditions is less efficient compared to irradiation in normoxia (Fig. 3.13). Hypoxia-induced radioresistance was more pronounced in NCI-H460 cells than in HCT116 cells. In both cell lines, IR-induced radioresistance could be overcome by co-treatment with DHA. For this effect, DHA concentration as low as 6.25 µM were sufficient. Moreover, the combinatory therapy was even slightly more efficient in hypoxia compared to normoxia. These results demonstrate that hypoxia-mediated radioresistance could be overcome in a combined therapy with the ROS-producing anti-malaria drug DHA.

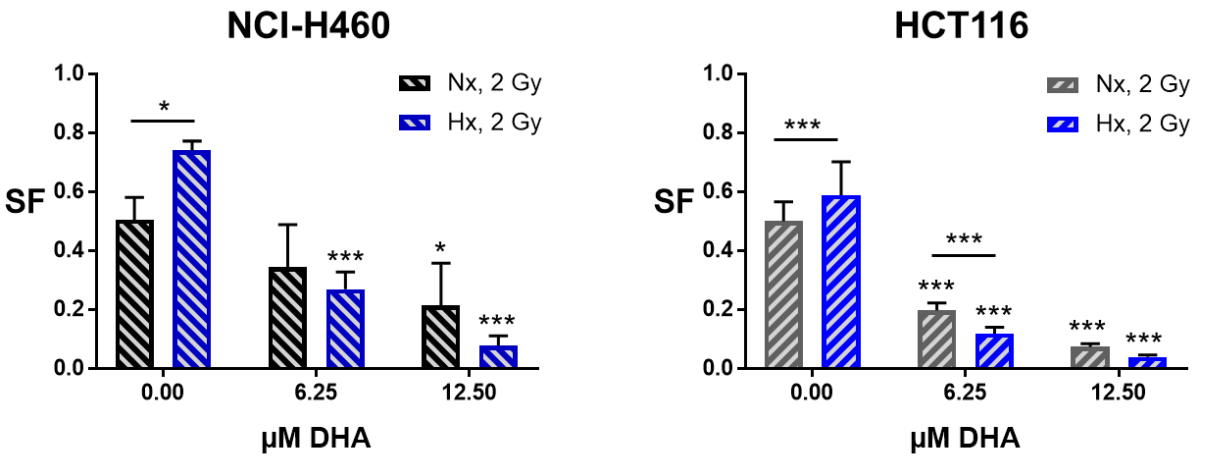

Figure 3.13 DHA improves the efficacy of radiotherapy more efficiently in hypoxia than in normoxia. *Clonogenic survival of NCI–H460 and HCT116 cells treated with IR (2 Gy) alone or in combination with DHA (0 µM, 6.25 µM, 12.5 µM) in normoxia or hypoxia was evaluated by colony formation assay. Cells treated in hypoxia were replaced to normoxia after 24 h to allow formation of colonies. In both conditions and both cell lines, the combined therapy decreased surviving fractions (SF) more efficient than radiation alone. Hypoxia-induced radioresistance was overcome in combination with DHA. Means ± SD (n=3). *, p < .05; ***, p < .0001; Significance was calculated to DMSO-treated (0 µM DHA) respective controls until otherwise indicated by bars.*

3.7 Pro-apoptotic proteins Bax and Bak decrease DHA-induced clonogenic survival in normoxia but are dispensable in hypoxia

The previous results have demonstrated that a combined treatment of DHA and IR can improve the efficacy of radiotherapy in normoxic and hypoxic conditions. In the following experiments, we therefore examined DHA-induced cytotoxicity in short-term and long-term experiments under both conditions, in normoxia (20% oxygen) and severe hypoxia (0.2% oxygen). In preceding experiments in our laboratory, Ontikatze et al. detected apoptosis induction in colorectal cancer cells [132]. Since the intrinsic apoptosis pathway is often deregulated in cancer [151, 152], we compared the impact of DHA on HCT116 colon cancer cells that are either proficient or deficient in apoptosis induction through the intrinsic pathway. HCT116 cells with deficient intrinsic apoptosis pathway were generated by knock-out of the pro-apoptotic Bcl-2 family protein Bax and knock-down of the pro-apoptotic protein Bak. Fig. 3.14 A shows the verification of the Bax knockout and Bak knockdown in HCT116 $Bax^{-/-}Bak^{sh}$ cells by Western blot. To analyze long-term survival, a colony formation assay was carried out with HCT116 wild type (wt) and HCT116 $Bax^{-/-}Bak^{sh}$ cells and treated with DHA in normoxic and hypoxic conditions. While treatment in normoxia occurred the whole time in presence of 20%

oxygen, treatment in hypoxia was performed for 24 h before returning to normoxic conditions to allow formation of colonies. In HCT116 wt cells, DHA treatment was slightly but insignificantly more efficient in hypoxia compared to normoxia (Fig 3.14 B). HCT116 Bax$^{-/-}$Bak^{sh} cells treated in normoxia were less sensitive to DHA than HCT116 wt cells, but DHA was similar effective in hypoxia in both cell lines. These results indicate, that intrinsic apoptosis is a crucial mechanism in cells treated under normoxic conditions, but becomes dispensable under oxygen-deprived conditions.

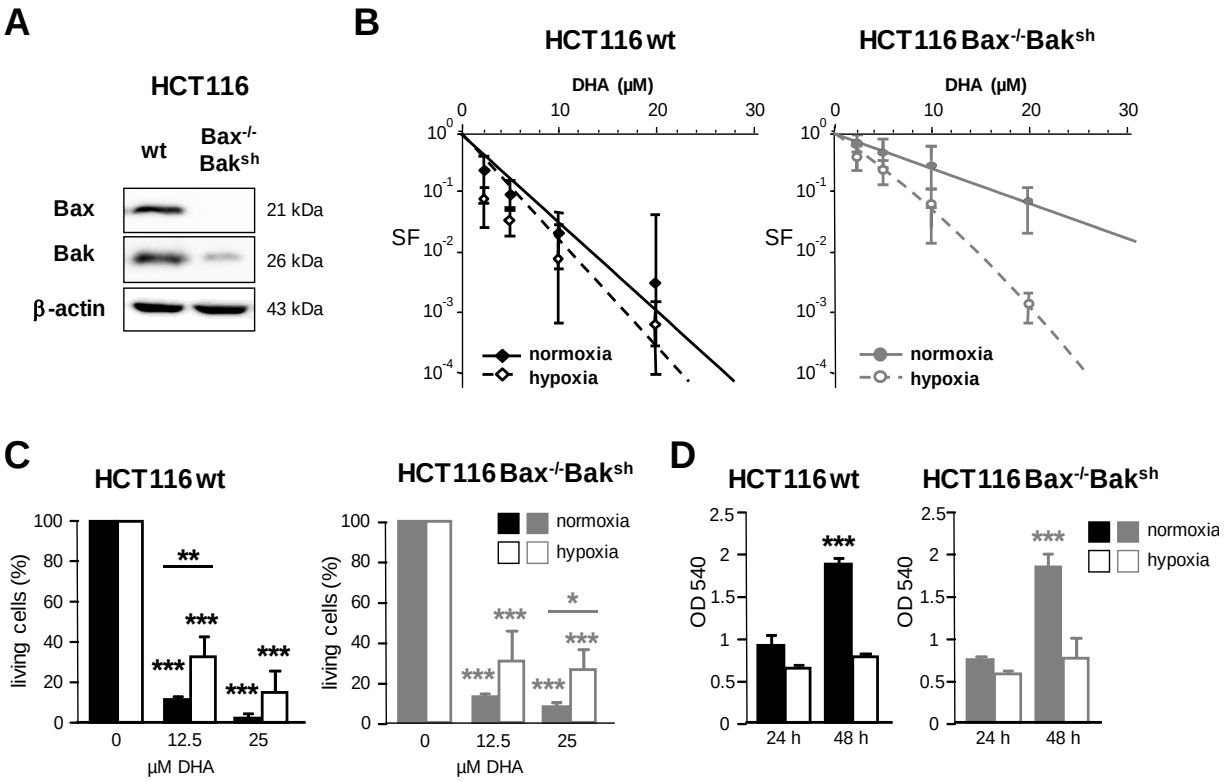

Figure 3.14 DHA-induced cytotoxicity in apoptosis-proficient HCT116 cells and with deficient intrinsic apoptosis pathway. *(A) Protein expression of Bax and Bak in HCT116 wild type (wt) and HCT116 Bax$^{-/-}$Bak^{sh} cells was detected by Western blot. (B) Long term survival of cells treated with different doses of DHA (0 µM, 2.5 µM, 5 µM, 10 µM, 20 µM) in normoxia or hypoxia was determined by colony formation assay. Cells treated in hypoxic conditions were replaced 24 h later to normoxia to allow formation of colonies. DHA was similar efficient when cells were treated in normoxia but in hypoxia, HCT116 Bax$^{-/-}$Bak^{sh} cells showed an increased resistance to DHA compared to HCT116 wt cells. (C) Cell viability was analyzed by crystal violet assay following treatment with DHA (0 µM, 12.5 µM, 25 µM) for 72 h in normoxia or hypoxia. 72 h following treatment, both cell lines respond to DHA more sensitive in normoxia than in hypoxia. (D) Analysis by crystal violet assay revealed similar OD540 values for both cell lines 24 h after plating. OD540 values doubled after incubation for another 24 h in normoxia but hardly increased in hypoxia, suggesting cell proliferation in normoxia, while proliferation was impaired in hypoxia. (A) Data shows representative Western blots. (B-D): Means ± SD (n=3). *, p < .05; **, p < .01; ***, p < .001 (ANOVA with Bonferroni post-hoc test)*

In contrast, short-term treatment for 48 h in normoxia or hypoxia revealed a similar decrease of the cell viability in both cell lines. DHA was more efficient when cells were treated under normoxic than hypoxic conditions (Fig. 3.14 C). Here, the cell viability was determined photometrically by the OD540 following crystal violet staining. To consider differences in the proliferation rates of non-treated cells in normoxia and hypoxia, the influence of oxygen availability on cell proliferation was also detected (Fig. 3.14 D). Therefore, cells were exposed for 24 and 48 h to normoxia and hypoxia respectively, and the absolute OD540 values were measured. Within 24 h, the values almost doubled in both cell lines under normoxic conditions. In hypoxia no considerable increase was detected, indicating that proliferation is obstructed by oxygen deprivation.

3.8 DHA induces cell cycle arrest in HCT116 $Bax^{-/-}$ Bak^{sh} cells

To further analyze the impact of DHA on cell proliferation, an EdU incorporation assay was performed 24 h after treatment with DHA (Fig. 3.15). In HCT116 wt cells, DHA decreased the number of proliferating cells more efficient in hypoxia, as depicted by the percentage of cells in S-phase (Fig. 3.15 A and B). In contrast, in HCT116 $Bax^{-/-}Bak^{sh}$ cells, DHA-induced inhibition of cell proliferation was similar efficient in both conditions. Concurrently, an increase of cells in G1 and G2 phase was observed after DHA treatment in normoxia, while incubation with DHA in hypoxia increased particularly the number of cells in G1 phase (Fig. 3.15 C). To further verify the observed impact of DHA on cell cycle progression, protein expression of the cell cycle inhibitors $p21^{WAF1/Cip1}$ and $p27^{KIP1}$ was detected (Fig. 3.15 E). Both cell cycle inhibitors block the progression from G1 to S phase. Treatment with DHA in hypoxia resulted in an increase of the protein levels in HCT116 $Bax^{-/-}Bak^{sh}$ cells but not in the control counterparts. The results disclose that cell proliferation is inhibited by DHA in HCT116 $Bax^{-/-}Bak^{sh}$ cells and indicates that the cell cycle inhibitors $p21^{WAF1/Cip1}$ and $p27^{KIP1}$ contributed to this effect, especially when treatment occurred in hypoxia.

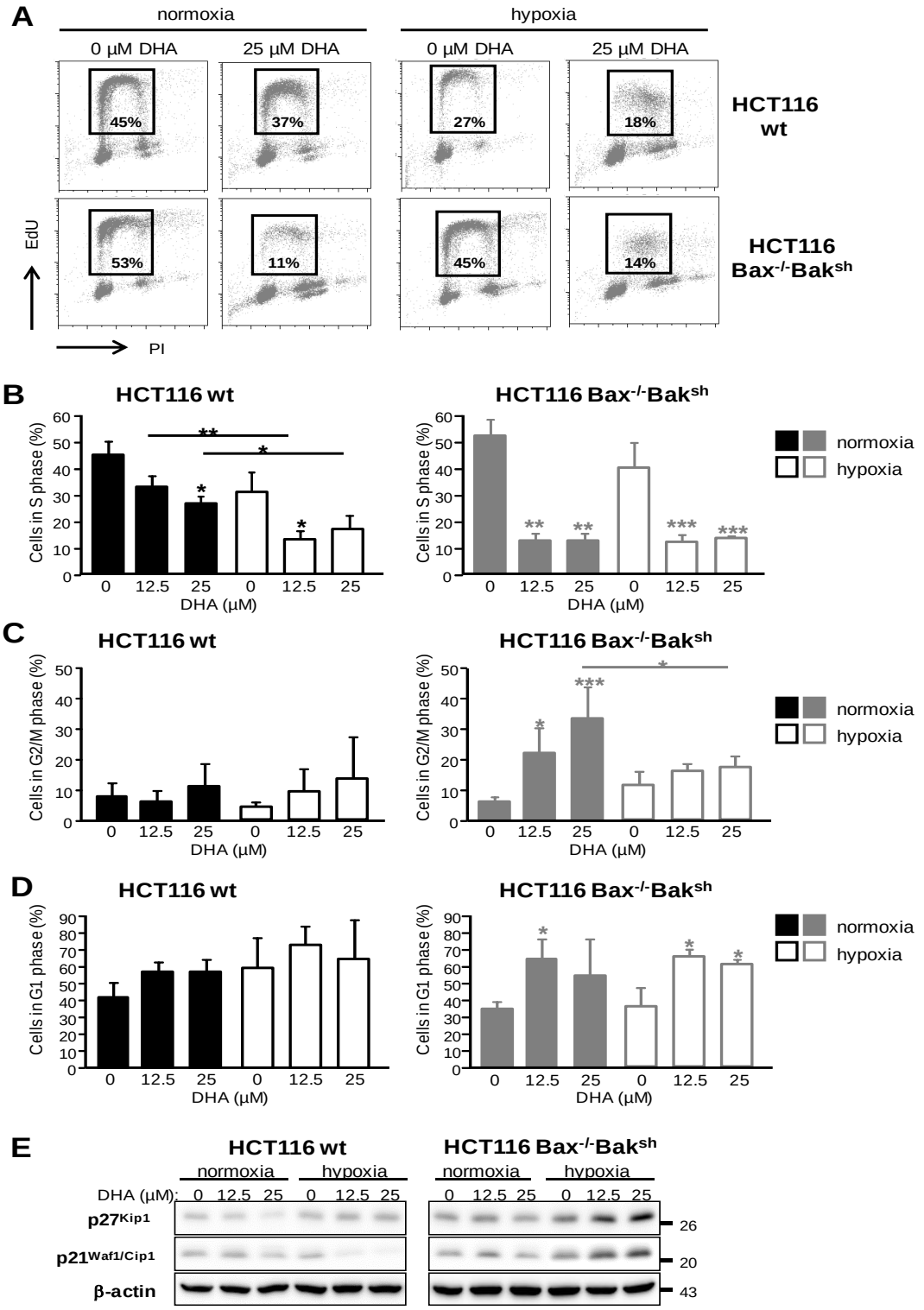

Figure 3.15 DHA induces cell cycle arrest preferentially in HCT116 Bax$^{-/-}$Bak^{sh} cells. *Cells were treated with DHA (0 µM, 12.5 µM, 25 µM) in normoxia or hypoxia. After 24 h EdU incorporation and intercalating propidium iodide (PI) was detected by flow cytometry (A-D). (A) Data shows representative dot plots of EdU incorporation. Squares tag cells in S phase. (B) Bars show cells in S phase, (C) in G2/M phase and (D) in G1 phase. DHA prevents proliferation more efficient in HCT116 Bax$^{-/-}$Bak^{sh} cells. (E) Protein expression of cell cycle inhibitors was detected by Western blot. Levels of p27^{Kip1} and p21$^{Waf1/Cip1}$ were increased only in HCT116 Bax$^{-/-}$Bak^{sh} cells following 24 h DHA treatment in hypoxia. Data shows representative Western blots. (B, C, D): Means ± SD (n=3). *, p < .05; **, p < .01; ***, p < .001 (ANOVA with Bonferroni post-hoc test).*

3.9 DHA-induced short-term cytotoxicity requires pro-apoptotic Bax and Bak

In the next set of experiments, DHA-induced cell death was analyzed. HCT116 wt and HCT116 Bax$^{-/-}$Bak^{sh} cells were treated with 12.5 and 25 µM DHA for 48 h in normoxia or hypoxia. Apoptosis induction was monitored by analysis of morphological changes using brightfield and fluorescence microscopy. DNA fragmentation, a hallmark of apoptosis, was quantified by flow cytometry analyzing the sub-G1 fraction, while activation of caspases was examined by Western blot, detecting cleavage of caspase-3 and of the caspase-3 substrate PARP (Fig. 3.16). Microscopic analysis demonstrates DHA-induced DNA condensation and formation of apoptotic bodies in HCT116 wt cells treated in normoxia (Fig. 3.16 A). In hypoxia, apoptotic cells were less frequent. In HCT116 Bax$^{-/-}$Bak^{sh} cells, DNA condensation and apoptotic bodies were scarce upon treatment in normoxia, while these features were completely absent after treatment in hypoxia. Interestingly, we observed detachment of HCT116 Bax$^{-/-}$Bak^{sh} cells after treatment with DHA in normoxia. In addition, the overall cell density was lower in DHA-treated HCT116 Bax$^{-/-}$Bak^{sh} cells compared to non-treated control cells, particularly when treatment was applied in normoxia. Quantification of DNA fragmentation by flow cytometry revealed a dose-dependent increase in apoptosis induction in HCT116 wt cells (Fig. 3.16 B). In normoxia, apoptosis was induced in more than 25% HCT116 wt cells after treatment with 12.5 µM DHA and almost 50% after treatment with 25 µM DHA. In hypoxia, apoptosis induction was less effective, reaching only 10 and 15%, respectively. In HCT116 Bax$^{-/-}$Bak^{sh} cells treated with DHA in normoxia, the apoptosis rate was further reduced to approximately 10%. In HCT116 Bax$^{-/-}$Bak^{sh} cells treated with DHA in hypoxia, apoptosis was hardly detectable. Correspondingly, Western blot analysis revealed a pronounced caspase-3 cleavage and cleavage of its substrate PARP in HCT116 wt cells treated with DHA in normoxia. Caspase-3 and PARP cleavage were reduced in HCT116 wt cells treated with DHA in hypoxia (Fig. 3.16 C). As expected, in HCT116 Bax$^{-/-}$Bak^{sh} cells that were incapable of inducing the intrinsic apoptosis pathway, no caspase-3 or PARP cleavage could be detected.

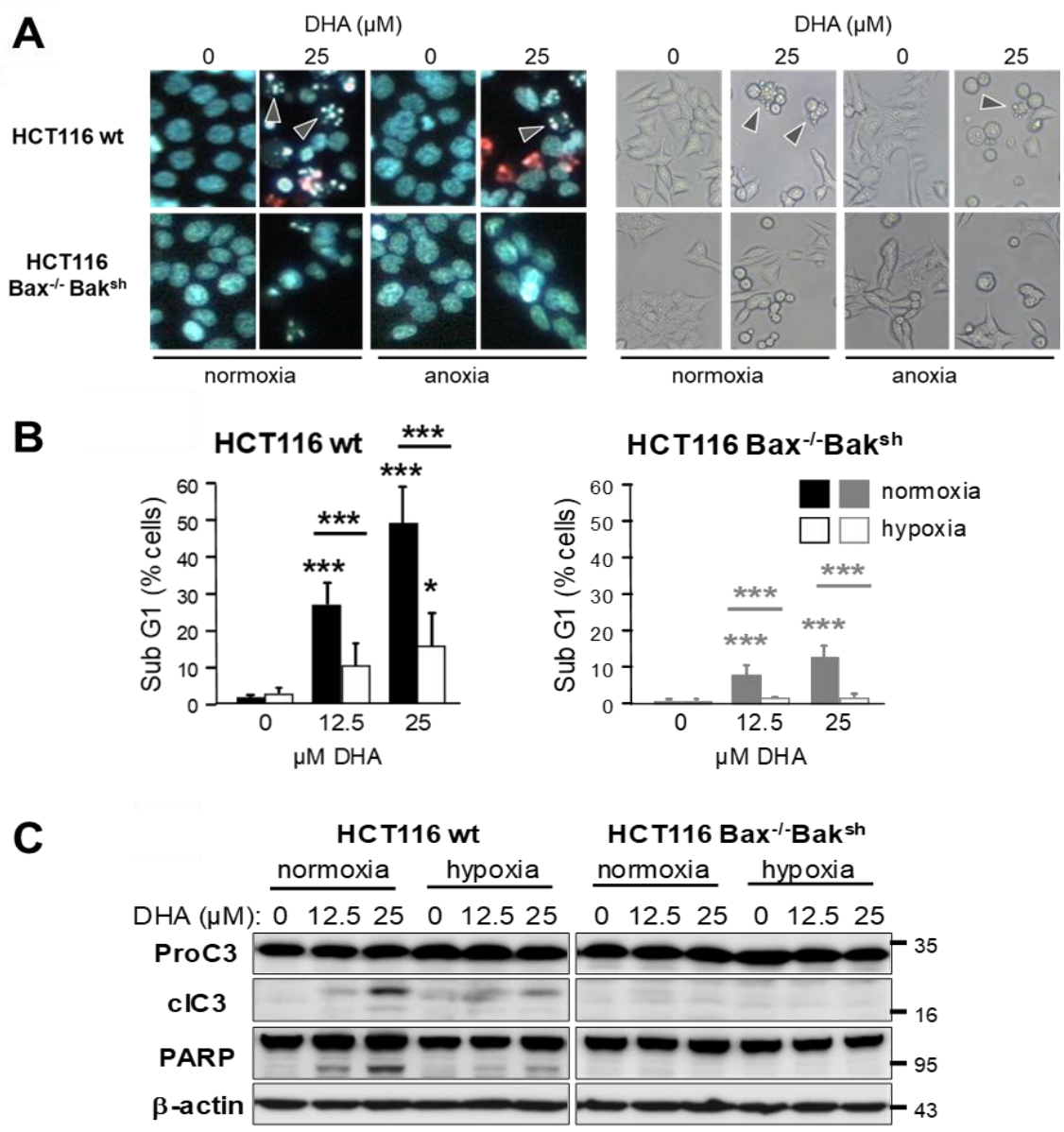

Figure 3.16 DHA-induced apoptosis is reduced in hypoxia and abrogated in HCT116 Bax$^{-/-}$Bak^{sh} cells. *Cells were treated with DHA (0 µM, 12.5 µM, 25 µM) for 48 h in normoxia or hypoxia. (A) DNA condensation was detected by Hoechst3342/PI-staining to distinguish between apoptotic and non-apoptotic cell death. Images were taken using fluorescence microscopy (left panel) and phase-contrast brightfield microscopy (right panel). Arrows point at apoptotic cells. Representative images are shown. Bars indicate 10 µm. (B) Apoptosis was quantified by flow cytometry, analyzing DNA fragmentation (sub-G1 cells) 48 h after treatment with DHA. DHA induced apoptosis particularly in HCT116 wt cells treated in normoxia. Means ± SD (n=3). *, p < .05; **, p < .01; ***, p < .001 (ANOVA with Bonferroni post-hoc test). (C) Apoptosis was analyzed by Western blot, detecting cleavage of caspase-3 and the caspase-3 substrate PARP 24 h after DHA treatment. Data shows representative Western blots.*

In addition, total cell death upon treatment with DHA was analyzed by PI exclusion assay and by detecting the dissipation of the mitochondrial membrane potential (ΔΨm low) (Fig. 3.17). In contrast to apoptosis induction, DHA induced death in

HCT116 wt cells with similar efficiency in normoxia and hypoxia (Fig. 3.17 A and B). Cell death induction in HCT116 Bax$^{-/-}$Bak^{sh} cells upon treatment with DHA in normoxia was considerably lower than in HCT116 wt cells. In hypoxia, cell death of HCT116 Bax$^{-/-}$Bak^{sh} cells was completely abrogated.

In conclusion, the results disclose that insufficient expression of pro-apoptotic Bax and Bak protects cells from DHA-induced cell death in the first 48 h after treatment with DHA. In HCT116 wt cells, apoptosis was the prevalent mechanism of DHA-induced cytotoxicity in normoxia, while oxygen deprivation shifts the cells towards a caspase-independent form of cell death. However, both modes of cell death obviously depend on expression of the Bcl-2 family proteins Bax and Bak.

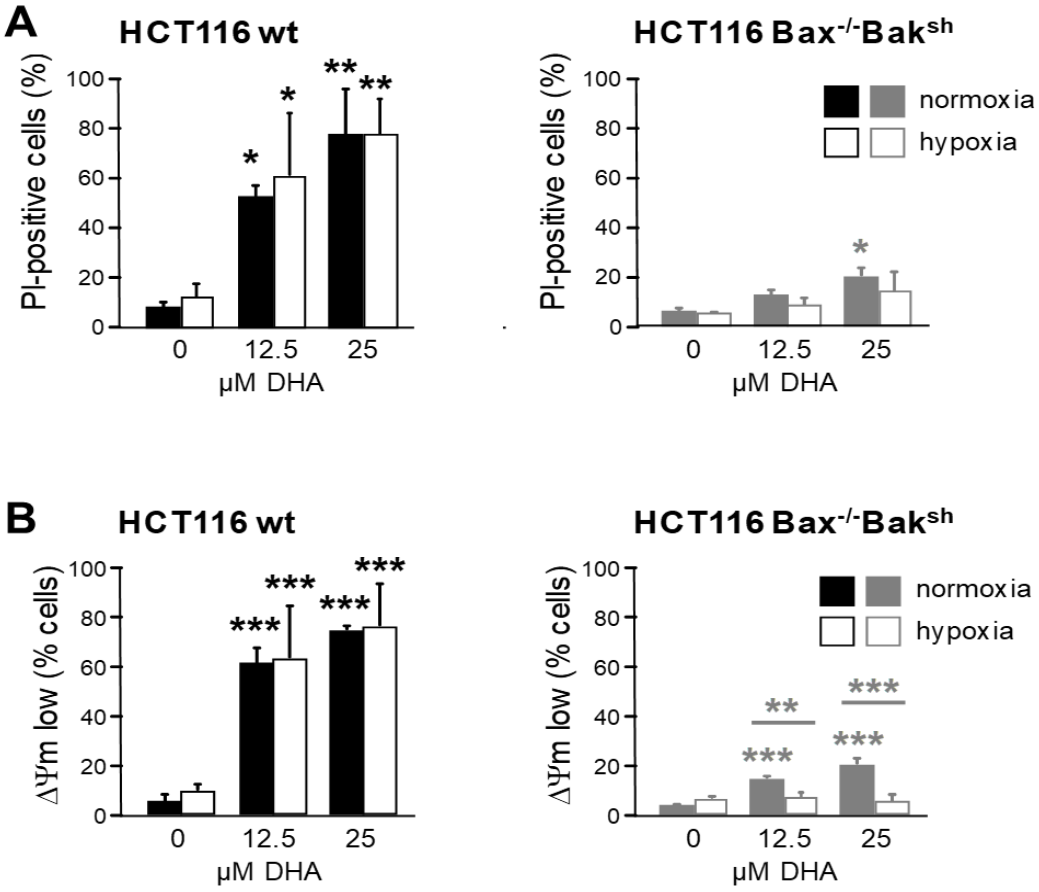

Figure 3.17 Loss of Bax and Bak abrogates DHA-induced cell death in normoxia and hypoxia. *Cells were treated with DHA (0 µM, 12.5 µM, 25 µM) for 48 h in normoxia or hypoxia. (A) Total cell death was analyzed by flow cytometry using propidium iodide (PI) exclusion assay and (B) by detecting cells with dissipated mitochondrial membrane potential (ΔΨm low). DHA induced cell death with similar efficiency in HCT116 wt cells in normoxia and hypoxia, but was inefficient in HCT116 Bax$^{-/-}$Bak^{sh} cells. (A, B): Means ± SD (n=3). *, p < .05; **, p < .01; ***, p < .001 (ANOVA with Bonferroni post-hoc test).*

3.10 Autophagy contributes to DHA-induced cell death in HCT116 wt cells in normoxia but not in hypoxia

Proteins of the Bcl-2 family regulate apoptosis execution, but are also involved in autophagy [153]. A widely accepted marker for autophagy induction is accumulation of LC3BII, the lipidated form of LC3BI [115]. We detected both forms of LC3B upon treatment with DHA by Western blot and quantified LC3BII by flow cytometry. Under basal conditions, we observed that loss of Bax and concurrent diminished Bak expression resulted in less LC3BII and increased LC3BI levels, indicating decreased autophagy in HCT116 $Bax^{-/-}Bak^{sh}$ cells compared to HCT116 wt cells (Fig. 3.18 A). Treatment with DHA for 24 h increased in the lipidated LC3BII, indicating autophagy induction. Autophagy induction was more efficient in HCT116 $Bax^{-/-}Bak^{sh}$ cells than in HCT116 wt cells (Fig. 3.18 B). In both cell lines, the increase was more pronounced in normoxia than in hypoxia. Since execution of autophagy is indicated by decreasing p62 levels, p62 protein was additionally detected by Western blot. We observed decreased p62 levels in response to DHA treatment in hypoxia, irrespective of Bax/Bak expression. Quantification of membrane-bound LC3BII levels was performed by flow cytometry following washout of cytosolic LC3BI (Fig. 3.18 C and D). Treatment with DHA for 24 h in normoxia significantly increased LC3BII insertion into membranes in HCT116 wt and HCT116 $Bax^{-/-}Bak^{sh}$ cells. Consistent with the previous results, this effect was more pronounced in HCT116 $Bax^{-/-}Bak^{sh}$ than HCT116 wt cells and more effective in normoxia than in hypoxia. In this assay, 20 µM chloroquine (CQ) was used as a positive control and resulted in a marked LC3BII accumulation. CQ disrupts the fusion of autophagosomes with lysosomes, thereby inhibiting the autophagic flux. To examine the impact of autophagy on DHA-induced cytotoxicity, cell death was quantified by flow cytometry using PI exclusion assay following co-treatment with CQ (Fig. 3.18 E). Treatment with 20 µM CQ did not affect cell survival but it significantly diminished DHA-induced cell death in HCT116 wt cells when treated in normoxia. When treatment occurred in hypoxia, co-treatment with CQ had no impact on DHA-induced cell death. These results demonstrate that autophagy induction contributes to DHA-induced cytotoxicity in normoxia but is dispensable in hypoxia. Since previous results have shown that DHA-induced cell death depends on Bax/Bak expression, inhibition of autophagy did not influence cell viability in HCT116 $Bax^{-/-}Bak^{sh}$ cells.

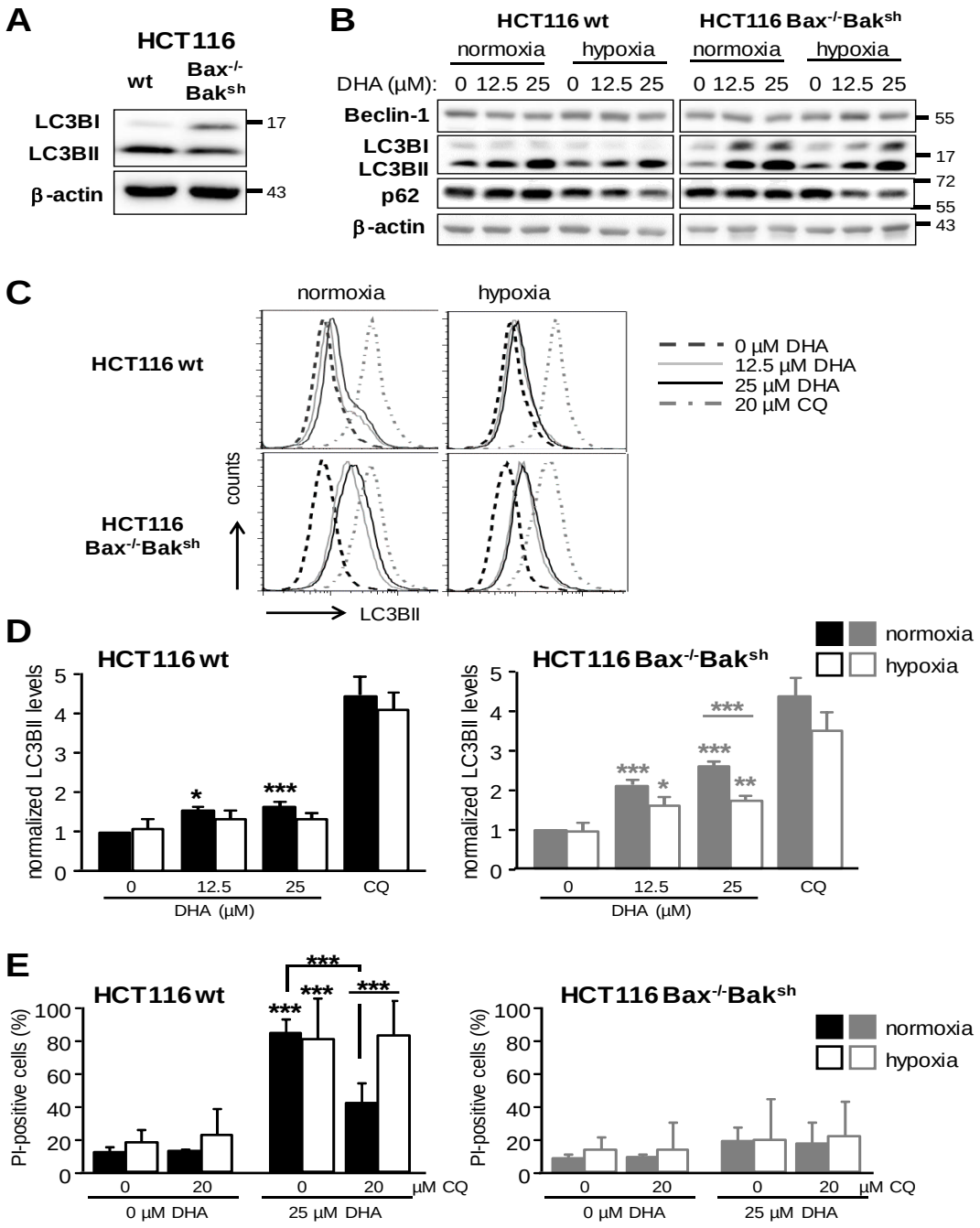

Figure 3.18 DHA-induced autophagy contributes to cell death induction in normoxia in HCT116 wt cells. *(A) Basal protein expression of LC3BI and LC3BII in non-treated HCT116 wt and HCT116 Bax$^{-/-}$Bak^{sh} cells in normoxia, detected by Western blot. Loss of Bax and Bak decreases autophagy induction under steady-state conditions. (B) Western blots analysis demonstrates increased LC3BII levels after treatment with DHA (0 μM, 12.5 μM, 25 μM) for 24 h in normoxia and less effective increase in hypoxia, indicating autophagy induction. DHA-induced execution of autophagy (decrease of p62 levels) was detected exclusively after treatment with DHA in hypoxia in both cell lines. (C, D) Quantification of membrane bound LC3BII after wash out of cytosolic LC3BI by flow cytometry 24 h after treatment with DHA (0 μM, 12.5 μM, 25 μM) in normoxia or hypoxia confirms the results in Western blot. In control experiment, cells were treated with CQ (20 μM) to interrupt autophagic flux and accumulate LC3BII. (C) shows representative histograms and (D) the mean fluorescence intensity of LC3BII. (E) Cell death following co-treatment with CQ was analyzed by flow cytometry using PI exclusion assay. Co-treatment with CQ reduced DHA-induced cell death in HCT116 wt cells. (D, E): Means ± SD (n=3). *, p < .05; **, p < .01; ***, p < .001 (ANOVA with Bonferroni post-hoc test).*

3.11 DHA increases ROS production

Previous publications linked DHA-induced cytotoxicity to intracellular ROS production [132]. For this reason, we first analyzed general ROS production in HCT116 wt and HCT Bax$^{-/-}$Bak^{sh} cells treated in normoxia and hypoxia by flow cytometry using DHE dye (Fig. 3.19 A). In both cell lines, DHA induced a dose-dependent increase in DHE-positive cells, but the increase was more pronounced in HCT116 wt compared to HCT Bax$^{-/-}$Bak^{sh} cells. DHA-induced ROS production was significantly higher in normoxic than in hypoxic conditions and could be diminished by co-treatment with the antioxidant N-acetylcyteine (NAC). Moreover, DHA-induced ROS production correlated with γH2A.X (p-H2A.X) levels, a marker for activation of DNA double strand break repair pathway (Fig. 3.19 B).

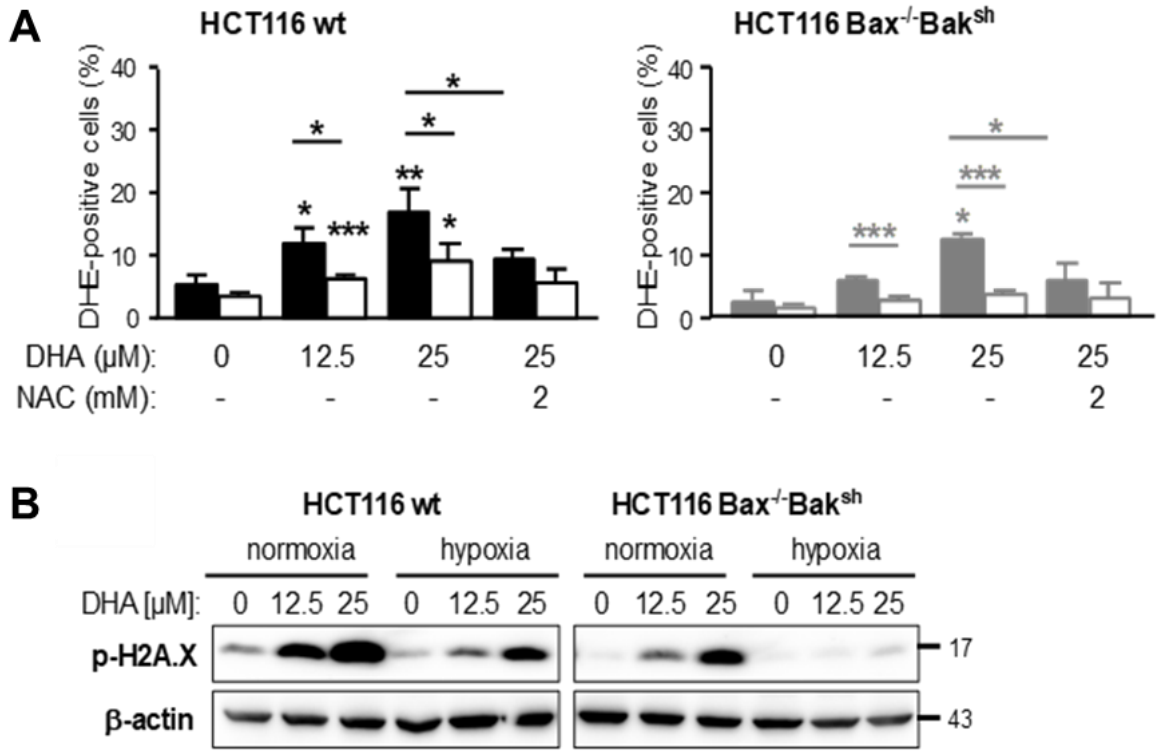

Figure 3.19 DHA-induced ROS production in normoxic and hypoxic HCT116 wt and HCT116 Bax$^{-/-}$Bak^{sh} cells. *Cells were treated with DHA (0 µM, 12.5 µM, 25 µM) in normoxia or hypoxia for 24 h. (A) Intracellular ROS production was analyzed by flow cytometry using the ROS-sensitive dye DHE. In normoxia, DHA increased ROS levels more efficient than in hypoxia. DHA-induced ROS production was more pronounced in HCT116 wt cells than in Bax$^{-/-}$Bak^{sh} cells. Co-treatment with 2 mM of the antioxidant N-acetylcysteine (NAC) reduced DHA-induced ROS production. (B) Protein expression of phosphorylated H2A.X (p-H2A.X) was analyzed by Western blot. Induction of p-H2A.X levels, indicating activation of DNA double strand break repair, correlated with DHA-induced ROS production. (A): Means ± SD (n=3). *, p < .05; **, p < .01; ***, p < .001 (ANOVA with Bonferroni post-hoc test).*

In previous experiments, we detected increased mitochondrial ROS production in NCI-H460 lung cancer cells expressing MitoTimer upon treatment with DHA in normoxia. Mitochondrial ROS production was accompanied by mitochondrial fragmentation and abrogation of mitochondrial function (Fig. 3.20). In addition to normoxia, we aimed to detect mitochondrial ROS production also in hypoxia in HCT116 wt and HCT116 $Bax^{-/-}Bak^{sh}$ colorectal cancer cells. To analyze mitochondrial ROS production, we used MitoSOX™ Red, a dye that reacts specifically with superoxide anions largely produced at mitochondria (Fig. 3.20 A and B). The mean fluorescence intensity of MitoSOX™ Red dye increased following treatment with DHA, indicating mitochondrial superoxide anion production. Surprisingly, DHA-induced superoxide anion production was similar in HCT116 wt and HCT116 $Bax^{-/-}Bak^{sh}$ cells. In both cell lines, mitochondrial ROS production was lower when cells were treated in hypoxia. In conclusion, the data suggests mitochondrial ROS production is not the underlying cause for the differences in total ROS production between HCT116 wt and HCT116 $Bax^{-/-}Bak^{sh}$ cells in response to DHA.

Since an increased mitochondrial ROS production is indicative for mitochondrial damage, we analyzed mitochondrial respiration and ATP production 24 h after treatment with DHA in normoxia and hypoxia (Fig. 3.20 D and E). In normoxia, no differences in basal oxygen consumption rate and ATP production were observed between HCT116 wt and HCT116 $Bax^{-/-}Bak^{sh}$ cells (Fig. 3.20 C). Both, basal oxygen consumption and ATP production significantly decreased after exposing the cells to hypoxia for 24 h. Hypoxia-induced decrease of mitochondrial function was even more pronounced in HCT116 wt cells than in HCT116 $Bax^{-/-}Bak^{sh}$ cells. Treatment with low dose of DHA (6.25 – 25 µM) significantly reduced mitochondrial respiration and ATP production in both cell lines, but was more efficient in HCT116 wt than in HCT116 $Bax^{-/-}Bak^{sh}$ cells (Fig. 3.20 D and E). In hypoxia, DHA scarcely influenced mitochondrial reparation and ATP production in HCT116 $Bax^{-/-}Bak^{sh}$ cells, but further decreased the already low levels in HCT116 wt cells. Taken together, the results suggest an adaptation process in response to oxygen deprivation by shutting down mitochondrial function, which was more effective in HCT116 wt cells than in HCT116 $Bax^{-/-}Bak^{sh}$ cells. In addition, DHA-induced inhibition of mitochondrial function was more efficient in HCT116 wt cells than in HCT116 $Bax^{-/-}Bak^{sh}$ cells.

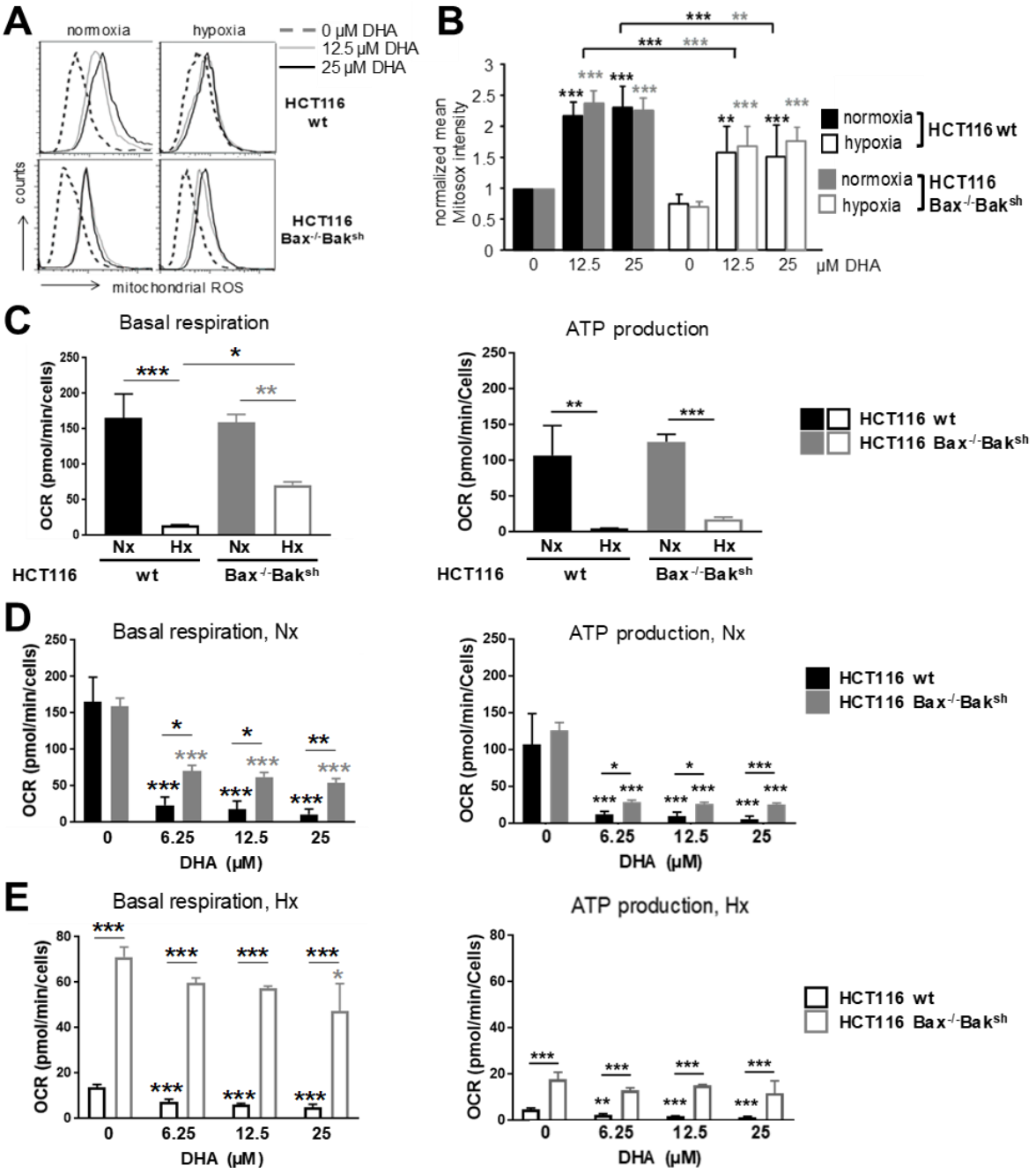

Figure 3.20 DHA-induced mitochondrial ROS production and abrogation of mitochondrial respiration in normoxic and hypoxic HCT116 wt and HCT116 Bax$^{-/-}$Bak^{sh} cells. *(A, B) 24 h after treatment with DHA (0 µM, 12,5 µM, 25 µM) in normoxia and hypoxia, mitochondrial ROS production was analyzed by flow cytometry after staining cells with MitoSOX. (A) shows representative histograms and (B) the mean fluorescence intensity. DHA-induced ROS production is more pronounced in normoxia compared to hypoxia. (C) Basal mitochondrial respiration and ATP production were detected with the Seahorse analyzer employing mitochondrial stress test. Oxygen deprivation downregulates mitochondrial respiration more efficiently in HCT116 wt than in HCT116 Bax$^{-/-}$Bak^{sh} cells. (D, E) Oxygen consumption was analyzed employing mitochondrial stress test 24 h after treatment with DHA with DHA (6,25 µM, 12,5 µM, 25 µM) in normoxia (Nx) and hypoxia (Hx). (D) Basal respiration and ATP production were reduced more efficiently in HCT116 wt than in HCT116 Bax$^{-/-}$Bak^{sh} cells following treatment with DHA in normoxia. (E) The already low basal respiration and ATP production were further decreased in HCT116 wt cell after treatment with DHA in hypoxia, while oxygen consumption was hardly affected in HCT116 Bax$^{-/-}$Bak^{sh} cells following treatment in same conditions. (B, C, D): Means ± SD (n=3). *, p < .05; **, p < .01; ***, p < .001 (ANOVA with Bonferroni post-hoc test).*

3.12 DHA-induced lipid peroxidation is more severe in hypoxia than in normoxia

We have demonstrated that treatment with DHA in normoxia induced oxidative damage to biomolecules, such as proteins and lipids, and organelles, such as mitochondria (Fig. 3.1, 3.2 and 3.3). Since previous experiments demonstrated an increased cytosolic and mitochondrial ROS production after treatment with DHA in normoxia and hypoxia, we intended to analyze the oxidative damage in both, HCT116 wt and Bax$^{-/-}$Bak^{sh} cells under normoxic and hypoxic conditions. Thus, lipid peroxidation was analyzed by flow cytometry and fluorescence microscopy using the lipophilic oxidation sensor BODIPY 581/591 C11 (Fig. 3.21 A and B). Treatment with 25 µM DHA for 24 h induced lipid peroxidation in HCT116 wt and HCT116 Bax$^{-/-}$Bak^{sh} cells. Interestingly, this effect was significantly more pronounced in hypoxia compared to normoxia (Fig. 3.21 A). Co-treatment with 50 µM of the iron chelating agent DFO completely abrogated DHA-induced lipid peroxidation in normoxia, but only partially decreased it in hypoxia. No differences between HCT116 wt and HCT116 Bax$^{-/-}$Bak^{sh} cells could be observed. Analysis by florescence microscopy revealed alterations in the localization of the oxidation sensor following exposure to hypoxia or incubation with DHA (Fig. 3.21 B). DHA treatment and oxygen deprivation resulted in accumulation of the oxidation sensor in lipophilic, droplet-like compartments. However, DHA facilitated lipid peroxidation in the plasma membrane of HCT116 wt and HCT116 Bax$^{-/-}$Bak^{sh} cells irrespective of the oxygen concentration. The latter effect was decreased by iron depletion using DFO.

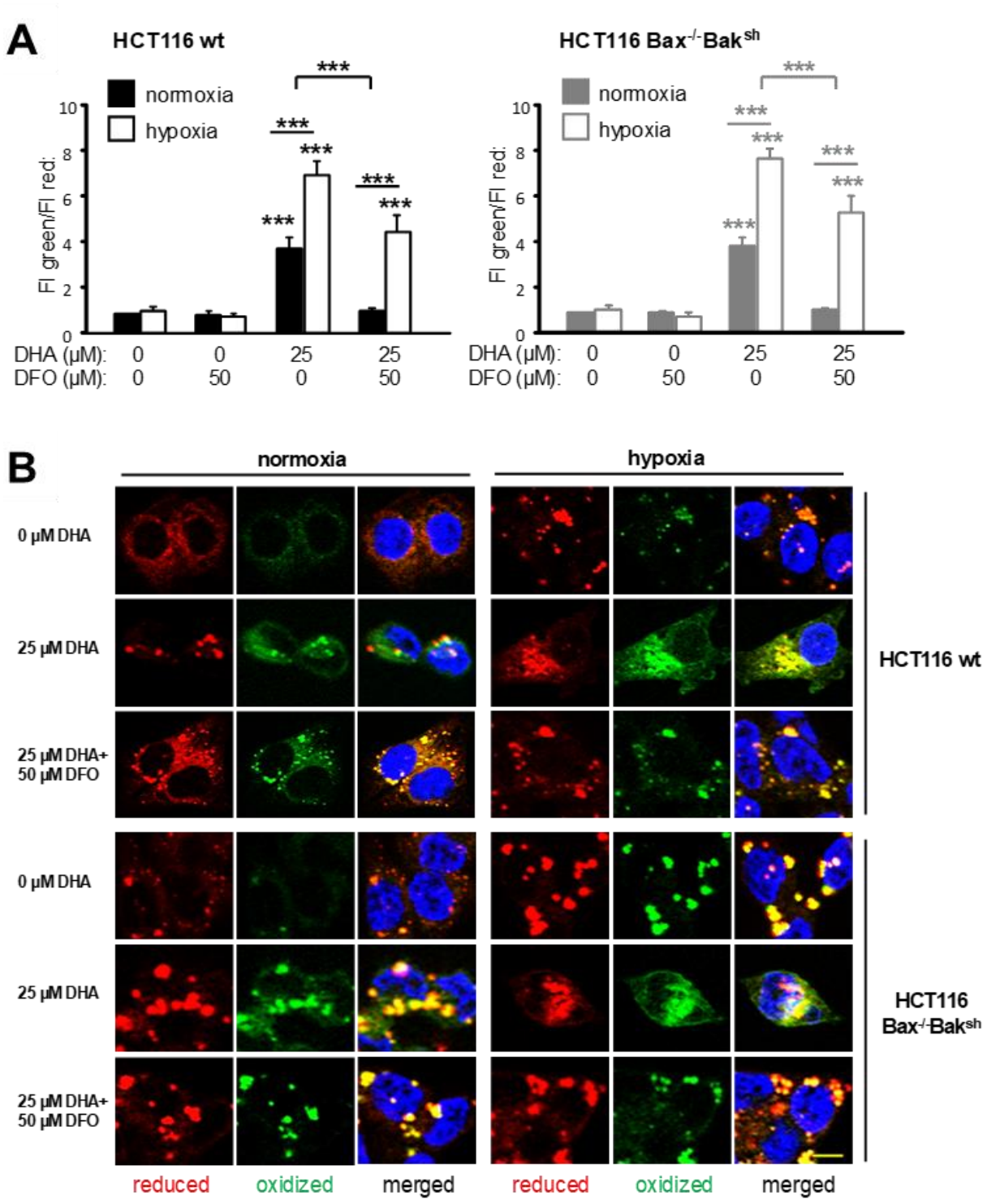

Figure 3.21 DHA-induced lipid peroxidation is higher in hypoxic than in normoxic cells. *Cells were treated with DHA (0 µM, 12.5 µM, 25 µM) for 24 h in normoxia or hypoxia. Lipid peroxidation was analyzed using the lipophilic oxidation sensor BODIPY 581/591 C11. (A) The ratio of oxidized (green)/reduced (red) dye was detected by flow cytometry measuring mean fluorescence intensity. Co-treatment with the iron-chelating compound deferoxamine (DFO) prevents DHA-induced lipid peroxidation in normoxia and partially lowers DHA-induced lipid peroxidation in hypoxia. (B) Representative images acquired by fluorescence microscopy are shown. (A): Means ± SD (n=3). ***, p < .001 (ANOVA with Bonferroni post-hoc test).*

The previous results have demonstrated that DHA-induced cytotoxicity is limited by activation of the antioxidative Keap1/Nrf2 pathway, accompanied by increased glutathione levels in HCT116 wt cells. Therefore, intracellular glutathione concentrations were also detected in HCT116 Bax$^{-/-}$Bak^{sh} cells 24 h after treatment with DHA in normoxia and hypoxia (Fig. 3.22). In normoxia, the basal glutathione levels were slightly but insignificantly higher in HCT116 Bax$^{-/-}$Bak^{sh} cells compared to HCT116 wt cells. Treatment with 25 µM DHA increased the levels to a similar extend in both cell lines. Oxygen deprivation for 24 h decreased glutathione concentrations by around 50% in HCT116 wt and HCT116 Bax$^{-/-}$Bak^{sh} cells. Treatment with DHA in hypoxia did not affect intracellular glutathione levels. In summary, the results revealed that DHA induces lipid peroxidation more efficiently in hypoxia than in normoxia. The lower glutathione levels are likely responsible for increased lipid peroxidation in hypoxia. The observed effect on lipid peroxidation is independent of Bax and Bak.

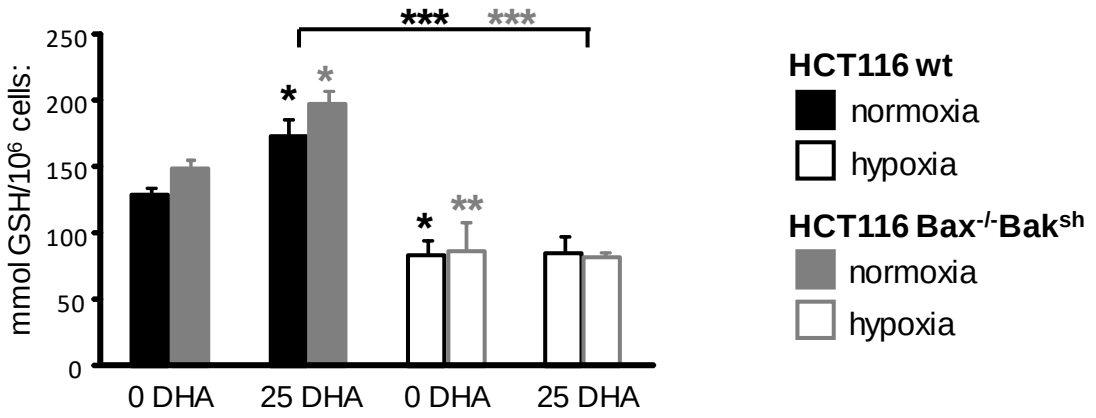

Figure 3.22 Incubation in hypoxia lowers glutathione levels and abrogates DHA-induced increase of glutathione levels observed in normoxia. *Intracellular glutathione concentration was analyzed biochemically. DHA induced an increase of glutathione levels exclusively in normoxia. Exposure to hypoxia decreased basal glutathione levels. Means ± SD (n=3). *, p < .05; ***, p < .001 (ANOVA with Bonferroni post-hoc test).*

3.13 DHA induced a delayed ferroptosis-like death in HCT116 Bax$^{-/-}$Bak^{sh} cells following treatment with DHA in hypoxia

The previous results demonstrated that treatment with DHA for 48 h only a marginally induced cell death in HCT116 Bax$^{-/-}$Bak^{sh} cells, but DHA-induced cell death at later time points has not been examined yet. This was analyzed in the next sets of experiments. HCT116 Bax$^{-/-}$Bak^{sh} cells were treated for 2 days with DHA in hypoxia and afterwards removed to normoxia for 7 days. HCT116 Bax$^{-/-}$Bak^{sh} cells treated with DHA in normoxia for 9 days served as a control. Microscopic analysis revealed decreased cell density after treatment with 25 µM DHA in normoxia compared to non-treated cells (Fig 3.23 A). In contrast, when HCT116 Bax$^{-/-}$Bak^{sh} cells were treated in hypoxia for the first 2 days, cell density was even lower and an excessive cell detachment was observed. This observation was confirmed by flow cytometric analysis detecting cell death with PI exclusion assay (PI-positive cells) and apoptosis by DNA fragmentation (sub-G1 fraction). After treatment with DHA in hypoxia, cell death was induced in 70 – 90% of HCT116 Bax$^{-/-}$Bak^{sh} cells, while cell death was only slightly and insignificantly elevated 9 days after treatment with DHA in normoxia (Fig. 3.23 B). Detection of DNA fragmentation revealed that only a minor part of DHA-induced cell death in hypoxia of approximately 20% could be linked to apoptosis (Fig. 3.23 C). Moreover, co-treatment with CQ did not affect cell death in HCT116 Bax$^{-/-}$Bak^{sh} cells treated with DHA in hypoxia, indicating that autophagic cell death was not involved in DHA-induced cytotoxicity under oxygen deprived conditions (Fig. 3.23 D). To sum up, the data demonstrates that insufficient expression of Bax and Bak prevented cell death induction after treatment with DHA in normoxia, but did not prevent the delayed cell death after initial treatment with DHA in hypoxia.

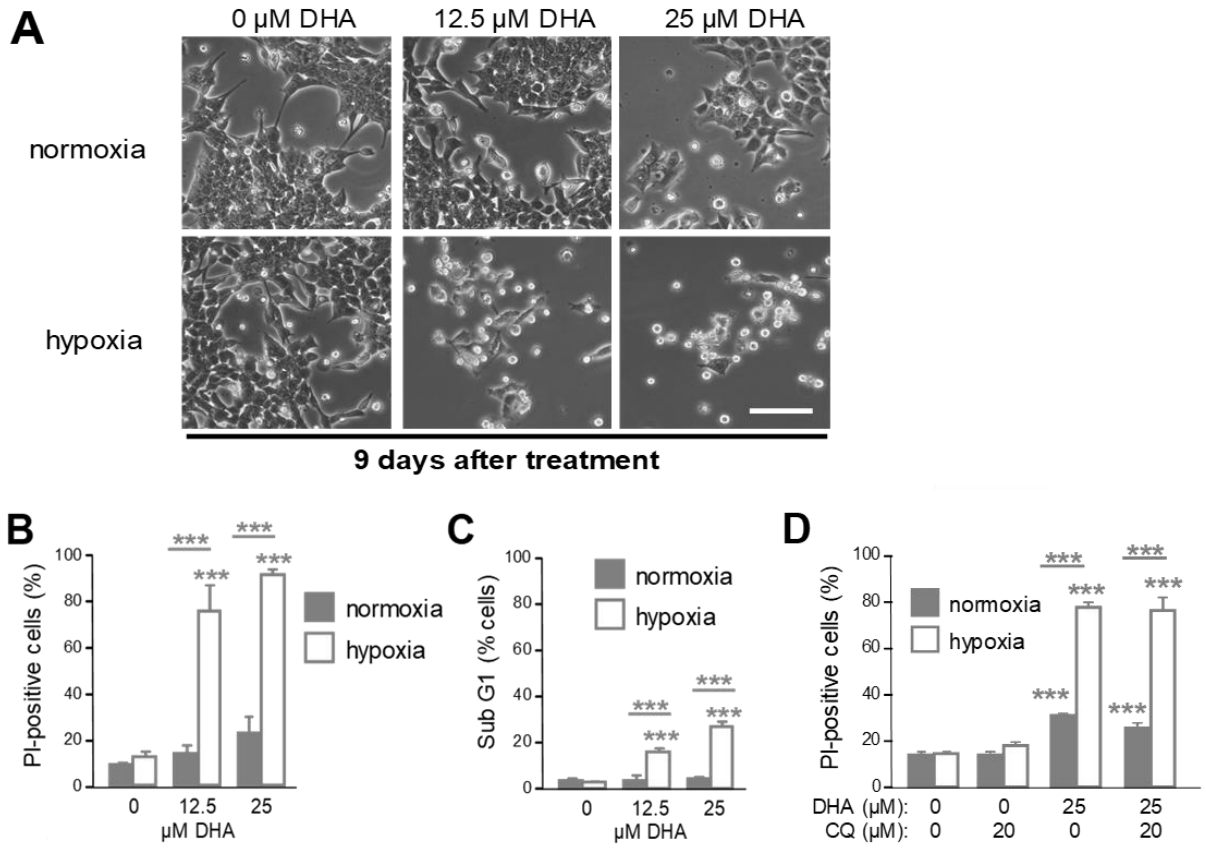

Figure 3.23 DHA induces delayed cell death in HCT116 Bax$^{-/-}$Bak^{sh} cells treated in hypoxia. *HCT116 Bax$^{-/-}$Bak^{sh} cells were treated with DHA (0 µM, 12.5 µM, 25 µM) in normoxic or hypoxic conditions for 9 days. Cells treated in hypoxia were returned to normoxia after 2 days and cultivated for another 7 days. Cell death was analyzed by phase-contrast microscopy (A) and by flow cytometry using propidium iodide (PI) exclusion assay (B and D). (A, B) Treatment with DHA in hypoxia induced massive cell death. (C) Apoptosis was analyzed by flow cytometry detecting DNA fragmentation (sub-G1 fraction). Only a minor part of DHA-induced cell death can be attributed to apoptosis. (D) Co-treatment with 20 µM chloroquine (CQ) did not affect DHA-induced delayed cell death. (A): Data show representative images. Bar indicates 20 µM. (B-D): Means ± SD (n=3). ***, p < .001 (ANOVA with Bonferroni post-hoc test).*

4 Discussion

4.1 The anti-malaria drug DHA in a combinatory therapy with ionizing radiation

Radiotherapy and surgery are common approaches in the treatment of lung and colorectal cancers. Radiation is either applied adjuvant to increase eradication of cancer cells that remained in tissue after surgery, or neoadjuvant to shrink tumor volume before surgery [154]. Cytotoxicity of ionizing radiation is based on a direct induction of DNA double strand breaks (DSB) and on indirectly induced oxidative damage of cellular biomolecules resulting from increased ROS production [155]. The importance of ROS production in IR-induced cytotoxicity becomes evident in tumor cells with activated antioxidant pathways, in which efficacy of radiotherapy is limited [131, 145]. In order to improve the anti-neoplastic effect of IR, radiotherapy is commonly combined with chemotherapeutic drugs, immunotherapy or molecular-targeting therapies. Enhanced normal tissue toxicity limits the doses applied in these anti-neoplastic therapies. Moreover, great costs and inaccessibility to these therapies, which is common in less developed countries, restrict the combat against cancer [3]. In order to evade the monetary and safety problems and improve radiotherapy, the present study intends to boost ROS production with DHA, a cheap drug with a high tolerability, that is already approved for treatment of malaria.

4.1.1 DHA induces iron-dependent oxidative damages

The first experiments of the present study were performed to improve our understanding of the anti-neoplastic effects induced by DHA. To examine the impact of the ROS-producing anti-malaria drug in different tumor entities, oxidative damage was detected in NCI-H460 lung adenocarcinoma and HCT116 colon cancer cells. In both cell lines, DHA damaged lipids and proteins by oxidation, depending on intracellular iron availability. These findings are in line with the postulated iron-dependent activation of DHA in the malaria parasite and recent observations, which linked iron-dependent ROS production with induction of ferroptosis in different cancer cells [86, 89, 156-158]. Iron-dependent DHA activation may not only result in ROS production, but also in direct interaction of the produced DHA radicals with reactive groups of cellular biomolecules. Unfortunately, less is known about such modifications. Further research is needed to resolve whether they are more difficult to repair than oxidative damage, to which extend they contribute to cell death and whether

preferential targets exist. Beside induction of ferroptosis, previous publications also detected other forms of cell death, such as apoptosis, necrosis and autophagy-associated cell death [132, 159, 160]. The severity of oxidative damage and the type of cell death induced by DHA most likely depend on the applied concentration, the molecular background of the targeted cell and the microenvironment.

The results obtained in the present study suppose that mitochondrial damage plays a major role in DHA-induced cytotoxicity, since DHA provoked a severe oxidation of thiol groups in mitochondrial proteins. Unfortunately, methanol was required for fixation of dimedone labeled cells, which fosters a wash out of cytosolic proteins. Hence, it cannot be excluded that DHA inflicts oxidative damage on cytosolic macromolecules.

The distinct oxidation of mitochondrial proteins in response to DHA was accompanied by a massive mitochondrial ROS production, indicating mitochondrial damage. Damaged mitochondria can produce even more ROS via the ETC than healthy mitochondria [140]. The continuing ROS stress could facilitate oxidation of the mitochondria-specific phospholipid cardiolipin which binds cytochrome c. Cardiolipin oxidation results in cytochrome c dissociation and subsequent induction of the cytochrome c peroxidase activity. Peroxidase activity can further propagate cardiolipin oxidation, resulting in execution of apoptosis through mitochondrial membrane permeabilization and cytochrome c release [161]. In addition to mitochondrial protein oxidation and ROS production, an increased mitochondrial fragmentation was observed by fluorescence microscopy. Mitochondrial fusion and fission occur constantly in the cell. These changes allow mitochondria to exchange content and adapt their metabolism to changing environmental conditions [162, 163]. Consequently, the morphological changes of mitochondria are indispensable for cell survival and growth. In addition, a recent observation detected a cytoprotective role of mitochondrial fission by regulating plasma membrane repair pathways [164]. On the contrary, excessive fragmentation of mitochondria is frequently associated with mitochondrial dysfunction and cell death [165]. In the present study, DHA-induced mitochondrial protein oxidation and fragmentation resulted in a hampered respiration and abrogated ATP-production in lung and colorectal cancer cells, indicating a massive mitochondrial damage.

4.1.2 Antioxidant Keap1/Nrf2 pathway limits DHA-induced cytotoxicity

4.1.2.1 Keap1 mutation protects against DHA-induced short-term cytotoxicity

DHA efficiently damaged biomolecules in an oxygen-dependent fashion, but the level of protein oxidation and the impairment of mitochondrial function were more pronounced in HCT116 cells than in NCI-H460 cells. Simultaneously with the mitochondrial changes, DHA induced short-term cell death more efficiently in HCT116 than in NCI-H460 cells. We hypothesized that the lower susceptibility of NCI-H460 cells to the prooxidative drug is attributed to an improved antioxidative defense. A recent publication identified a constant activation of the Keap1/Nrf2 pathway, a major regulator of the oxidative stress response in this lung adenocarcinoma cell line [142]. In healthy unstressed cells, the cytosolic protein Keap1 facilitates degradation of the transcription factor Nrf2. Oxidative stress causes dissociation of Nrf2 from the degrading protein complex, followed by nuclear translocation of the transcription factor Nrf2 and expression of antioxidant and detoxification genes [59, 60]. Among these target genes is SLC7A11, a subunit of the glutamate-cystine antiporter providing the cell with cysteine, the rate limiting amino acid in glutathione biosynthesis [48, 54].

In the present study, we detected a nuclear localization of Nrf2 in non-treated NCI-H460 cells, which was accompanied by low basal Keap1 protein levels and high expression levels of the target gene SLC7A11 as well as high intracellular glutathione concentrations. The identified mutation in the Nrf2 binding domain of Keap1 in NCI-H460 lung cancer cells [142] could disrupt the interaction of Keap1 with Nrf2, allowing the transcription factor to permanently accumulate in the nucleus and activate transcription of genes involved in cystine import and glutathione synthesis. Accordingly, high SLC7A11 and glutathione levels detected in NCI-H460 cells are most likely a result of a constant activation of this pathway, resulting in an improved antioxidant defense. As a consequence, NCI-H460 cells respond less sensitive to DHA with less oxidative damage and lower cell death rates than HCT116 cells.

Other researchers linked mutations in Keap1 to lung cancer progression and a poor patient survival [142, 143, 166]. The clinical relevance of this protective pathway in lung tumors was demonstrated by our pancancer study, which identified lung cancer as the tumor entity with the most frequent alterations in Keap1 gene. In addition, previous publications revealed Nrf2-dependent resistance towards chemo- and radiotherapy in several lung cancer cell lines [131, 167]. These findings emphasize the

Keap1/Nrf2 pathway as a potential target in the treatment of lung cancer with chemotherapeutic drugs as well as ionizing radiation.

4.1.2.2 DHA-induced activation of Keap1/Nrf2 pathway limits short-term cytotoxicity

In contrast to Keap1 mutant NCI-H460 cells, Keap1 wildtype HCT116 cells reacted more sensitive towards DHA-induced cell death. The lower basal glutathione levels in association with increased oxidative damage upon treatment with DHA demonstrate a less efficient oxidative defense in HCT116 than NCI-H460 cells. The cytosolic localization of Nrf2 and the high expression levels of Keap1 corroborated the inactive status of this pathway in HCT116 cells under unstressed control conditions. This was further confirmed by steady glutathione levels upon single treatment with the Nrf2 inhibitor ML385. In the lung carcinoma cell line with constantly activated Keap1/Nrf2 pathway, high basal glutathione levels were only marginally affected by Nrf2 inhibition and were still almost three times higher than in HCT116 cells. In contrast, high protein expression of SLC7A11 in NCI-H460 cells was decreased by Nrf2 inhibition but was still conclusively higher than in non-treated HCT116 cells. The ability of the Nrf2 inhibitor to decrease SLC7A11 protein levels but its failure to lower glutathione levels seems to be contradictory on the first sight. It is likely, however, that SLC7A11 protein is less stable and more quickly degraded than glutathione. In this case, a longer exposure to ML385 would also significantly drop glutathione levels.

In NCI-H460 cells, treatment with DHA increased SLC7A11 gene expression and protein levels in a Nrf2-dependent manner. However, intracellular glutathione levels were not affected. These results suggest a further activation of the Keap1/Nrf2 pathway in NCI-H460 cells by DHA and indicate that other factors than the cysteine availability restrict an additional increase of already high glutathione concentrations. In accordance with the unchanged glutathione levels upon Nrf2 inhibition in NCI-H460 cells, cell death was also not affected in response to co-treatment with DHA and the Nrf2-inhibitor in the first 48 h. In contrast, treatment with DHA dramatically increased glutathione levels in HCT116 cells in a Nrf2-dependent fashion, indicating an activation of the protective Keap1/Nrf2 pathway. This conclusion was supported by decreased Keap1 protein levels, Nrf2 nuclear translocation and increased expression of the Nrf2 target gene SLC7A11. Accordingly, inhibition of Nrf2 prevented DHA-induced increase of glutathione levels and further enhanced DHA-induced cell death in HCT116 cells. These observations reveal that DHA-induced activation of the Keap1/Nrf2 pathway limits the cytotoxicity of the prooxidative drug in Keap1 wildtype HCT116 cells.

Interestingly, cotreatment with erastin enhanced DHA-induced cell death after 48 h in both cell lines. Erastin directly blocks xCT transporter and cystine import [168]. Thus, erastin exerts a direct and faster impact on glutathione levels than the inhibition of Nrf2-regulated transcription of SLC7A11 using ML385. These results imply a subsequent erastin-induced decrease of cytoprotective glutathione concentrations, thereby enhancing DHA-induced cell death in both, Keap1 wildtype HCT116 and Keap1 mutant NCI-H460 cells.

4.1.2.3 Inhibition of Keap1/Nrf2 pathway increases DHA-induced long-term cytotoxicity irrespective of Keap1 mutation

Although concentrations of 12.5 µM DHA failed to induce short-term cell death in NCI-H460 lung cancer cells, long-term exposure to DHA significantly reduced the clonogenic survival. As stated above, we hypothesized that Nrf2 inhibition takes longer than 48 h to lower the constantly upregulated antioxidant defense and sensitize NCI-H460 cells to ROS-induced cytotoxicity. Longer exposure to the Nrf2 inhibitor ML385 together with DHA should further decrease NCI-H460 cell survival. Indeed, we observed a significant DHA-induced decline of the surviving fraction by concurrent Nrf2 inhibition in both, HCT116 and NCI-H460 cells, supporting this line of argumentation. In accordance with these findings, other researchers detected an enhanced cytotoxicity in lung cancer cells with Keap1 mutations when combining ML385 with carboplatin [143]. In addition, a further publication revealed Nrf2 as a resistance factor regulating cis-platin resistance in HCT116 colorectal cancer cells [169]. Taken together, the results obtained in the present study corroborate previous findings and clearly reveal that inhibition of Nrf2 improves the outcome of anti-cancer therapies, irrespective of Keap1 mutations.

4.1.3 DHA improves efficacy of radiotherapy

4.1.3.1 Combined therapy of DHA and IR is more efficient than single treatments

Resistance of tumor cells to ionizing radiation is a central obstacle in cancer therapy. Previous publications have demonstrated that activation of the antioxidant defense via Nrf2 confers resistance towards ROS-based therapies, due to an improved neutralization of drug- and radiation-induced ROS production [77, 131, 166, 167, 170] [131, 171]. Conversely, depletion of Nrf2 restored drug sensitivity and increased susceptibility to ionizing radiation in therapy resistant cancer cells [77, 131, 167, 172]. A wide range of tumors overexpresses Nrf2 and its target genes, which is often

correlated with a poor clinical outcome in patients [54]. In this study, analyzing the survival of patients with lung carcinoma undergoing radiotherapy, we detected SLC7A11 as a key molecule of the Keap1/Nrf2 pathway influencing the response to radiotherapy. In patients with a high SLC7A11 expression, radiotherapy correlated with a poor survival. Unfortunately, no data was available to examine the survival of patients with colorectal cancer after receiving radiotherapy. Collectively, the results of previous publications and our patient data analysis reveal that an activation of the antioxidative defense limits radiation-induced cytotoxicity and highlights the importance of ROS in conferring radiation-induced cytotoxicity.

Therefore, the present study aimed to improve the therapeutic efficacy of IR by further boosting ROS production with DHA. This strategy is based on the proposed *threshold concept for cancer therapy* [173], which implicates that an excessive amount of ROS triggers cell death by exhausting the cellular antioxidative capacity of cancer cells. In addition, it is suggested that the amount of ROS needed to exceed the toxic threshold is lower in tumor cells compared to normal cells, due to higher steady state ROS levels in malignant cells. Thus, therapies based on the combination of ROS-producing agents or depletion of the antioxidative capacity might constitute a strategy to specifically eradicate cancer cells without damaging normal tissue. This hypothesis was confirmed in a study, in which melanoma cells and fibroblasts were treated with the ROS-producing chemotherapeutic drug doxorubicin in combination with redox-active cerium oxide nanoparticles [174]. The researchers revealed an increased ROS production and a synergistic cytotoxicity in tumor cells, while fibroblasts were not affected. In addition, Yi et al. combined the ROS-producing therapeutic agent arsenic trioxide with the ROS-generating natural anthraquinone derivative emodin [175]. The cytotoxicity of arsenic trioxide was selectively enhanced in malignant cells, but not in fibroblasts, by emodin-induced ROS production. In the present study, concurrent application of DHA and IR revealed an increased efficacy of radiotherapy by additional application of the ROS-generating drug DHA in HCT116 colon cancer cells with wild type Keap1 and in lung cancer cells with a constitutively activated protective Keap1/Nrf2 pathway. A synergistic anti-cancer activity of radiotherapy and DHA was previously described in non-small cell lung cancer and glioma cells [176-178], but in colorectal cancer it has not been tested so far.

Another strategy to elevate intracellular ROS levels and exceed the toxic threshold is an interference with the antioxidant system. Previous publications described an improved response to radiotherapy by lowering glutathione levels via inhibition of xCT

or glutaminolysis [12, 130]. Conversely, enhanced glutathione levels could be correlated with cancer progression and resistance to anticancer therapy [46, 54] . The results of this study revealed Nrf2-dependent increase of glutathione levels in response to the prooxidative drug DHA in HCT116 colorectal cancer cells with wildtype Keap1. Previous publications also described an activation of the antioxidative Keap1/Nrf2 pathway in a ROS-dependent manner by radiotherapy [171, 179]. Therefore, we expected that activation of this protective pathway by DHA or IR could limit the response to the combinatory therapy when treatments were applied sequentially. This is of particular interest, since radiotherapy is usually applied in fractionated doses [5]. Particularly, we presumed a Nrf2-dependent protection by DHA and IR in HCT116 colorectal cancer cells with wildtype Keap1. Protective effects were not expected in NCI-H460 cells, due to the constitutive activation of this pathway and constantly high glutathione levels. Our results revealed that treatment with DHA 24 h before irradiation abrogated the additional effect of the combinatory therapy in HCT116 colorectal cancer cells that respond to DHA. Most likely, the Keap1/Nrf2 pathway activated by DHA provides protection against additional radiotherapy. We suggest that Nrf2-activated and cysteine-dependent elevation of intracellular glutathione levels induced by DHA, neutralize subsequent IR-induced ROS production, thereby preventing the cytotoxic, oxidative boost. Surprisingly, in Keap1 wildtype HCT116 cells treatment with DHA 24 h after irradiation did not abrogate the additional effect, although researchers described a radiation-induced activation of the Keap1/Nrf2 pathway [171, 179]. Supposably, IR activates the antioxidant Keap1/Nrf2 pathway less efficient than the prooxidative drug DHA in HCT116 cells, resulting in a minor protection by radiotherapy against the DHA-forced oxidative boost. Due to the failure to increase glutathione levels in NCI-H460 cells in response to treatment with DHA and – probably - to irradiation, the efficacy of the combinatory therapy was not changed by modulation of the treatment regimen.

Taken together, the results of the present study disclose an improved efficacy of IR in a combined therapy that is based on excessive ROS production, irrespective of Keap1 mutations. However, the treatment regimen needs to be considered and requires optimization to achieve a synergistic effect and the best possible outcome in a combined therapy when treating cancer cells with an inducible Keap1/Nrf2 pathway.

4.1.3.2 DHA overcomes hypoxia-induced radioresistance

The efficacy of radiotherapy is strongly restricted in an oxygen-deficient environment. The low oxygen availability results in decreased ROS production and impedes the induction of irreparable DNA strand breaks, responsible for cell death. The limited success of chemo- and radiotherapy, which exert cytotoxicity through ROS production, is a central issue in the treatment of hypoxic tumors [14, 26]. Treatment of hypoxic tumors with the prooxidant drug DHA might increase ROS production and improve the efficacy of radiotherapy.

So far, most studies on DHA and other artemisinin derivatives were conducted in a normoxic environment [96, 97, 156, 158-160, 180-182]. Only few experiments were carried out in hypoxia, but the few published analysis point towards an even better anti-neoplastic function in hypoxic than in normoxic conditions, particularly when DHA was used at low concentrations [132, 147-150]. The promising effect of DHA on hypoxic colon cancer cells was also detected in former experiments conducted in our lab [132]. However, the combinatory effect of DHA and radiation in a hypoxic environment has not been tested yet. This study revealed that combining radiation with DHA completely overcomes hypoxia-mediated radioresistance in Keap1 wildtype HCT116 as well as Keap1 mutant NCI-H460 cells. In both cell lines, the additive effect of IR and DHA was even more pronounced in hypoxia than in normoxia. Based on these observations, the present study intended to elucidate more detailed the mechanisms behind DHA-induced cytotoxicity in normoxia and hypoxia.

4.2 Mechanism of DHA-induced cytotoxicity in normoxia and hypoxia

Although many researchers observed an anti-neoplastic effect of DHA and other artemisinin derivatives on several cancer cell lines, the precise mechanism underlying DHA-mediated cytotoxicity remains largely elusive. This applies even more to the DHA-activated pathways in hypoxia, since experimental data in an oxygen-deficient microenvironment is rare [132, 148-150]. Most groups analyzed DHA-induced cytotoxicity in normoxia and focused on the first 24 h to 48 h after treatment, in which apoptosis was the most often observed type of cell death induced by DHA in a wide array of tumor cells [94, 97, 132, 159, 160, 176, 180, 183]. In addition, ferroptosis and autophagy-associated cell death were observed [158, 160, 184, 185]. When used at lower concentrations, DHA efficiently induced cell cycle arrest, decreased cancer cell

proliferation and, moreover, inhibited migration and invasion [94, 96, 180-183]. Certain publications linked DHA-induced effects to an iron-dependent ROS production [148, 156, 158, 178]. In preceding experiments in our laboratory, Ontikatze et al. detected apoptosis induction in HCT116 colorectal cancer cells after application of lower DHA concentrations (≤ 25 µM), while treatment with higher DHA concentrations (> 50 µM) resulted in necrosis-like cell death [132]. The publication also described decreased clonogenic survival of HCT116 cells treated with DHA in normoxia and severe hypoxia. In addition, previous results of the present study revealed that combining DHA with IR overcomes hypoxia-mediated radioresistance. Based on these findings, the present study aimed to shed more light on the mechanisms of DHA-induced short-term and long-term cytotoxicity in normoxia and severe hypoxia. Therefore, DHA-induced cell death and the clonogenic survival were examined in HCT116 cells (HCT116 wt) with an intact intrinsic apoptosis pathway and compared to the effect in HCT116 $Bax^{-/-}Bak^{sh}$ cells with an impaired intrinsic apoptosis pathway due to Bax knock-out and Bak knock-down.

4.2.1 DHA-induced cytotoxicity in normoxia

In compliance with previous observations [132], HCT116 wt cells underwent apoptosis following treatment with DHA at concentrations up to 25 µM in normoxia. In addition, the results of the present study revealed that autophagy-associated cell death contributes to DHA-induced cytotoxicity in HCT116 wt cells treated in normoxia. Moreover, pro-apoptotic proteins Bax and Bak regulated DHA-induced short- and long-term cytotoxicity in normoxia, since an impaired expression of Bax and Bak largely prevented DHA-induced cell death and decrease of the clonogenic survival. Therefore, the results clearly demonstrate the importance of the pro-apoptotic proteins Bax and Bak for DHA-induced short- and long-term cytotoxicity in normoxia.

The here present work additionally demonstrated that treatment with DHA in normoxia caused oxidative damage to lipids and proteins in an iron-dependent manner. Analysis upon treatment with DHA in HCT116 $Bax^{-/-}Bak^{sh}$ cells revealed a similar severity of DHA-induced iron-dependent lipid peroxidation as detected in HCT116 wt cells. Moreover, DHA increased intracellular glutathione levels in both HCT116 cell lines equally and independent of Bax and Bak expression. Elevated glutathione levels upon treatment with DHA in HCT116 $Bax^{-/-}Bak^{sh}$ cells are likely a consequence of DHA-induced activation of the protective Keap1/Nrf2 pathway, as previously detected in

HCT116 wt cells [186]. Presumably, the antioxidative defense pathway is not influenced by an inefficient expression of the anti-apoptotic proteins Bax and Bak. However, subsequent analysis of cellular ROS production revealed a dose-dependent increase in HCT116 wt cells but a minor increase in HCT116 $Bax^{-/-}Bak^{sh}$ cells. Moreover, ROS levels correlated with DHA-induced DNA DSB repair, which was more pronounced in HCT116 wt cells. Unfortunately, it remains obscure how the anti-apoptotic proteins Bax and Bak contribute to cellular ROS production. We hypothesize that the diminished autophagy induction under basal conditions in Bax/Bak-deficient cells lowered degradation of the iron storage protein ferritin. This autophagic process is termed ferritinophagy and results in the release of redox-active iron into the cytosol [187]. Thus, a lowered autophagic flux might result in a decreased cytosolic iron pool, a reduced initial DHA activation and subsequent lowered ROS production within the first 24 h of treatment. A previous publication by Yang et al. disclosed the importance of ferritin degradation in artesunate-induced cell death. Knockdown of the adaptor protein for ferritin degradation inhibited ferritinophagy and prevented artesunate-induced cytotoxicity [188].

In the previous section of this study, we demonstrated that DHA facilitated oxidation of mitochondrial proteins and increased mitochondrial ROS production in NCI-H460 MitoTimer cells. It was suggested that mitochondrial ROS production is a consequence of DHA-induced oxidative damage, since damaged mitochondria produce even more ROS, particularly superoxide anions, than healthy mitochondria [140]. Usually, superoxide dismutase quickly converts superoxide anions into the highly diffusible H_2O_2, followed by enzymatically catalyzed detoxification [32]. Thus, mitochondrial damage can result in excessive production of H_2O_2, thereby increasing cytosolic ROS levels. However, no differences in mitochondrial ROS production between HCT116 wt and HCT116 $Bax^{-/-}Bak^{sh}$ cells were overserved, suggesting a similar damage induction at mitochondria independent of Bax and Bak expression.

In addition to mitochondrial ROS production, previous results of this study revealed a DHA-induced decrease of mitochondrial function in NCI-H460 and HCT116 wt cells. A previous publication described a major role of Bax in the regulation of cellular bioenergetics in HCT116 cells and linked Bax deficiency to reduced energy production via aerobic respiration [189]. Assuming that Bax-deficient cells are less dependent on energy supply via oxidative phosphorylation than Bax-expressing control cells, we expected that the adverse impact of DHA on mitochondrial function would have a minor role in HCT116 $Bax^{-/-}Bak^{sh}$ cells. Thus, HCT116 $Bax^{-/-}Bak^{sh}$ cells should have a

survival advantage over HCT116 wt cells. However, the present study neither detected differences in mitochondrial basal respiration, nor in ATP production between non-treated HCT116 wt and HCT116 Bax$^{-/-}$Bak^{sh} cells in normoxic conditions. Treatment with DHA, however, exerted a marked inhibitory effect on mitochondrial function in both cell lines, but the intensity was more severe in HCT116 wt than in HCT116 Bax$^{-/-}$Bak^{sh} cells. These data demonstrated that an impaired expression of the pro-apoptotic factors Bax and Bak partially prevented DHA-induced inhibition of mitochondrial respiration and ATP production. Presumably, a less severe inhibition of mitochondrial function upon DHA treatment provided HCT116 Bax$^{-/-}$Bak^{sh} cells with a survival advantage over wild type cells and contributed to an improved long-term survival in normoxia.

Collectively, the intensity of DHA-induced cellular ROS production, DNA damage and abrogation of mitochondrial function were marginally lower in HCT116 Bax$^{-/-}$Bak^{sh} cells than in HCT116 wildtype cells. Concurrently, DHA efficiently induced cell cycle arrest in G2/M phase in cells with impaired Bax and Bak expression. We assume that HCT116 Bax$^{-/-}$Bak^{sh} cells induce cell cycle arrest instead of cell death in response to DHA, which allows HCT116 Bax$^{-/-}$Bak^{sh} cells to repair DHA-induced oxidative damage, resulting in enhanced long-term survival.

Taken together, the here obtained results revealed apoptosis as the prevalent form of DHA-induced cell death in HCT116 colorectal cancer cells treated in normoxia and identified the pro-apoptotic proteins Bax and Bak as factors conferring DHA-induced short- and long-term cytotoxicity in normoxia.

4.2.2 DHA-induced cytotoxicity in hypoxia

In HCT116 wt cells, DHA-induced short- and long-term cytotoxicity were similar efficient under normoxic and hypoxic conditions. In normoxia short-term cytotoxicity based on induction of apoptosis and autophagy, while cell death did not rely anymore on apoptosis and autophagy in an oxygen-deficient environment. Since an apoptosis-independent type of cell death was detected in HCT116 wt cells treated in hypoxia, we assumed that DHA induced cell death in a similar fashion and with comparable effectivity in HCT116 Bax$^{-/-}$Bak^{sh} cells. Surprisingly, HCT116 Bax$^{-/-}$Bak^{sh} cells remained insensitive to DHA-induced cytotoxicity in hypoxia in the first 48 h after treatment. These results point towards an apoptosis-independent but Bax and Bak-dependent

form of cell death in HCT116 wt cells in the first 48 h after treatment with DHA in hypoxic conditions.

Although HCT116 Bax$^{-/-}$Bak^{sh} cells reacted refractory to DHA-induced cell death in the first phase after treatment with DHA in hypoxia, they efficiently induced cell cycle arrest 24 h after treatment. Moreover, the clonogenic survival of HCT116 Bax$^{-/-}$Bak^{sh} cells was efficiently decreased upon treatment with DHA for 24 h in hypoxia with following incubation in normoxia. The cytotoxic effect of DHA on HCT116 Bax$^{-/-}$Bak^{sh} cells was comparable to that on HCT116 wt cells, indicating activation of a Bax/Bak-independent cytotoxic mechanism in a hypoxic environment. Further analysis of cell death induction by DHA after treatment in hypoxia followed by reoxygenation revealed that DHA efficiently induced cell death in HCT116 Bax$^{-/-}$Bak^{sh} cells nine days later, while the cytotoxic effect remained negligible upon treatment in normoxia. Thus, sensitivity to DHA-induced long-term cytotoxicity in a hypoxic environment was independent of Bax and Bak expression. Moreover, this delayed cell death was also independent of autophagy.

The absence of molecular oxygen attenuated DHA-induced ROS production in HCT116 wt cells and completely abolished DHA-induced ROS production in HCT116 Bax$^{-/-}$Bak^{sh} cells. As observed in normoxia, cellular ROS levels correlated with DHA-induced DNA DSB repair. Moreover, compared to normoxia, the basal as well as DHA-induced mitochondrial ROS production was lower in hypoxia. Most likely, this is a consequence of the decreased energy production via oxidative phosphorylation in hypoxic conditions [190]. Exposure to hypoxia for 24 h significantly decreased mitochondrial function in both cell lines. Interestingly, hypoxia-induced reduction of the basal respiration and ATP production were less pronounced in HCT116 Bax$^{-/-}$Bak^{sh} cells compared to HCT116 wt cells. This indicates that an impaired expression of the pro-apoptotic proteins Bax and Bak facilitates adaptation to low oxygen availability. Moreover, treatment with DHA did not affect ATP production in HCT116 Bax$^{-/-}$Bak^{sh} cells but further decreased ATP levels in wild type cells treated in hypoxia. Hence, an impaired expression of the pro-apoptotic factors Bax and Bak mitigates DHA-induced abrogation of mitochondrial function in normoxia and hypoxia.

Decreased ATP levels in hypoxia might limit the antioxidant capacity by decreasing glutathione levels, since glutathione biosynthesis depends on the availability of ATP [48]. The lowered glutathione levels detected in HCT116 wt and HCT116 Bax$^{-/-}$Bak^{sh} cells confirm this assumption, revealing a lowered antioxidant capacity in hypoxia,

independent of Bax and Bak expression. Compared to normoxia, treatment with DHA in hypoxia had no impact on intracellular glutathione levels. In the previous section of the study a DHA-induced increase of glutathione levels in HCT116 wt cells was detected when treatment occurred in normoxia. This effect was ascribed to an activation of the antioxidant Keap1/Nrf2 pathway by ROS [186]. Supposably, the lowered DHA-induced ROS production upon treatment in hypoxia failed to activate this protective pathway, resulting in constantly low glutathione levels and a higher susceptibility to oxidative damages. A higher susceptibility to oxidative damage was confirmed by markedly increased levels of oxidized lipids, when cells were treated in a hypoxic environment. DHA-induced lipid peroxidation was similar efficient in HCT116 wt and HCT116 $Bax^{-/-}Bak^{sh}$ cells, but cotreatment with an iron-chelator marginally lowered lipid peroxidation in hypoxia, in contrast to a complete prevention in normoxia. The failure to avert DHA-induced lipid peroxidation by iron depletion in hypoxia could be attributed to different intracellular iron levels in normoxic and hypoxic cells. Hypoxia-induced HIF1α activation increases iron accumulation via upregulation of transferrin receptor 1 (TfR1) and heme oxygenase 1 (HO-1), an enzyme which degrades heme, resulting in an increase in cytosolic iron [191, 192]. Iron-dependent DHA activation generates highly reactive DHA radicals that could directly interact with cellular biomolecules to create adducts [86], which, probably, are more difficult to repair. An excessive iron-dependent generation of DHA radicals in a hypoxic environment could explain the elevated lipid peroxidation in association with a lowered total ROS production upon treatment with DHA in hypoxia compared to normoxia. Consequently, increased cytosolic iron levels and decreased glutathione levels in hypoxic cells could facilitate long lasting damage to lipids upon treatment with DHA, independent of Bax and Bak expression. Thus, we conclude that DHA induced a delayed, ferroptosis-like cell death in hypoxic HCT116 cells.

Finally, the results suggest that DHA-induced oxidative damage results in subsequent cell cycle arrest in HCT116 $Bax^{-/-}Bak^{sh}$ cells instead of cell death induction as observed in wild type cells. Low glutathione levels in hypoxia might limit the repair of the inflicted damage even after return to normoxic conditions, thereby promoting induction of a delayed cell death. In contrast, an activated oxidative stress response and enhanced glutathione levels in normoxia could explain the improved cell survival of HCT116 $Bax^{-/-}Bak^{sh}$ cells compared to hypoxia.

Taken together, this study identified apoptosis and autophagy-associated cell death as the major pathways contributing to DHA-induced cytotoxicity of HCT116 colon cancer cells in normoxia. Moreover, we established pro-apoptotic proteins Bax and Bak as factors regulating sensitivity to DHA in normoxic HCT116 cells. In hypoxia, sensitivity to DHA was independent of Bax and Bak expression. Collectively, the present study established DHA as a hypoxia-active drug with radiosensitizing properties. These two qualities of DHA could improve the clinical outcome of lung and colorectal cancer patients. Thus, the application of DHA in cancer therapy seems to be particularly suitable for the treatment of highly aggressive hypoxic tumors with a low apoptosis rate or an activated antioxidative stress response.

4.3 Prospect on the applicability and limitations of DHA in cancer therapy

Previous publications and the present study could demonstrate that DHA and the related derivatives exert anti-neoplastic effects and are favorable candidates for anti-cancer therapy, since these compounds are reasonably cost-efficient with a good safety profile and already approved for medical use in malaria. The selectivity of artemisinin and its derivatives to preferably eradicate the malaria parasite *Plasmodium* and, moreover, cancer cells might be attributed to the iron-dependent activation of these compounds [81, 85, 86, 156]. It is supposed that, digestion of hemoglobin results in an increased amount of redox-active iron in the acidic food vacuole of *Plasmodium*, thereby conferring an efficient drug activation and toxicity in the parasite [89]. An altered iron metabolism is a hallmark of cancer cells and was detected in a wide array of tumor cells and tissue samples [193]. Moreover, we speculate that particularly hypoxic cells are provided with an increased amount of iron, since HIF1α activation induces upregulation of the transferrin receptor 1, facilitating iron uptake [192]. Thus, the iron-dependency of DHA reflects a beneficial feature for targeting normoxic and even hypoxic cancer cells.

In clinical studies, plasma concentrations in malaria patients reached up to 0.71 µg/ml DHA (approximately 2.5 µM) [194], while the concentrations used for *in vitro* experiments in this study are much higher. Within the normal dosage in malaria therapy, only a small number of patients undergo a mild and transient reduction in reticulocytes [194]. Increasing the dosage in cancer therapy might implicate the occurrence of anemia. Therefore, DHA-treated cancer patients would require a

continuous control of blood values. Unfortunately, clinical studies applying DHA or the related derivatives in cancer therapy are scarce. The few ones available indicate a good tolerability with concurrent anti-cancer activity using moderately higher administration doses than these in malaria therapy [99-101]. However, the clinical application in cancer therapy is limited by the pharmacokinetic properties of artemisinin and the related derivatives. The poor water solubility, short plasma half-life and low bioavailability upon oral administration most likely hinder to achieve an appropriate drug concentration at the targeted tumor tissue. In order to address this issue, researchers develop new compounds with structural modifications or drug carrier and delivery systems [94]. Recent publications reported an enhanced antitumor activity in diverse cancer cell lines using mitochondria-targeted artemisinin derivatives [195]. A further promising approach is the use of pharmacophore hybridization products, such as DHA-coumarin hybrids or artemisinin-chemotherapeutic agent conjugates, that provoked a much higher anti-cancer activity than either agent alone [196, 197]. The development of nano-formulations such as liposomes [198, 199], nanospheres [200], nanocapsules [201] or nanoparticles [202] increased the efficacy and distinctly improved the bioavailability of the drugs. An improved water solubility, blood circulation half-life and anti-cancer activity was reported for instance using a polyethylene glycol-DHA conjugate in non-small cell lung cancer xenograft models [203]. Moreover, a tumor-targeted distribution could be achieved using magnetic nanoliposomes and artemisinin-loaded transferrin-conjugated nanostructured lipid carriers, that revealed a greater therapeutic efficacy and a decreased likelihood for neurotoxicity compared to conventional artemisinin [199, 204]. Even though these new drug formulations appear promising, clinical studies are needed to approve the applicability in cancer therapy. In addition, studies on combined treatments with conventional therapies are needed to evaluate possible combination strategies.

The present study revealed that combining DHA with IR improves the efficacy of radiotherapy and moreover, overcomes hypoxia-mediated radioresistance. Thus, we could demonstrate that combining ROS-based therapies is an effective anti-cancer strategy. At the same time, we revealed an activation of the protective antioxidative Keap1/Nrf2 pathway in response to DHA, that could limit the efficacy of the combinatory therapy in Keap1 wildtype cancer cells. Although our results demonstrate that inhibition of Nrf2 increased the anti-neoplastic impact of DHA, we cannot recommend the use of an Nrf2-inhibitor to further maximize the synergistic effect of DHA and IR. This estimation is based on a previous publication which indicated an

increased radiation-induced pulmonary fibrosis and revealed a reduced life span of Nrf2-deficient mice following thoracic irradiation [205]. These observations demonstrated that activation of the antioxidative Keap1/Nrf2 pathway is crucial in normal cells for protection against radiation-induced cytotoxicity and indicate, that inhibition of Nrf2 is probably not suitable for combinatory therapies with IR. Instead, we suppose an optimization of the treatment regimen when combining radiotherapy with ROS-producing drugs such as DHA. We observed the most efficient anti-cancer activity by concurrent administration of IR and DHA and thus, propose a treatment schedule in which DHA is administered directly after radiotherapy. Since radiotherapy is usually applied at 5 fractions per week, occurring Monday to Friday [5], we suggest DHA administration immediately after the last dose fraction on Friday to avoid a protective effect by DHA-induced Keap1/Nrf2 pathway activation. In addition, the results of this study revealed a strong anti-cancer activity of a combined treatment in cancer cells with a constantly upregulated antioxidative defense. Thus, IR-induced upregulation of the antioxidative system by a fractionated regimen would probably not limit the anti-neoplastic impact of the combined therapy. We expect that application of DHA following the last dose fraction of the week induced an oxidative boost that exceeds the repair capacity of tumor cells, irrespective of Keap1 mutations, thereby increasing radiation-induced cytotoxicity.

In addition, DHA could reduce the toxic side effects of radiotherapy. Other researchers described a protective effect of DHA on inflammatory cardiovascular diseases by suppressing inflammation in bleomycin-induced pulmonary fibrosis in mice and rats [206-208]. Since the risk of cardiovascular disease and lung fibrosis increases after thorax irradiation during radiotherapy [209], patients might profit from an additional health benefit by averting radiation-induced lung fibrosis when combining radiotherapy with DHA.

Taken together, the research of the past decades and our recent findings provide evidence on DHA as a promising anti-cancer drug. DHA is particularly able to revers therapy resistance when combined with chemotherapeutics or radiotherapy. However, further research, especially clinical trials, are needed to validate the applicability of DHA and the new developed formulations in cancer therapy.

5 Summary

The efficacy of radiotherapy depends on DNA damage induced either directly by IR or, most of all, indirectly in response to oxidative stress via ROS production. Massive ROS stress can either induce cell death or activate protective mechanisms such as the Keap1/Nrf2 pathway, improving the antioxidative defense and limiting IR-induced lethal damage. Moreover, hypoxic areas in tumor tissues restrict the efficacy of radiotherapy. Reduced ROS production and a lowered induction of irreparable, oxidative damage in an oxygen-deficient environment is a reason for this limitation. The present study aimed to improve the efficacy of radiotherapy in normoxia and hypoxia by inducing an additional and cytotoxic ROS boost with the prooxidative anti-malaria drug DHA. Due to its anti-neoplastic effects, low toxicity and known safety, DHA has received increasing attention in cancer research.

Initially, the oxidative response was analyzed in the colorectal cancer cell line HCT116 and the lung cancer cell line NCI-H460 treated with DHA in normoxia. DHA efficiently induced iron-dependent oxidative damage to lipids, proteins and mitochondria. At the same time, DHA activated the protective Keap1/Nrf2 pathway in HCT116 cells, while, in NCI-H460 cells, Nrf2 was already constitutively activated due to a Keap1 mutation. An activated Keap1/Nrf2 pathway is related to resistance towards chemo- and radiotherapy. However, the results of the present thesis revealed that a concurrent combined treatment of IR and DHA markedly improved radiotherapy, independent of Keap1 mutations. In HCT116 cells responding to DHA with an activation of the protective Keap1/Nrf2 pathway, the treatment regimen can limit the combinatory effect when DHA is applied prior to IR. An application of the prooxidative drug after IR was more toxic than either treatment alone in the colon cancer cell line. The cytotoxic impact evoked by the combinatory therapy was even more efficient when cells were treated under hypoxic conditions. The results revealed, that hypoxia-mediated radioresistance was overcome when combining IR with DHA. Thus, the present study demonstrates that combining ROS-based therapies is an effective anti-cancer strategy.

In order to improve our understanding on the mechanisms behind DHA-induced cytotoxicity in normoxia and hypoxia, short-term cell death and long-term survival were analyzed in HCT116 wild type (wt) cells and in HCT116 $Bax^{-/-}Bak^{sh}$ cells with a defective intrinsic apoptosis pathway. The results revealed apoptosis and autophagy-associated cell death as the prevalent mechanisms contributing to DHA-induced cell death of HCT116 colon cancer cells treated in normoxia. Our data identified the pro-

apoptotic proteins Bax and Bak as factors regulating sensitivity to DHA in normoxic conditions. In addition, in HCT116 $Bax^{-/-}Bak^{sh}$ cells, treatment with DHA in normoxia initially induced cell cycle arrest, which most likely allows repair of DHA-induced oxidative damage, resulting in an improved long-term survival. In hypoxia, sensitivity to DHA was independent of Bax and Bak expression. While DHA induced cell death shortly after treatment with DHA in hypoxic HCT116 wt cells, treatment with DHA in hypoxia initially induced cell cycle arrest in HCT116 $Bax^{-/-}Bak^{sh}$ cells, followed by a delayed ferroptosis-like cell death. Lower glutathione levels correlated with a higher lipid peroxidation in hypoxic HCT116 $Bax^{-/-}Bak^{sh}$ cells. Moreover, incubation in hypoxia resulted in reduced oxidative phosphorylation after returning to normoxia, providing the cells with reduced energy production. This effect was less pronounced in HCT116 $Bax^{-/-}Bak^{sh}$ than in HCT116 wt cells, providing HCT116 $Bax^{-/-}Bak^{sh}$ cells with a better energy supply via oxidative phosphorylation than HCT116 wt cells after return to normoxia.

In summary, we identified a) DHA-induced activation of Keap1/Nrf2 pathway leading to improved antioxidant defense and b) the pro-apoptotic proteins Bax and Bak as critical factors regulating sensitivity to DHA in HCT116 colon cancer cells in normoxia, while impaired Nrf2 activation and reduced glutathione levels improved the cytotoxic response to DHA in hypoxia despite less ROS production and independent of Bax and Bak expression.

6 Zusammenfassung

Die Wirksamkeit der Strahlentherapie basiert einerseits auf der direkten Induktion von DNA-Schäden durch ionisierende Strahlung, anderseits aber vor allem auf der Generierung von oxidativem Stress durch ROS. Hohe ROS-Level induzieren entweder den Zelltod oder protektive Mechanismen, wie den Keap1/Nrf2-Signalweg, der die antioxidative Abwehr aktiviert, die wiederum den strahleninduzierten Schaden begrenzt. Darüber hinaus ist die Hypoxie in Tumoren ein weiterer Einflussfaktor, der die Wirksamkeit der Strahlentherapie deutlich einschränkt. In Hypoxie werden weniger ROS produziert, und die Induktion von irreparablen Schäden ist aufgrund des Mangels an molekularem Sauerstoff begrenzt. Die vorliegende Studie zielt darauf ab die Wirksamkeit der Bestrahlung in Normoxie und Hypoxie zu verbessern, indem ein zusätzlicher, zytotoxischer ROS-Anstieg mithilfe des prooxidativen Malaria-medikaments DHA erzeugt werden soll. Aufgrund seiner antineoplastischen Wirkung, geringen Toxizität und der guten Verträglichkeit gewann das Antimalariamittel DHA auch in der Krebsforschung an Bedeutung.

Zunächst wurde das oxidative Potential von DHA in der Kolorektalkarzinom-Zelllinie HCT116 und der Lungenkarzinom-Zelllinie NCI-H460 untersucht. DHA induzierte eisenabhängig oxidative Schäden an Lipiden, Proteinen und den Mitochondrien. Gleichzeitig aktivierte DHA den protektiven Keap1/Nrf2-Signalweg in HCT116-Zellen, wohingegen dieser Signalweg in NCI-H460 Zellen aufgrund einer Keap1-Mutation bereits konstitutiv aktiviert war. Eine Aktivierung des Keap1/Nrf2-Signalwegs wird mit Chemo- und Strahlenresistenz in Zusammenhang gebracht. Dennoch belegen die Ergebnisse der vorliegenden Arbeit, dass eine Kombinationstherapie aus ionisierender Strahlung und DHA die Wirksamkeit der Strahlentherapie, unabhängig von einer Keap1-Mutation, deutlich verbessern kann. In HCT116 Zellen, in denen DHA den protektiven Keap1/Nrf2-Signalweg aktiviert, kann die Behandlungsabfolge die Wirksamkeit der Kombinationstherapie limitieren, sofern DHA vor der Bestrahlung appliziert wird. Es empfiehlt sich daher die Applikation von DHA direkt nach der Bestrahlung vorzunehmen, um so einen oxidativen und zytotoxischen ROS-Anstieg zu induzieren. Darüber hinaus war die zytotoxische Wirkung der Kombinationstherapie unter hypoxischen Bedingungen noch stärker ausgeprägt. Die Ergebnisse konnten sogar eine Überwindung der Hypoxie-vermittelten Strahlenresistenz durch die Kombinationsbehandlung mit DHA belegen. Folglich zeigt die vorliegende Arbeit deutlich, dass die Kombination von ROS-basierten Therapien eine potentielle Strategie in der Bekämpfung von Krebs ist.

Um die zugrundeliegenden Mechanismen der DHA-induzierten Zytotoxizität in Normoxie und Hypoxie besser zu verstehen, wurde der Zelltod sowie das Langzeitüberleben von HCT116 Wildtyp (wt)-Zellen und HCT116 $Bax^{-/-}Bak^{sh}$ Zellen mit defektem intrinsischen Apoptoseweg untersucht. Die Ergebnisse haben Apoptose und Autophagie-assoziierten Zelltod als primäre Mechanismen der DHA-induzierten Zytotoxizität in Normoxie offengelegt. Aus den Daten wird deutlich, dass die pro-apoptotischen Proteine Bax und Bak die Sensitivität gegenüber der DHA-Behandlung unter normoxischen Bedingungen beeinflussen. Die DHA-induzierte Beeinträchtigung der mitochondrialen Funktion war in HCT116 $Bax^{-/-}Bak^{sh}$ Zellen weniger stark ausgeprägt als in HCT116 wt Zellen. Darüber hinaus induzierte DHA zunächst einen Zellzyklusarrest in HCT116 $Bax^{-/-}Bak^{sh}$-Zellen, der den Zellen vermutlich die Reparatur von DHA-induzierten oxidativen Schäden ermöglicht und somit zu einem verbesserten Langzeitüberleben beiträgt. In Hypoxie wurde die Sensitivität gegenüber DHA durch die pro-apoptotischen Proteine Bax und Bak nicht beeinflusst. Während DHA in hypoxischen HCT116 wt-Zellen bereits zu einem frühen Zeitpunkt den Zelltod induzierte, wurde in hypoxischen HCT116 $Bax^{-/-}Bak^{sh}$-Zellen zunächst der Zellzyklusarrest eigeleitet und zu einem späteren Zeitpunkt ein verzögerter Zelltod induziert. In Hypoxie wurden niedrigere Konzentrationen des anti-oxidativ wirkenden Glutathion detektiert als in Normoxie, die mit einer stärkeren Lipidperoxidation korrelierten. Abschließend wird daher ein verzögerter, ferroptoseartiger Zelltod durch die DHA-Behandlung in Hypoxie angenommen.

Zusammenfassend wurden a) der durch DHA aktivierte Keap1/Nrf2-Signalweg als auch b) die pro-apoptotischen Proteine Bax und Bak als Faktoren identifiziert, die die Sensitivität der kolorektalen Karzinomzelllinie HCT116 gegenüber DHA in Normoxie regulieren. In Hypoxie wird Nrf2 nicht aktiviert und sorgt zusammen mit den niedrigeren Glutathion-level für eine gute Zytotoxizität bei geringerer ROS-Produktion und unabhängig von Bax- und Bak-Expression.

7 References

1. Sung, H., et al., *Global cancer statistics 2020: GLOBOCAN estimates of incidence and mortality worldwide for 36 cancers in 185 countries.* CA CANCER J CLIN 2021. 0: p. 1 - 41.

2. Wu, G., et. al., *Overcoming treatment resistance in cancer: Current understanding and tactics.* Cancer Lett, 2017. 387: p. 69-76.

3. Baskar, R., et al., *Cancer and Radiation Therapy: Current Advances and Future Directions.* International Journal of Medical Sciences, 2012. 9(3): p. 193-199.

4. Liauw, S.L., P.P. Connell, and R.R. Weichselbaum, *New paradigms and future challenges in radiation oncology: an update of biological targets and technology.* Science translational medicine, 2013. 5(173): p. 173sr2-173sr2.

5. Withers, H.R., *The Four R's of Radiotherapy*, in *Advances in Radiation Biology*, J.T. Lett and H. Adler, Editors. 1975, Elsevier. p. 241-271.

6. Hall, E.J. and A.J. Giaccia, *Radiobiology for the radiologist*. 2012, Philadelphia, PA: Wolters Kluwer/Lippincott Williams & Wilkins.

7. Jaffray DA, G.M., *Radiation Therapy for Cancer.*, in *Cancer: Disease Control Priorities*, J.P. Gelband H, Sankaranarayanan R, et al., editors., Editor. 2015: Washington (DC): The International Bank for Reconstruction and Development / The World Bank.

8. Jaffray, D.A., *Image-guided radiotherapy: from current concept to future perspectives.* Nat Rev Clin Oncol, 2012. 9(12): p. 688-99.

9. Reisz, J.A., et al., *Effects of ionizing radiation on biological molecules--mechanisms of damage and emerging methods of detection.* Antioxid Redox Signal, 2014. 21(2): p. 260-92.

10. Loh, Z.-H., et al., *Observation of the fastest chemical processes in the radiolysis of water.* Science, 2020. 367(6474): p. 179-182.

11. Wang, J.S., H.J. Wang, and H.L. Qian, *Biological effects of radiation on cancer cells.* Mil Med Res, 2018. 5(1): p. 20.

12. Matschke, J., et al., *Targeted Inhibition of Glutamine-Dependent Glutathione Metabolism Overcomes Death Resistance Induced by Chronic Cycling Hypoxia.* Antioxid Redox Signal, 2016. 25(2): p. 89-107.

13. Vaupel, P. and A. Mayer, *Hypoxia in cancer: significance and impact on clinical outcome.* Cancer and Metastasis Reviews, 2007. 26(2): p. 225-239.

14. Wang, H., et al., *Hypoxic Radioresistance: Can ROS Be the Key to Overcome It?* Cancers, 2019. 11(1): p. 112.

15. Held, K.D., *Radiobiology for the Radiologist, 6th ed., by Eric J. Hall and Amato J. Giaccia.* Radiation Research, 2006. 166(5): p. 816-817.

16. Mah, L.J., A. El-Osta, and T.C. Karagiannis, *γH2AX: a sensitive molecular marker of DNA damage and repair.* Leukemia, 2010. 24(4): p. 679-686.

17. Mladenov, E., et al., *DNA double-strand break repair as determinant of cellular radiosensitivity to killing and target in radiation therapy.* Front Oncol, 2013. 3: p. 113.

18. Sia, J., et al., *Molecular Mechanisms of Radiation-Induced Cancer Cell Death: A Primer.* Frontiers in Cell and Developmental Biology, 2020. 8(41).

19. Vaupel, P. and L. Harrison, *Tumor hypoxia: causative factors, compensatory mechanisms, and cellular response.* Oncologist, 2004. 9 Suppl 5: p. 4-9.

20. Durand, R.E. and E. Sham, *The lifetime of hypoxic human tumor cells.* Int J Radiat Oncol Biol Phys, 1998. 42(4): p. 711-5.

21. Semenza, G.L., *Hypoxia-inducible factor 1 (HIF-1) pathway.* Sci STKE, 2007. 2007(407): p. cm8.

22. Kallinowski, F., et al., *Growth-related changes of oxygen consumption rates of tumor cells grown in vitro and in vivo.* J Cell Physiol, 1989. 138(1): p. 183-91.

23. Vaupel, P., F. Kallinowski, and P. Okunieff, *Blood flow, oxygen and nutrient supply, and metabolic microenvironment of human tumors: a review.* Cancer Res, 1989. 49(23): p. 6449-65.

24. Bayer, C. and P. Vaupel, *Acute versus chronic hypoxia in tumors: Controversial data concerning time frames and biological consequences.* Strahlenther Onkol, 2012. 188(7): p. 616-27.

25. Dong, Z., et al., *Apoptosis-resistance of hypoxic cells: multiple factors involved and a role for IAP-2.* The American journal of pathology, 2003. 163(2): p. 663-671.

26. Codony, V.L. and M. Tavassoli, *Hypoxia-induced therapy resistance: Available hypoxia-targeting strategies and current advances in head and neck cancer.* Transl Oncol, 2021. 14(3): p. 101017.

27. Graham K, U.E., *Overcoming tumor hypoxia as a barrier to radiotherapy, chemotherapy and immunotherapy in cancer treatment.* Int J Nanomedicine, 2018. 13: p. 6049-6058.

28. Wilson, W.R. and M.P. Hay, *Targeting hypoxia in cancer therapy.* Nature Reviews Cancer, 2011. 11(6): p. 393-410.

29. Kohan, R., et al., *Reactive oxygen species in cancer: a paradox between pro- and anti-tumour activities.* Cancer Chemother Pharmacol, 2020. 86(1): p. 1-13.

30. Zhang, J., et al., *Small molecules regulating reactive oxygen species homeostasis for cancer therapy.* Med Res Rev, 2021. 41(1): p. 342-394.

31. Brillo, V., et al., *Mitochondrial Dynamics, ROS, and Cell Signaling: A Blended Overview.* Life, 2021. 11(4): p. 332.

32. Dan Dunn, J., et al., *Reactive oxygen species and mitochondria: A nexus of cellular homeostasis.* Redox Biology, 2015. 6: p. 472-485.

33. Feng, H. and B.R. Stockwell, *Unsolved mysteries: How does lipid peroxidation cause ferroptosis?* PLoS biology, 2018. 16(5): p. e2006203-e2006203.

34. Narayanan, D., S. Ma, and D. Özcelik, *Targeting the Redox Landscape in Cancer Therapy.* Cancers (Basel), 2020. 12(7).

35. Cremers, C.M. and U. Jakob, *Oxidant Sensing by Reversible Disulfide Bond Formation.* Journal of Biological Chemistry, 2013. 288(37): p. 26489-26496.

36. Cross, J.V. and D.J. Templeton, *Regulation of signal transduction through protein cysteine oxidation.* Antioxid Redox Signal, 2006. 8(9-10): p. 1819-27.

37. Radzinski, M., et al., *The Cys Sense: Thiol Redox Switches Mediate Life Cycles of Cellular Proteins.* Biomolecules, 2021. 11(3): p. 469.

38. Di Monte, D., et al., *Menadione-induced cytotoxicity is associated with protein thiol oxidation and alteration in intracellular Ca2+ homeostasis.* Arch Biochem Biophys, 1984. 235(2): p. 343-50.

39. Ayala, A., M.F. Muñoz, and S. Argüelles, *Lipid peroxidation: production, metabolism, and signaling mechanisms of malondialdehyde and 4-hydroxy-2-nonenal.* Oxidative medicine and cellular longevity, 2014. 2014: p. 360438-360438.

40. Cozza, G., et al., *Glutathione peroxidase 4-catalyzed reduction of lipid hydroperoxides in membranes: The polar head of membrane phospholipids binds the enzyme and addresses the fatty acid hydroperoxide group toward the redox center.* Free Radic Biol Med, 2017. 112: p. 1-11.

41. Fruhwirth, G.O., A. Loidl, and A. Hermetter, *Oxidized phospholipids: From molecular properties to disease.* Biochimica et Biophysica Acta (BBA) - Molecular Basis of Disease, 2007. 1772(7): p. 718-736.

42. Gaschler, M. and B. Stockwell, *Lipid peroxidation in cell death.* Biochemical and biophysical research communications, 2017. 482 3: p. 419-425.

43. Cooke, M.S., et al., *Oxidative DNA damage: mechanisms, mutation, and disease.* Faseb j, 2003. 17(10): p. 1195-214.

44. Croteau, D.L. and V.A. Bohr, *Repair of Oxidative Damage to Nuclear and Mitochondrial DNA in Mammalian Cells *.* Journal of Biological Chemistry, 1997. 272(41): p. 25409-25412.

45. Forman, H.J., H. Zhang, and A. Rinna, *Glutathione: overview of its protective roles, measurement, and biosynthesis.* Molecular aspects of medicine, 2009. 30(1-2): p. 1-12.

46. Traverso, N., et al., *Role of Glutathione in Cancer Progression and Chemoresistance.* Oxidative Medicine and Cellular Longevity, 2013. 2013: p. 972913.

47. Hatem, E., N. El Banna, and M.E. Huang, *Multifaceted Roles of Glutathione and Glutathione-Based Systems in Carcinogenesis and Anticancer Drug Resistance.* Antioxid Redox Signal, 2017. 27(15): p. 1217-1234.

48. Ortega, A.L., S. Mena, and J.M. Estrela, *Glutathione in cancer cell death.* Cancers, 2011. 3(1): p. 1285-1310.

49. Bonifácio, V.D.B., et al., *Cysteine metabolic circuitries: druggable targets in cancer.* British Journal of Cancer, 2021. 124(5): p. 862-879.

50. Shin, C.-S., et al., *The glutamate/cystine xCT antiporter antagonizes glutamine metabolism and reduces nutrient flexibility.* Nature Communications, 2017. 8(1): p. 15074.

51. Koppula, P., L. Zhuang, and B. Gan, *Cystine transporter SLC7A11/xCT in cancer: ferroptosis, nutrient dependency, and cancer therapy.* Protein & Cell, 2020.

52. Lin, W., et al., *SLC7A11/xCT in cancer: biological functions and therapeutic implications.* American journal of cancer research, 2020. 10(10): p. 3106-3126.

53. Lo, M., et al., *The xc− cystine/glutamate antiporter: a mediator of pancreatic cancer growth with a role in drug resistance.* British Journal of Cancer, 2008. 99(3): p. 464-472.

54. Bansal, A. and M.C. Simon, *Glutathione metabolism in cancer progression and treatment resistance.* Journal of Cell Biology, 2018. 217(7): p. 2291-2298.

55. Kansanen, E., et al., *The Keap1-Nrf2 pathway: Mechanisms of activation and dysregulation in cancer.* Redox Biology, 2013. 1(1): p. 45-49.

56. Jaramillo, M.C. and D.D. Zhang, *The emerging role of the Nrf2-Keap1 signaling pathway in cancer.* Genes Dev, 2013. 27(20): p. 2179-91.

57. Motohashi, H. and M. Yamamoto, *Nrf2-Keap1 defines a physiologically important stress response mechanism.* Trends Mol Med, 2004. 10(11): p. 549-57.

58. Tong, Y.-H., et al., *Keap1-Nrf2 pathway: A promising target towards lung cancer prevention and therapeutics.* Chronic diseases and translational medicine, 2015. 1(3): p. 175-186.

59. Kobayashi, A., et al., *Oxidative stress sensor Keap1 functions as an adaptor for Cul3-based E3 ligase to regulate proteasomal degradation of Nrf2.* Mol Cell Biol, 2004. 24(16): p. 7130-9.

60. Suzuki, T., et al., *Molecular Mechanism of Cellular Oxidative Stress Sensing by Keap1.* Cell Rep, 2019. 28(3): p. 746-758 e4.

61. Kensler, T.W., N. Wakabayashi, and S. Biswal, *Cell survival responses to environmental stresses via the Keap1-Nrf2-ARE pathway.* Annu Rev Pharmacol Toxicol, 2007. 47: p. 89-116.

62. Annalisa Lo Gerfo, L.P., Lucia Chico and Gabriele Siciliano *Nrf2 Signaling: An Adaptive Response Pathway for Neurodegenerative Disorders*, in *A Master Regulator of Oxidative Stress - The Transcription Factor Nrf2*, A.M.-G.a.E.O.M.-S. Jose Antonio Morales-Gonzalez, Editor. 2016, IntechOpen.

63. Olinski, R., et al., *DNA base modifications in chromatin of human cancerous tissues.* FEBS Lett, 1992. 309(2): p. 193-8.

64. Pelicano, H., D. Carney, and P. Huang, *ROS stress in cancer cells and therapeutic implications.* Drug Resistance Updates, 2004. 7(2): p. 97-110.

65. Panieri, E. and M.M. Santoro, *ROS homeostasis and metabolism: a dangerous liason in cancer cells.* Cell Death & Disease, 2016. 7(6): p. e2253-e2253.

66. Perillo, B., et al., *ROS in cancer therapy: the bright side of the moon.* Experimental & Molecular Medicine, 2020. 52(2): p. 192-203.

67. Liou, G.-Y., et al., *Mutant KRas-Induced Mitochondrial Oxidative Stress in Acinar Cells Upregulates EGFR Signaling to Drive Formation of Pancreatic Precancerous Lesions.* Cell Reports, 2016. 14(10): p. 2325-2336.

68. Vafa, O., et al., *c-Myc can induce DNA damage, increase reactive oxygen species, and mitigate p53 function: a mechanism for oncogene-induced genetic instability.* Mol Cell, 2002. 9(5): p. 1031-44.

69. Irani, K., et al., *Mitogenic signaling mediated by oxidants in Ras-transformed fibroblasts.* Science, 1997. 275(5306): p. 1649-52.

70. Yuan, Y., et al., *Comprehensive molecular characterization of mitochondrial genomes in human cancers.* Nature Genetics, 2020. 52(3): p. 342-352.

71. Carew, J.S. and P. Huang, *Mitochondrial defects in cancer.* Molecular cancer, 2002. 1: p. 9-9.

72. Chandel, N.S., et al., *Mitochondrial reactive oxygen species trigger hypoxia-induced transcription.* Proc Natl Acad Sci U S A, 1998. 95(20): p. 11715-20.

73. Behrend, L., G. Henderson, and R.M. Zwacka, *Reactive oxygen species in oncogenic transformation.* Biochem Soc Trans, 2003. 31(Pt 6): p. 1441-4.

74. de Sá Junior, P.L., et al., *The Roles of ROS in Cancer Heterogeneity and Therapy.* Oxidative Medicine and Cellular Longevity, 2017. 2017: p. 2467940.

75. Suh, Y.-A., et al., *Cell transformation by the superoxide-generating oxidase Mox1.* Nature, 1999. 401(6748): p. 79-82.

76. Glasauer, A. and N.S. Chandel, *Targeting antioxidants for cancer therapy.* Biochem Pharmacol, 2014. 92(1): p. 90-101.

77. Wang, X.J., et al., *Nrf2 enhances resistance of cancer cells to chemotherapeutic drugs, the dark side of Nrf2.* Carcinogenesis, 2008. 29(6): p. 1235-43.

78. Sullivan, L.B. and N.S. Chandel, *Mitochondrial reactive oxygen species and cancer.* Cancer & metabolism, 2014. 2: p. 17-17.

79. Klayman, D., *Qinghaosu (artemisinin): an antimalarial drug from China.* Science, 1985. 228(4703): p. 1049-1055.

80. Dhingra, V., K.V. Rao, and M.L. Narasu, *Current status of artemisinin and its derivatives as antimalarial drugs.* Life Sciences, 1999. 66(4): p. 279-300.

81. Rudrapal, M. and D. Chetia, *Endoperoxide antimalarials: development, structural diversity and pharmacodynamic aspects with reference to 1,2,4-trioxane-based structural scaffold.* Drug design, development and therapy, 2016. 10: p. 3575-3590.

82. Nontprasert, A., et al., *Assessment of the neurotoxicity of parenteral artemisinin derivatives in mice.* Am J Trop Med Hyg, 1998. 59(4): p. 519-22.

83. Nontprasert, A., et al., *Studies of the neurotoxicity of oral artemisinin derivatives in mice.* Am J Trop Med Hyg, 2000. 62(3): p. 409-12.

84. Schmuck, G., et al., *Neurotoxic mode of action of artemisinin.* Antimicrob Agents Chemother, 2002. 46(3): p. 821-7.

85. Meshnick, S.R., *Artemisinin: mechanisms of action, resistance and toxicity.* International Journal for Parasitology, 2002. 32(13): p. 1655-1660.

86. Pasupureddy, R., et al., *Current scenario and future strategies to fight artemisinin resistance.* Parasitology Research, 2019. 118(1): p. 29-42.

87. Brossi, A., et al., *Arteether, a new antimalarial drug: synthesis and antimalarial properties.* J Med Chem, 1988. 31(3): p. 645-50.

88. Kaiser, M., et al., *Peroxide bond-dependent antiplasmodial specificity of artemisinin and OZ277 (RBx11160).* Antimicrobial agents and chemotherapy, 2007. 51(8): p. 2991-2993.

89. Zhang, F., D.K. Gosser, Jr., and S.R. Meshnick, *Hemin-catalyzed decomposition of artemisinin (qinghaosu).* Biochem Pharmacol, 1992. 43(8): p. 1805-9.

90. Pandey, N. and S. Pandey-Rai, *Updates on artemisinin: an insight to mode of actions and strategies for enhanced global production.* Protoplasma, 2016. 253(1): p. 15-30.

91. Krishna, S., et al., *Artemisinins: their growing importance in medicine.* Trends in pharmacological sciences, 2008. 29(10): p. 520-527.

92. Ho, W.E., et al., *Artemisinins: pharmacological actions beyond anti-malarial.* Pharmacol Ther, 2014. 142(1): p. 126-39.

93. Li, Q., et al., *Dihydroartemisinin as a Sensitizing Agent in Cancer Therapies.* Onco Targets Ther, 2021. 14: p. 2563-2573.

94. Dai, X., et al., *Dihydroartemisinin: A Potential Natural Anticancer Drug.* Int J Biol Sci, 2021. 17(2): p. 603-622.

95. Dong, F., et al., *Dihydroartemisinin targets VEGFR2 via the NF-κB pathway in endothelial cells to inhibit angiogenesis.* Cancer Biology & Therapy, 2014. 15(11): p. 1479-1488.

96. Jiang, J., et al., *Repurposing the anti-malarial drug dihydroartemisinin suppresses metastasis of non-small-cell lung cancer via inhibiting NF-κB/GLUT1 axis.* Oncotarget, 2016. 7(52).

97. Xu, C., Liu, Y., Xiao, L., Guo, C., Zheng, S., Zeng, E., & Li, D. , *Dihydroartemisinin treatment exhibits antitumor effects in glioma cells through induction of apoptosis.* Molecular Medicine Reports, 2017. 16: p. 9528-9532.

98. Efferth, T., *From ancient herb to modern drug: Artemisia annua and artemisinin for cancer therapy.* Seminars in Cancer Biology, 2017. 46: p. 65-83.

99. Jansen, F.H., et al., *First study of oral Artenimol-R in advanced cervical cancer: clinical benefit, tolerability and tumor markers.* Anticancer Res, 2011. 31(12): p. 4417-22.

100. von Hagens, C., et al., *Prospective open uncontrolled phase I study to define a well-tolerated dose of oral artesunate as add-on therapy in patients with metastatic breast cancer (ARTIC M33/2).* Breast Cancer Res Treat, 2017. 164(2): p. 359-369.

101. Krishna, S., et al., *A Randomised, Double Blind, Placebo-Controlled Pilot Study of Oral Artesunate Therapy for Colorectal Cancer.* EBioMedicine, 2015. 2(1): p. 82-90.

102. Henson, P.M. and D.A. Hume, *Apoptotic cell removal in development and tissue homeostasis.* Trends Immunol, 2006. 27(5): p. 244-50.

103. Elmore, S., *Apoptosis: a review of programmed cell death.* Toxicologic pathology, 2007. 35(4): p. 495-516.

104. Igney, F.H. and P.H. Krammer, *Death and anti-death: tumour resistance to apoptosis.* Nature Reviews Cancer, 2002. 2(4): p. 277-288.

105. Li, J. and J. Yuan, *Caspases in apoptosis and beyond.* Oncogene, 2008. 27(48): p. 6194-6206.

106. Riedl, S.J. and Y. Shi, *Molecular mechanisms of caspase regulation during apoptosis.* Nat Rev Mol Cell Biol, 2004. 5(11): p. 897-907.

107. Youle, R.J. and A. Strasser, *The BCL-2 protein family: opposing activities that mediate cell death.* Nature Reviews Molecular Cell Biology, 2008. 9(1): p. 47-59.

108. Glowacki, S., E. Synowiec, and J. Blasiak, *The role of mitochondrial DNA damage and repair in the resistance of BCR/ABL-expressing cells to tyrosine kinase inhibitors.* Int J Mol Sci, 2013. 14(8): p. 16348-64.

109. Hanahan, D. and R.A. Weinberg, *Hallmarks of cancer: the next generation.* Cell, 2011. 144(5): p. 646-74.

110. Fulda, S. and K.M. Debatin, *Extrinsic versus intrinsic apoptosis pathways in anticancer chemotherapy.* Oncogene, 2006. 25(34): p. 4798-4811.

111. Abbas, R. and S. Larisch, *Targeting XIAP for Promoting Cancer Cell Death-The Story of ARTS and SMAC.* Cells, 2020. 9(3): p. 663.

112. Carneiro, B.A. and W.S. El-Deiry, *Targeting apoptosis in cancer therapy.* Nat Rev Clin Oncol, 2020. 17(7): p. 395-417.

113. Li, Y.-J., et al., *Autophagy and multidrug resistance in cancer.* Chinese Journal of Cancer, 2017. 36(1): p. 52.

114. Arroyo, D.S., et al., *Autophagy in inflammation, infection, neurodegeneration and cancer.* Int Immunopharmacol, 2014. 18(1): p. 55-65.

115. Tanida, I., T. Ueno, and E. Kominami, *LC3 and Autophagy.* Methods Mol Biol, 2008. 445: p. 77-88.

116. Feng, Y., et al., *The machinery of macroautophagy.* Cell Research, 2014. 24(1): p. 24-41.

117. Liu, G., et al., *Role of Autophagy and Apoptosis in Non-Small-Cell Lung Cancer.* Int J Mol Sci, 2017. 18(2).

118. Jung, S., H. Jeong, and S.-W. Yu, *Autophagy as a decisive process for cell death.* Experimental & Molecular Medicine, 2020. 52(6): p. 921-930.

119. Panda, P.K., et al., *Chemical Screening Approaches Enabling Drug Discovery of Autophagy Modulators for Biomedical Applications in Human Diseases.* Frontiers in Cell and Developmental Biology, 2019. 7(38).

120. Dixon, S.J., et al., *Ferroptosis: an iron-dependent form of nonapoptotic cell death.* Cell, 2012. 149(5): p. 1060-72.

121. Li, J., et al., *Ferroptosis: past, present and future.* Cell Death & Disease, 2020. 11(2): p. 88.

122. Stockwell, B.R., et al., *Ferroptosis: A Regulated Cell Death Nexus Linking Metabolism, Redox Biology, and Disease.* Cell, 2017. 171(2): p. 273-285.

123. Tang, D., et al., *Ferroptosis: molecular mechanisms and health implications.* Cell Research, 2021. 31(2): p. 107-125.

124. Galluzzi, L., et al., *Molecular mechanisms of cell death: recommendations of the Nomenclature Committee on Cell Death 2018.* Cell Death & Differentiation, 2018. 25(3): p. 486-541.

125. Gao, M., et al., *Role of Mitochondria in Ferroptosis.* Mol Cell, 2019. 73(2): p. 354-363.e3.

126. Yang, W.S. and B.R. Stockwell, *Ferroptosis: Death by Lipid Peroxidation.* Trends in Cell Biology, 2016. 26(3): p. 165-176.

127. Doll, S. and M. Conrad, *Iron and ferroptosis: A still ill-defined liaison.* IUBMB Life, 2017. 69(6): p. 423-434.

128. Xie, Y., et al., *Ferroptosis: process and function.* Cell Death & Differentiation, 2016. 23(3): p. 369-379.

129. Battaglia, A.M., et al., *Ferroptosis and Cancer: Mitochondria Meet the "Iron Maiden" Cell Death.* Cells, 2020. 9(6): p. 1505.

130. Sleire, L., et al., *Drug repurposing: sulfasalazine sensitizes gliomas to gamma knife radiosurgery by blocking cystine uptake through system Xc−, leading to glutathione depletion.* Oncogene, 2015. 34(49): p. 5951-5959.

131. Singh, A., et al., *Gain of Nrf2 function in non-small-cell lung cancer cells confers radioresistance.* Antioxid Redox Signal, 2010. 13(11): p. 1627-37.

132. Ontikatze, T., et al., *Dihydroartemisinin is a Hypoxia-Active Anti-Cancer Drug in Colorectal Carcinoma Cells.* Front Oncol, 2014. 4: p. 116.

133. Laker, R.C., et al., *A Novel MitoTimer Reporter Gene for Mitochondrial Content, Structure, Stress, and Damage in Vivo*.* Journal of Biological Chemistry, 2014. 289(17): p. 12005-12015.

134. Nicoletti, I., et al., *A rapid and simple method for measuring thymocyte apoptosis by propidium iodide staining and flow cytometry.* J Immunol Methods, 1991. 139(2): p. 271-9.

135. Scaduto, R.C., Jr. and L.W. Grotyohann, *Measurement of mitochondrial membrane potential using fluorescent rhodamine derivatives.* Biophysical journal, 1999. 76(1 Pt 1): p. 469-477.

136. Eng, K.E., et al., *A novel quantitative flow cytometry-based assay for autophagy.* Autophagy, 2010. 6(5): p. 634-641.

137. Technologies, A. *Seahorse Bioscience, a part of Agilent Technology*. 2021; Available from: https://www.agilent.com/cs/library/usermanuals/public/Report_Generator_User_Guide_Seahorse_XF_Cell_Mito_Stress_Test_Single_File.pdf.

138. Livak, K.J. and T.D. Schmittgen, *Analysis of relative gene expression data using real-time quantitative PCR and the 2(-Delta Delta C(T)) Method.* Methods, 2001. 25(4): p. 402-8.

139. Thomas J.A., P.E., Chai YC., Brooks R., Rokutan K., Johnston R.B. , *S-Thiolation of Protein Sulfhydryls.* , in *Biological Reactive Intermediates IV. Advances in Experimental Medicine and Biology*, S.R.R. Witmer C.M., Jollow D.J., Kalf G.F., Kocsis J.J., Sipes I.G. (eds), Editor. 1991, Springer, Boston, MA.

140. Murphy, Michael P., *How mitochondria produce reactive oxygen species.* Biochemical Journal, 2008. 417(1): p. 1-13.

141. Bach, D., et al., *Mitofusin-2 Determines Mitochondrial Network Architecture and Mitochondrial Metabolism: A NOVEL REGULATORY MECHANISM ALTERED IN OBESITY*.* Journal of Biological Chemistry, 2003. 278(19): p. 17190-17197.

142. Gong, M., et al., *Loss-of-function mutations in KEAP1 drive lung cancer progression via KEAP1/NRF2 pathway activation.* Cell communication and signaling : CCS, 2020. 18(1): p. 98-98.

143. Singh, A., et al., *Small Molecule Inhibitor of NRF2 Selectively Intervenes Therapeutic Resistance in KEAP1-Deficient NSCLC Tumors.* ACS Chem Biol, 2016. 11(11): p. 3214-3225.

144. Singh, A. and H. Singh, *Time-scale and nature of radiation-biological damage: Approaches to radiation protection and post-irradiation therapy.* Progress in Biophysics and Molecular Biology, 1982. 39: p. 69-107.

145. Hlouschek, J., et al., *Targeting SLC25A10 alleviates improved antioxidant capacity and associated radioresistance of cancer cells induced by chronic-cycling hypoxia.* Cancer Lett, 2018. 439: p. 24-38.

146. Győrffy, B., et al., *Online survival analysis software to assess the prognostic value of biomarkers using transcriptomic data in non-small-cell lung cancer.* PLoS One, 2013. 8(12): p. e82241.

147. D'Alessandro, S., et al., *Hypoxia modulates the effect of dihydroartemisinin on endothelial cells.* Biochem Pharmacol, 2011. 82(5): p. 476-84.

148. Huang, X.J., et al., *Dihydroartemisinin exerts cytotoxic effects and inhibits hypoxia inducible factor-1alpha activation in C6 glioma cells.* J Pharm Pharmacol, 2007. 59(6): p. 849-56.

149. Murray, J., et al., *In vitro oxygen availability modulates the effect of artesunate on HeLa cells.* Anticancer research, 2014. 34(12): p. 7055-7060.

150. Vandewynckel, Y.P., et al., *Therapeutic effects of artesunate in hepatocellular carcinoma: repurposing an ancient antimalarial agent.* Eur J Gastroenterol Hepatol, 2014. 26(8): p. 861-70.

151. Adams, J.M. and S. Cory, *The Bcl-2 apoptotic switch in cancer development and therapy.* Oncogene, 2007. 26(9): p. 1324-1337.

152. Ramesh, P. and J.P. Medema, *BCL-2 family deregulation in colorectal cancer: potential for BH3 mimetics in therapy.* Apoptosis : an international journal on programmed cell death, 2020. 25(5-6): p. 305-320.

153. Mukhopadhyay, S., et al., *Autophagy and apoptosis: where do they meet?* Apoptosis, 2014. 19(4): p. 555-66.

154. M. Früh, D. De Ruysscher, S. Popat, L. Crinò, S. Peters and E. Felip, Small-cell lung cancer (SCLC): ESMO Clinical Practice Guidelines for diagnosis, treatment and follow-up. Annals of Oncology, 2013. 24: p.99-105

155. Maier, P., et al., *Cellular Pathways in Response to Ionizing Radiation and Their Targetability for Tumor Radiosensitization.* International Journal of Molecular Sciences, 2016. 17(1): p. 102.

156. Shen, Y., et al., *Iron Promotes Dihydroartemisinin Cytotoxicity via ROS Production and Blockade of Autophagic Flux via Lysosomal Damage in Osteosarcoma.* Frontiers in Pharmacology, 2020. 11(444).

157. Chen, G.Q., et al., *Artemisinin compounds sensitize cancer cells to ferroptosis by regulating iron homeostasis.* Cell Death Differ, 2020. 27(1): p. 242-254.

158. Chen, Y., et al., *Dihydroartemisinin-induced unfolded protein response feedback attenuates ferroptosis via PERK/ATF4/HSPA5 pathway in glioma cells.* J Exp Clin Cancer Res, 2019. 38(1): p. 402.

159. Poupel, F., et al., *Dihydroartemisinin Induces Apoptosis in Human Bladder Cancer Cell Lines Through Reactive Oxygen Species, Mitochondrial Membrane Potential, and Cytochrome C Pathway.* International journal of preventive medicine, 2017. 8: p. 78-78.

160. Thongchot, S., et al., *Dihydroartemisinin induces apoptosis and autophagy-dependent cell death in cholangiocarcinoma through a DAPK1-BECLIN1 pathway.* Mol Carcinog, 2018. 57(12): p. 1735-1750.

161. Kalpage, H.A., et al., *Tissue-specific regulation of cytochrome c by post-translational modifications: respiration, the mitochondrial membrane potential, ROS, and apoptosis.* The FASEB Journal, 2019. 33(2): p. 1540-1553.

162. Liesa, M. and O.S. Shirihai, *Mitochondrial dynamics in the regulation of nutrient utilization and energy expenditure.* Cell metabolism, 2013. 17(4): p. 491-506.

163. Popov, L.-D., *Mitochondrial biogenesis: An update.* Journal of cellular and molecular medicine, 2020. 24(9): p. 4892-4899.

164. Horn, A., et al., *Mitochondrial fragmentation enables localized signaling required for cell repair.* Journal of Cell Biology, 2020. 219(5).

165. Coronado, M., et al., *Physiological Mitochondrial Fragmentation Is a Normal Cardiac Adaptation to Increased Energy Demand.* Circulation Research, 2018. 122(2): p. 282-295.

166. Hellyer, J.A., et al., *Clinical Implications of KEAP1-NFE2L2 Mutations in NSCLC.* Journal of Thoracic Oncology, 2021. 16(3): p. 395-403.

167. Homma, S., et al., *Nrf2 enhances cell proliferation and resistance to anticancer drugs in human lung cancer.* Clin Cancer Res, 2009. 15(10): p. 3423-32.

168. Dixon, S.J., et al., *Pharmacological inhibition of cystine-glutamate exchange induces endoplasmic reticulum stress and ferroptosis.* eLife, 2014. 3: p. e02523-e02523.

169. Luo, P., et al., *LncRNA MIR4435-2HG mediates cisplatin resistance in HCT116 cells by regulating Nrf2 and HO-1.* PLoS One, 2020. 15(11): p. e0223035.

170. Jeong, Y., et al., *Role of KEAP1/NRF2 and TP53 Mutations in Lung Squamous Cell Carcinoma Development and Radiation Resistance.* Cancer Discov, 2017. 7(1): p. 86-101.

171. McDonald, J.T., et al., *Ionizing radiation activates the Nrf2 antioxidant response.* Cancer Res, 2010. 70(21): p. 8886-95.

172. Singh, A., et al., *RNAi-mediated silencing of nuclear factor erythroid-2-related factor 2 gene expression in non-small cell lung cancer inhibits tumor growth and increases efficacy of chemotherapy.* Cancer Res, 2008. 68(19): p. 7975-84.

173. Kong, Q., J.A. Beel, and K.O. Lillehei, *A threshold concept for cancer therapy.* Med Hypotheses, 2000. 55(1): p. 29-35.

174. Sack, M., et al., *Combination of conventional chemotherapeutics with redox-active cerium oxide nanoparticles--a novel aspect in cancer therapy.* Mol Cancer Ther, 2014. 13(7): p. 1740-9.

175. Yi, J., et al., *Emodin enhances arsenic trioxide-induced apoptosis via generation of reactive oxygen species and inhibition of survival signaling.* Cancer Res, 2004. 64(1): p. 108-16.

176. Chen, T., M. Chen, and J. Chen, *Ionizing radiation potentiates dihydroartemisinin-induced apoptosis of A549 cells via a caspase-8-dependent pathway.* PloS one, 2013. 8(3): p. e59827-e59827.

177. Zhang, H., et al., *Eliminating Radiation Resistance of Non-Small Cell Lung Cancer by Dihydroartemisinin Through Abrogating Immunity Escaping and Promoting Radiation Sensitivity by Inhibiting PD-L1 Expression.* Front Oncol, 2020. 10: p. 595466.

178. Kim, S.J., et al., *Dihydroartemisinin enhances radiosensitivity of human glioma cells in vitro.* Journal of Cancer Research and Clinical Oncology, 2006. 132(2): p. 129-135.

179. Chen, N., et al., *ROS/Autophagy/Nrf2 Pathway Mediated Low-Dose Radiation Induced Radio-Resistance in Human Lung Adenocarcinoma A549 Cell.* International Journal of Biological Sciences, 2015. 11(7): p. 833-844.

180. Du, X.X., et al., *Initiation of apoptosis, cell cycle arrest and autophagy of esophageal cancer cells by dihydroartemisinin.* Biomed Pharmacother, 2013. 67(5): p. 417-24.

181. Li, N., et al., *The Effect of Dihydroartemisinin on the Malignancy and Epithelial-Mesenchymal Transition of Gastric Cancer Cells.* Curr Pharm Biotechnol, 2019. 20(9): p. 719-726.

182. Wu, B., et al., *Dihydroartiminisin inhibits the growth and metastasis of epithelial ovarian cancer.* Oncol Rep, 2012. 27(1): p. 101-8.

183. Liao, K., J. Li, and Z. Wang, *Dihydroartemisinin inhibits cell proliferation via AKT/GSK3β/cyclinD1 pathway and induces apoptosis in A549 lung cancer cells.* Int J Clin Exp Pathol, 2014. 7(12): p. 8684-91.

184. Du, J., et al., *DHA inhibits proliferation and induces ferroptosis of leukemia cells through autophagy dependent degradation of ferritin.* Free Radic Biol Med, 2019. 131: p. 356-369.

185. Lin, R., et al., *Dihydroartemisinin (DHA) induces ferroptosis and causes cell cycle arrest in head and neck carcinoma cells.* Cancer Lett, 2016. 381(1): p. 165-75.

186. Bader, S., et al., *Activation of anti-oxidant Keap1/Nrf2 pathway modulates efficacy of dihydroartemisinin-based monotherapy and combinatory therapy with ionizing radiation.* Free Radic Biol Med, 2021. 168: p. 44-54.

187. Gao, M., et al., *Ferroptosis is an autophagic cell death process.* Cell Res, 2016. 26(9): p. 1021-32.

188. Yang, N.D., et al., *Artesunate induces cell death in human cancer cells via enhancing lysosomal function and lysosomal degradation of ferritin.* J Biol Chem, 2014. 289(48): p. 33425-41.

189. Boohaker, R.J., et al., *BAX supports the mitochondrial network, promoting bioenergetics in nonapoptotic cells.* Am J Physiol Cell Physiol, 2011. 300(6): p. C1466-78.

190. Fuhrmann, D.C. and B. Brüne, *Mitochondrial composition and function under the control of hypoxia.* Redox biology, 2017. 12: p. 208-215.

191. Brown, R.A.M., et al., *Altered Iron Metabolism and Impact in Cancer Biology, Metastasis, and Immunology.* Frontiers in Oncology, 2020. 10(476).

192. Tacchini, L., et al., *Transferrin receptor induction by hypoxia. HIF-1-mediated transcriptional activation and cell-specific post-transcriptional regulation.* J Biol Chem, 1999. 274(34): p. 24142-6.

193. Brown, R.A.M., et al., *Altered Iron Metabolism and Impact in Cancer Biology, Metastasis, and Immunology.* Frontiers in oncology, 2020. 10: p. 476-476.

194. Tu, Y., *Chapter 22 - Clinical Studies of Dihydroartemisinin*, in *From Artemisia Annua L. to Artemisinins*, Y. Tu, Editor. 2017, Academic Press. p. 335-349.

195. Zhang, C.J., et al., *Mechanism-Guided Design and Synthesis of a Mitochondria-Targeting Artemisinin Analogue with Enhanced Anticancer Activity.* Angew Chem Int Ed Engl, 2016. 55(44): p. 13770-13774.

196. Li, X., et al., *Preclinical Efficacy and Safety Assessment of Artemisinin-Chemotherapeutic Agent Conjugates for Ovarian Cancer.* EBioMedicine, 2016. 14: p. 44-54.

197. Yu, H., et al., *Design, synthesis, cytotoxicity and mechanism of novel dihydroartemisinin-coumarin hybrids as potential anti-cancer agents.* Eur J Med Chem, 2018. 151: p. 434-449.

198. Li, H., et al., *Effects of magnetic dihydroartemisinin nano-liposome in inhibiting the proliferation of head and neck squamous cell carcinomas.* Phytomedicine, 2019. 56: p. 215-228.

199. Gharib, A., et al., *Preparation, characterization and in vitro efficacy of magnetic nanoliposomes containing the artemisinin and transferrin.* Daru : journal of Faculty of Pharmacy, Tehran University of Medical Sciences, 2014. 22(1): p. 44-44.

200. Chen, J., et al., *Mn(ii) mediated degradation of artemisinin based on Fe3O4@MnSiO3-FA nanospheres for cancer therapy in vivo.* Nanoscale, 2015. 7(29): p. 12542-12551.

201. Meng, H., et al., *Nanocapsules based on mPEGylated artesunate prodrug and its cytotoxicity.* Colloids and Surfaces B: Biointerfaces, 2014. 115: p. 164-169.

202. Wang, D., et al., *Magnetically guided delivery of DHA and Fe ions for enhanced cancer therapy based on pH-responsive degradation of DHA-loaded Fe3O4@C@MIL-100(Fe) nanoparticles.* Biomaterials, 2016. 107: p. 88-101.

203. Dai, L., et al., *Novel multiarm polyethylene glycol-dihydroartemisinin conjugates enhancing therapeutic efficacy in non-small-cell lung cancer.* Sci Rep, 2014. 4: p. 5871.

204. Emami, J., H. Yousefian, and H. Sadeghi, *Targeted Nanostructured Lipid Carrier for Brain Delivery of Artemisinin: Design, Preparation, Characterization, Optimization and Cell Toxicity.* J Pharm Pharm Sci, 2018. 21(1s): p. 225s-241s.

205. Travis, E.L., et al., *NRF2 deficiency reduces life span of mice administered thoracic irradiation.* Free radical biology & medicine, 2011. 51(6): p. 1175-1183.

206. Yang, D., et al., *Dihydroartemisinin supresses inflammation and fibrosis in bleomycine-induced pulmonary fibrosis in rats.* Int J Clin Exp Pathol, 2015. 8(2): p. 1270-81.

207. Yang, D.-x., et al., *Dihydroartemisinin alleviates oxidative stress in bleomycin-induced pulmonary fibrosis.* Life Sciences, 2018. 205: p. 176-183.

208. Yin, J., et al., *Role of dihydroartemisinin in regulating prostaglandin E2 synthesis cascade and inflammation in endothelial cells.* Heart and Vessels, 2018. 33(11): p. 1411-1422.

209. Ghobadi, G., et al., *Physiological Interaction of Heart and Lung in Thoracic Irradiation.* International Journal of Radiation Oncology*Biology*Physics, 2012. 84(5): p. e639-e646.

210. Ramroth, J., et al., *Dose and Fractionation in Radiation Therapy of Curative Intent for Non-Small Cell Lung Cancer: Meta-Analysis of Randomized Trials.* International journal of radiation oncology, biology, physics, 2016. 96(4): p. 736-747.

211. Winegar, R.A., et al., *Radiation-induced point mutations, deletions and micronuclei in lacI transgenic mice*. Mutat Res, 1994. 307(2): p. 479-87

212. Iliakis, G., et al., *Mechanisms of DNA double strand break repair and chromosome aberration formation.* Cytogenet Genome Res, 2004. 104(1-4): p. 14-20

213. Manova, V., Singh, S. K. and Iliakis, G., *Processing of DNA double strand breaks by alternative non-homologous end-joining in hyperacetylated chromatin.* Genome Integr, 2012. 3(1): p. 4

214. Salem, A., et al., *Targeting Hypoxia to Improve Non–Small Cell Lung Cancer Outcome*. Journal of the National Cancer Institute, 2017. 110(1): p. 14-30

215. Muz, B., et al, *The role of hypoxia in cancer progression, angiogenesis, metastasis, and resistance to therapy.* Hypoxia (Auckland, N.Z.), 2015. 3: p. 83-92

216. Huang, L.E., et al., *Regulation of hypoxia-inducible factor 1alpha is mediated by an O_2-dependent degradation domain via the ubiquitin-proteasome pathway.* Proc Natl Acad Sci U S A, 1998. 95(14): p. 7987-92

217. Höckel, M. and Vaupel, P., *Tumor Hypoxia: Definitions and Current Clinical, Biologic, and Molecular Aspects.* Journal of the National Cancer Institute, 2001, 93 (4): p. 266-276

218. Sørensen, B.S. and Horsman, M. R., *Tumor Hypoxia: Impact on Radiation Therapy and Molecular Pathways.* Frontiers in Oncology, 2020. 10(562)

219. Dewhirst, M.W., Cao, Y. and Moeller, B., *Cycling hypoxia and free radicals regulate angiogenesis and radiotherapy response.* Nature Reviews Cancer 2008, 8(6): p. 425-437

8 Appendix

8.1 Abbreviation Index

γH2A.X	Phosphorylated H2A histone family member X
ΔΨm	Mitochondrial membrane potential
·OH	hydroxyl radical
$^1O_2$	singlet oxygen
4HNE	4-hydroxynonenal
ACT	Artemisinin combination therapies
ANOVA	Analysis of variance
APAF1	Apoptotic protease activating factor 1
APS	Ammonium persulfate
ATCC	American Type Culture Collection
ATP	Adenosine triphosphate
Bak	Bcl-2 homologous antagonist/killer
Bax	Bcl-2 associated X protein
Bcl-2	B-cell lymphoma 2
BER	Base excision repair
BH3	Bcl-2 homology domain 3
BSA	Bovine serum albumin
BSO	Buthionine sulfoximine
cDNA	Complementary deoxyribonucleic acid
CFA	Colony formation assay
CO_2	Carbon dioxide
CQ	Chloroquine
Ct	Cycle threshold
DFO	Deferoxamine
DHA	Dihydroartemisinin
DISC	Death-inducing signaling complex
DMSO	Dimethyl sulfoxide
DNA	Deoxyribonucleic acid
DSB	Double strand break
DTNB	Dithiobis-(2-nitrobenzoic) acid
EBRT	External beam radiation therapy
ECAR	Extracellular acidification rate

EDTA	Ethylendiaminetetraacetic acid
EdU	5-ethynyl-2´-deoxyuridine
ELISA	Enzyme-linked immunosorbent assay
ER	Endoplasmic reticulum
ETC	Electron transport chain
FADD	Fas-associated protein with death domain
FCCP	Fluoro-carbonyl cyanide phenylhydrazone
FCS	Fetal calf serum
FI	Fluorescence intensity
FSC	Forward scattering
GAPDH	Glycerinaldehyd-3-phosphat-Dehydrogenase
GCL	Glutamate-Cysteine Ligase
GCLC	Glutamate-Cysteine Ligase Catalytic Subunit
GCLM	Glutamate-Cysteine Ligase Modifier Subunit
GPx	Glutathione peroxidase
Grx	Glutaredoxin
GSH	Glutathione
GSSG	Glutathione disulfide
GST	Glutathione-S-transferase
H_2O^+	Ionized water
H_2O_2	Hydrogen peroxide
HEPES	4-(2-hydroxyethyl)-1-piperazineethanesulfonic acid
HIF	hypoxia-inducible factor
HRR	Homologous recombination repair
Hx	Hypoxia
IAP-2	Inhibitor of apoptosis protein 2
IR	Ionizing radiation
Keap1	Kelch Like ECH Associated Protein 1
$L^{\cdot}$	Lipid radicals
LC3	Microtubule-associated protein 1A/1B-light chain 3
LC3II	LC3-phosphatidylethanolamine conjugate
$LOO^{\cdot}$	Lipid peroxide radicals
LOOH	Lipid hydroperoxides
MDA	Malondialdehyde
MMP	Mitochondrial membrane potential

MOMP	Mitochondrial outer membrane permeabilization
mRNA	Messenger ribonucleic acid
mtDNA	Mitochondrial deoxyribonucleic acid
mTOR	Mammalian target of rapamycin complex 1
NAC	N-acetylcyteine
NaCl	Sodium chloride
NADPH	Nicotinamide adenine dinucleotide phosphate
NER	Nucleotide excision repair
NHEJ	Non-homologous end-joining
Nrf2	Nuclear factor erythroid 2-related factor 2
Nx	Normoxia
O_2	Oxygen
$O_2^{\cdot-}$	superoxide anion
OCR	Oxygen consumption rate
OD	Optical density
OER	Oxygen enhancement ratio
PAGE	Polyacrylamide gel electrophoresis
PBS	Phosphate-buffered saline
PCR	Polymerase chain reaction
PE	Plating efficiency
PFA	Para-formaldehyde
PHD	Prolyl hydroxylase domain
PI	Propidium iodide
PUFA	Polyunsaturated fatty acid
PVDF	Polyvinylidene fluoride
qRT-PCR	Quantitative real time polymerase chain reaction
R-OOH	Hydroperoxide group
RCD	Regulated cell death
ROS	Reactive oxygen species
rpm	Rounds per minute
R-SSG	S-glutathionylated
SD	Standard deviation
SDS	Sodium dodecyl sulfate
SF	Survival fraction
SLC7A11	Solute Carrier Family 7 Member 11

SOD	Superoxide dismutase
SSC	Sideward scattering
TBS-T	Tris-buffered saline with Tween-20 (0.2%)
TCA	Tricarboxylic acid
TCGA	The Cancer Genome Atlas
TEMED	Tetramethylethylenediamine
TfR1	Transferrin receptor 1
TMRE	Tetramethylrhodaminethylester
TNF	Tumor necrosis factor
Tris	Tris(hydroxymethyl)aminomethane
Trx	Thioredoxin reductase
VEGF	Vascular endothelial growth factor
VHL	Von Hippel-Lindau
WHO	World Health Organization
xCT	Cystine–glutamate antiporter
XIAP	X-linked inhibitor of apoptosis

8.2 Figure Index

8.3 Table Index

9 Acknowledgement

First of all, I would like to thank my supervisor Dr. Justine Rudner for giving me the chance to work on this exciting project, for her kind support and excellent scientific guidance during the last three years, while allowing to pursue my own scientific curiosity. Furthermore, I would like to thank Prof. Verena Jendrossek for giving me the opportunity to work in her lab and her valuable and continuous endorsement.

Special thanks to Dr. Johann Matschke for supporting me and share his knowledge and expertise, especially in the field of hypoxia research and experimental methods such as the Seahorse Analyzer.

I warmly want to thank Angelika Warda for the excellent technical assistance and, especially, for the mental support during the last year.

I would also like to offer my special thanks to the whole AG1 for the constructive support and daily help. I am very grateful for the pleasant and confiding working atmosphere all of you created.

Finally, I want to thank my family and friends for their love and continuous encouragement, especially my parents and stepfather for supporting me whenever possible. Thank you Basko for your calming influence during the last months.

10 Declarations

Erklärung:

Hiermit erkläre ich, gem. § 6 Abs. (2) g) der Promotionsordnung der Fakultät für Biologie zur Erlangung der Dr. rer. nat., dass ich das Arbeitsgebiet, dem das Thema „*Dihydroartemisinin efficiently Induces Cytotoxicity in Normoxic and Hypoxic Cancer Cells and Improves Radiotherapy“* zuzuordnen ist, in Forschung und Lehre vertrete und den Antrag von Sina Bader befürworte und die Betreuung auch im Falle eines Weggangs, wenn nicht wichtige Gründe dem entgegenstehen, weiterführen werde.

Essen, den _____ _____

PD Dr. rer. nat. Justine Rudner

Erklärung:

Hiermit erkläre ich, gem. § 7 Abs. (2) d) + f) der Promotionsordnung der Fakultät für Biologie zur Erlangung des Dr. rer. nat., dass ich die vorliegende Dissertation selbständig verfasst und mich keiner anderen als der angegebenen Hilfsmittel bedient, bei der Abfassung der Dissertation nur die angegeben Hilfsmittel benutzt und alle wörtlich oder inhaltlich übernommenen Stellen als solche gekennzeichnet habe.

Essen, den _____ _____

Sina Bader

Erklärung:

Hiermit erkläre ich, gem. § 7 Abs. (2) e) + g) der Promotionsordnung der Fakultät für Biologie zur Erlangung des Dr. rer. nat., dass ich keine anderen Promotionen bzw. Promotionsversuche in der Vergangenheit durchgeführt habe und dass diese Arbeit von keiner anderen Fakultät/Fachbereich abgelehnt worden ist.

Essen, den _____ _____

Sina Bader